Coordination of innate behaviors by GABAergic cells in lateral hypothalamus

DISSERTATION
zur Erlangung des akademischen Grades

Doctor rerum naturalium
(Dr. rer. nat.)

eingereicht an der
Lebenswissenschaftlichen Fakultät der Humboldt-Universität zu Berlin

von
M.Sc. Marta Carus-Cadavieco

Präsidentin
der Humboldt-Universität zu Berlin

Prof. Dr.-Ing. Dr. Sabine Kunst

Dekan der Lebenswissenschaftlichen Fakultät
der Humboldt-Universität zu Berlin

Prof. Dr. Bernhard Grimm

Gutachter/innen

1. Dr. Tatiana Korotkova
2. Prof. Dr. Peter Hegemann
3. Prof. Dr. Rüdiger Krahe

Tag der mündlichen Prüfung: 28.2.2018

The experimental work of this thesis was performed from January 2013 to October 2017 under supervision of Dr. Tatiana Korotkova and Dr. Alexey Ponomarenko at the Leibniz Institute for Molecular Pharmacology (FMP), Berlin, Germany.

Abstract

Lateral hypothalamus (LH) is crucial for regulation of innate behaviors, including sleep-wake cycle, locomotion and feeding behavior. However, it remained unknown whether and how temporal coordination of hypothalamic neuronal populations regulates transitions between different behavioral states. This work combined optogenetics with neuronal recordings in behaving mice and revealed that optogenetic stimulation of LH_{Vgat} cells and their connections regulates arousal, food intake and food seeking. LH_{Vgat} cells were optogenetically identified by expressing a Cre-dependent excitatory opsin (ChETA) in VGAT-Cre mice. LH_{Vgat} neurons increased firing rates upon transitions from non-REM (NREM) sleep to wakefulness, and their optogenetic stimulation during NREM sleep induced a rapid transition to wakefulness. LH_{Vgat} cells project to the reticular thalamic nucleus (RTN). Optogenetic activation of LH_{Vgat} terminals in the RTN area exerted a strong frequency-dependent inhibition of RTN cells and replicated state-dependent changes in RTN neurons activity. Recordings of LH neurons during exploration revealed that 65% of LH neurons increased their activity upon the onset of locomotion. Top-down forebrain innervation of LH is provided, to a great extent, by inhibitory inputs from the lateral septum (LS), a key region for regulating innate behaviors according to environmental context; LS is connected, in turn, with cortical networks. During spontaneous exploration in a free-feeding model, LS and LH displayed prominent gamma oscillations (30-90 Hz) which entrained neuronal activity within and across the two regions. Optogenetic gamma-frequency stimulation of somatostatin-positive GABAergic (LS-SST) projections to LH facilitated food-seeking, i.e. shortened latency to reach the food zone but not the drinking zone or a control zone. It also increased the probability of entering the food zone prior to food-free zones, located in other corners of the enclosure. LS inhibitory input enabled separate signaling by LH neurons according to their feeding-related activity, making them fire at distinct phases of the gamma oscillation. Interestingly, in contrast to increased food intake during optogenetic stimulation of LH_{Vgat} cells, food intake during gamma-rhythmic LS-LH stimulation was not changed.

Overall this works provides new insight into the function of LH circuitry, which employs signalling at different time scales, which in coordination with upstream and downstream circuits regulates transitions between innate behaviors.

Zusammenfassung

Der laterale Hypothalamus (LH) reguliert angeborene Verhaltensweisen, einschließlich den Schlaf-Wach-Zyklus, Fortbewegung und Nahrungsaufnahme. Ob und wie die Koordination von hypothalamischen Neuronengruppen Übergänge zwischen Verhaltenszuständen reguliert, blieb jedoch unbekannt. In dieser Arbeit wurde Optogenetik mit neuronalen Ableitungen in verhaltenden Mäusen kombiniert und ergab, dass optogenetische Stimulation von LH_{Vgat} Zellen und deren Verbindungen Wachzustand, Nahrungsaufnahme und Nahrungssuche steuert. LH_{Vgat} Zellen wurden optogenetisch durch Exprimierung von Cre-abhängigem Opsin (ChETA) in VGAT-Cre Mäusen identifiziert. LH_{Vgat} Neurone erhöhten ihre Aktivitätsrate während Übergängen vom NREM-Schlaf zum Wachzustand. Dieser Übergang konnte durch optogenetische Stimulation der Zellen induziert werden. LH_{Vgat} Zellen projizieren zum Nucleus reticularis des Thalamus (RTN). Optogenetische Aktivierung von Vgat Ausgängen im RTN führte eine starke, frequenzabhängige Inhibierung von RTN Zellen herbei und replizierte Verhaltenszustands-abhängige Aktivitätsraten in RTN Neuronen. Ableitungen von LH Neuronen währen Umgebungserkundung ergaben, dass 65% der LH Neurone ihre Aktivitätsrate erhöhten, wenn das Tier began sich fortzubewegen. 'Top-down' Innervation des LH erfolgt größtenteils durch inhibitorische Signale ausgehend vom lateralen Septums (LS), einer Schlüsselregion bei der Regulierung von angeborenen Verhaltensweisen entsprechend dem Umgebungskontext. Das LS ist wiederum mit kortikalen Netzwerken verbunden. Während spontaner Umgebungserkundung und freiem Zugang zu Futter wiesen der LH und das LS charakteristische Gamma-Oszillationen (30-90 Hz) auf, welche neuronale Aktivität innerhalb und zwischen diesen beiden Gehirnregionen synchronisierten. Optogenetische Stimulation von Somatostatin-positiven GABAergen (LS-SST) Projektionen zum LH mit Gamma-Frequenz förderte die Nahrungssuche, d.h. die Zeit bis zum Erreichen der Nahrungs-, aber nicht einer Trink- oder Kontrollzone, wurde verringert. Weiterhin erhöhte sich die Wahrscheinlichkeit des Betretens der Nahrungszone im Vergleich zu den anderen Ecken der Umgebung, wo sich keine Nahrung befand. Inhibitorische Signale des LS bewirkten eine Unterteilung der LH Neurone: entsprechend ihrer Aktivität im Bezug zur Nahrungsstelle wurden sie während bestimmter Phasen der Gamma-Oszillation aktiviert. Interessanterweise führte optogenetische Stimulation von LS-LH Neuronen mit Gamma-Frequenz, im Gegensatz zu optogenetischer Stimulation von LH_{Vgat} Zellen, keine Veränderung bei der Nahrungsaufnahme selbst herbei.

Insgesamt liefert diese Arbeit neue Einsichten über die Funktion der neuronalen Netzwerke des LH, welche durch Signalgebung mit unterschiedlichen Zeitskalen über die Koordination mit vor- und nachgeschalteten neuronalen Netzwerken Übergange zwischen verschiedenen angeborenen Verhaltensweisen regeln.

Glosary

AAV	adeno-associated virus
AD	Alzheimer's disease
AgRP	agouti-related protein
AN	anorexia nervosa
AP	anteroposterior
ARAS	ascending reticular activating systems
Arc	arcuate nucleus
ATP	adenosine triphosphate
BF	basal forebrain
BLA	basolateral amygdala
BN	bulimia nervosa
BNST	bed nucleus of the stria terminalis
BR	bacteriorhodopsin
CaMKII	calmodulin-dependent protein kinase II
CART	cocaine- and amphetamine-related transcript
CCK	cholecystokinin
CeA	central nucleus of the amygdala
ChETA	channelrhodpsin 2 E123T Accelerated
ChR	channelrhodopsin
CNS	central nervous system
CT	corticothalamic
CV	coefficient of variance
D1R	dopamine receptor-1
DR	dorsal raphe
DV	dorsoventral
Dyn	dynorphin
EEG	electroencephalogram
EMG	electromyogram
eYFP	enhanced yellow fluorescent protein

FFT	fast Fourier transform
FZ	food zone
GLP1	glucagon-like peptide 1
Glu	glutamate
Hcrt	hypocretins
HSVs	herpes simplex viruses
icv	intracerebroventricullar
IPSPs	inhibitory postsynaptic potentials
ISIs	interspike intervals
I_T	T-type current
LC	locus coeruleus
LDT	laterodorsal
LED	light-emitting diode
LepRB	long-form of the leptin receptor
LFP	local field potential
LH	lateral hypothalamus
LHb	lateral habenular nucleus
LS	lateral septum
LV	lentivirus
MCH	melanin-concentrating hormone
ML	mediolateral
MnPO	median preoptic nucleus
mPFC	medial prefrontal cortex
MRF	midbrain reticular formation
MS	medial septum
NAc	nucleus accumbens
NAcSh	nucleus accumbens shell
NpHR	*Natromonas pharaonis* halorhodopsin
NPY	neuropeptide-y
NREM	non-rapid eye movement (sleep)
Nts	neurotensin
NTS	nucleus of the solitary tract

Ox	orexin
PAG	periaqueductal grey
PB	parabrachial nucleus
PBS	phosphate-buffered saline
PFA	paraformaldehyde
POMC	pro-opiomelanocortin
PPT	pedunculopontine
PV	parvalbumin
PVN	hypothalamic paraventricular nucleus
PVT	paraventricular nucleus of the thalamus
RMg	nucleus raphe magnus
RTMg	rostromedial tegmental nucleus
RTN	reticular thalamic nucleus
Sst	somatostatin
SWA	slow wave activity
TC	thalamocortical
TMN	tuberomammillary nucleus
TTL	transistor-transistor logic
Vgat	vesicular gaba transporter
Vglut2	vesicular glutamate transporter-2
VLPO	ventrolateral preoptic nucleus
VMH	ventromedial hypothalamus
VTA	ventral tegmental area

Contents

List of Figures

List of Tables

1 Introduction

Innate behaviors such as food intake, locomotion, sleep and wakefulness aim to preserve homeostasis, which in a long term leads to the survival and propagation of the individual and its species. The term *homeostasis* was first conceived in 1925 by a physiologist, Walter Cannon, who later developed the concept (Cannon 1932) and it means maintaining a stable internal state. The modern homeostasis concept requires several mechanisms in the brain: a setpoint, a system able to detect errors, if there is a deficit or excess in the actual physiological situation compared to the setpoint, and an error correction mechanism, such as a motivated drive to activate appropriate response (Berridge 2004).

Many behavioral responses provide homeostatic outcomes before a real physiological need occurs. If there is no depletion in the organism yet, these anticipatory mechanisms cannot be rigorously referred to as homeostatic. However, they supply substrate that eventually will be needed, and many of the brain mechanisms activated during the course of these responses are the same ones activated during 'proper homeostatic responses' (Berridge 2004). Anticipatory responses can therefore provide an advantage by preparing the individual for upcoming challenges.

Precise coordination of innate behaviors, including fast transitions between them, which should happen at the right time, in order to adapt to changing environment, is therefore essential for survival. Adequate sleep is required for good health and performance, however sleeping animals are more vulnerable to potential threats, hence neural systems, which enable quick awakening, if necessary, are required in order to later escape or defend themselves (Saper, Fuller et al. 2010). Consequently, successful food seeking and food intake must occur with a sufficient level of arousal, but an excess of hyperactivity can keep animals from their goals and expose them to possible predators (Korotkova and Ponomarenko 2017).

Pathologies of innate behaviors can cause eating and sleep disorders, whose prevalence is increasing in developed countries, affecting individuals from all age groups (Haslam 2007; Roth 2007). Obesity is rapidly becoming a major health problem, and is normally associated with cardiovascular disease, hypertension and diabetes mellitus (Williams, Mesidor et al. 2015). Anorexia nervosa (AN) constitutes a very difficult to treat psychiatric disorder with a very complex aetiology, in which biological, genetic, psychological and sociocultural factors possibly interact to contribute to its progression (Kaye, Fudge et al. 2009). Likewise, the insufficient sleep associated with insomnia can have dangerous

consequences for the individuals, eventually contributing to cognitive impairment (McCoy and Strecker 2011).

Moreover, alterations of innate behaviors are normally not isolated (Korotkova and Ponomarenko 2017). Sleep irregularities are linked to hormonal imbalances, which can lead to eating and metabolic disorders, such as obesity and diabetes (Adamantidis and de Lecea 2008). In turn, eating disorders like AN or Bulimia nervosa (BN) co-occur with excessive and compulsive locomotor activity (Davis, Katzman et al. 1997).

Thus, understanding the neuronal substrates for the regulation of innate behaviors can also provide insights into mechanisms of eating and sleep disorders, and lead to the development of potential treatments (Korotkova and Ponomarenko 2017). Through the last decades the hypothalamus has been appointed as an orchestrator of innate behaviors (Bernardis and Bellinger 1996).

1.1 Hypothalamus

The hypothalamus is a very phylogenetically conserved through vertebrates species brain region. By integrating signals originated in the brain, body and external environment, it is responsible for a variety of functions, including sleep and arousal, fatigue, thermoregulation, hunger and thirst, locomotion, mating and aggression, therefore playing a critical role in maintaining physiological and behavioral homeostasis (Sternson 2013; Waterson and Horvath 2015; Bonnavion, Mickelsen et al. 2016). All these behavioral responses are essential for ensuring the survival both of the individual and the species (Canteras 2012).

1.1.1 Morphological/anatomical

The hypothalamus is composed of multiple nuclei and fiber tracts located in the ventral part of the diencephalon (Felten and Shetty 2010; Simerly 2015). The most rostral part of the hypothalamus is the preoptic region, anterior boundaries of which are the anterior commissure (dorsally) and the lamina terminalis (ventrally). The nucleus of the diagonal band of Broca is also considered as an anteroventral border of the hypothalamus (Simerly 2015) since the medial preoptic area does not elongate beyond the lamina terminalis, but the lateral preoptic area appears to extend medially, eventually replacing the medial preoptic area at rostral levels (Simerly and Swanson 1988). The posterior boundary of the hypothalamus are the mammillary bodies, where it merges with the periaqueductal gray and ventral tegmental area of the midbrain. Le Gros Clark (1938) subdivided the hypothalamic nuclei along the rostrocaudal axis in four hypothalamic zones: preoptic, supraoptic (commonly designated as anterior), tuberal and mammillary

(or posterior). Medially, the hypothalamus is bounded by the III ventricle, and dorsally by the zona inserta (along most of its length) (Le Gros Clark 1938). Crosby and Woodburne (1939) subdivided the hypothalamus from its medial border to the lateral one in three distinct longitudinal zones: periventricular, medial and lateral (Crosby and Woodburne 1939). The combination of both compartmentalization systems (Le Gros Clark's with Crosby and Woodburne's) organizes the hypothalamus into 12 compartments where all the recognized hypothalamic nuclei are enclosed (Simerly 2015).

1.1.2 Functional neural systems

In addition to morphoanatomical definitions, subgroups of hypothalamic neurons were also originally described based on functional criteria (e.g feeding centers, waking centers, etc). Already in the early 20th century, based on the symptoms displayed by patients suffering from *Encephalitis Lethargica*, and on the post-mortem analysis of brain lesions caused by the disease, Von Economo proposed that the anterior hypothalamus and preoptic area constitute a 'sleep center', whereas the posterior hypothalamus constitutes a 'waking area' (Von Economo 1930). Further experimental studies confirmed this notion and sleep-active neurons were subsequently identified both in inhibitory neurons in VLPO and the median preoptic area, reviewed in (Saper, Fuller et al. 2010).
Likewise, early experiments pointed to the role of hypothalamus in regulating food intake. Hetherington and Ranson found in 1940 that bilateral electrolytic lesions, performed in the medial hypothalamic region, caused hyperphagia and obesity. These lesion sites included the dorsomedial and ventromedial hypothalamic nuclei, the arcuate nucleus, and the ventral premamillary nucleus. On the contrary, lesions in the adjacent lateral hypothalamic area led to a prominent reduction of food intake (Hetherington and Ranson 1940). Subsequent studies proved that lesions in the ventromedial hypothalamus (VMH) of the rat led to a significant increase in food intake (Brobeck, Tepperman et al. 1943) and that electrical stimulation of the lateral hypothalamus (LH) evoked food intake and positive reinforcement, while LH ablation produced aphagia (Hoebel and Teitelbaum 1962). These findings led to the general notion that the ventromedial hypothalamus constitutes a 'satiety center' while the lateral hypothalamic area constitutes a 'feeding center'.
These concepts were challenged over the following decades, and the hypothalamic map became progressively complexified, especially after the identification of neuropeptides expressed in subsets of hypothalamic neurons and the discovery of leptin.

1.1.3 Behavioral control column

Results from successive anatomical studies analyzing afferent and efferent hypothalamic axonal projections combined with the notions about diverse functional centres in the hypothalamus, led to the concept of the ‘behavior control column' (Swanson 2000). This column comprises several circuits and nuclei in the hypothalamus and midbrain, which are involved in mediating different motivated behaviors (Thompson and Swanson 2003). Neuronal groups from this column display a shared pattern in their output connections: a primary branch including descending projections to the motor circuits in the brainstem, that generate behavior, and a secondary branch of ascending projections to the thalamocortical system (Swanson 2000; Thompson and Swanson 2003). As it was conceived in (Swanson 2000), two segments can be distinguished in the behavioral control column: rostral and caudal. The rostral segment comprises the medial preoptic, anterior hypothalamic descending paraventricular, ventromedial and premamillary nucleus, which are implicated in mediating three basic classes of motivated innate behaviors: ingestive (eating and drinking), reproductive and defensive. The caudal segment includes the mammillary body, the reticular substantia nigra and ventral tegmental area, and is suggested to play a role in the expression of locomotor and foraging behaviors employed to reach any and all goal objects.

Further, three components can be distinguished in the behavioral control column, controlling the three fundamental classes of goal-oriented behavior. The anterior hypothalamic nucleus, the dorsomedial part of the ventromedial nucleus, and the dorsal premamillary nucleus display a high level of interconnectivity, and can be partially separated from other elements in column, constituting the circuit for defensive behaviors (Canteras 2012). In turn, the medial preoptic, the ventrolateral part of the ventromedial, the tuberal and ventral premamillary nuclei share wide interconnections among them, forming the component involved in the control of reproductive behaviors (Canteras 2012). The third component of the behavior control column comprises the descending division of the paraventricular hypothalamic nucleus, which controls ingestive behaviors (eating and drinking) (Swanson 2000). Although to the date is not yet fully elucidated how the paraventricular nucleus controls feeding, it probably mediates eating responses over its descending projections to the brainstem (Canteras 2012).

1.2 Lateral hypothalamus

The lateral hypothalamus (LH) is a homeostasis center that coordinates sleep-wake states, food intake, metabolism balance, and motivated behavior. Unlike the clear laminar structure presented by cortical or hippocampal networks, LH circuits form an

intricate local and extensive network, of excitatory and inhibitory neurons that present no obvious anatomical characteristics (Herrera, Ponomarenko et al. 2017). Despite this complex reticular cytoarchitecture, the LH constitutes a functionally distinct formation within the hypothalamus, comprised of an intricate assemble of multiple cell types with unique neurochemical profiles, membrane receptors, functions and unique patterns of inputs and outputs that interconnect with various physiological systems (Bonnavion, Mickelsen et al. 2016; Herrera, Ponomarenko et al. 2017). In this section, some of the main neuronal types that compose LH, including neurons that release classical neurotransmitters as well as neurons, which express neuropeptides, are described.

1.2.1 Glutamatergic neurons

Subsets of LH neurons can be defined by the expression of classical excitatory neurotransmitter glutamate. This glutamatergic population appears to be heterogeneous in terms of co-expression with neurochemical markers and of functionality (Bonnavion, Mickelsen et al. 2016). Many glutamatergic neurons in LH co-express the neuropeptide hypocretin /orexin (Hcrt/Ox), which promotes food intake (see section 1.2.3). In contrast, optogenetic stimulation of LH neurons defined by the expression of the vesicular glutamate transporter (Vglut2) abolished food intake and induced aversive behavioral effects (Jennings, Rizzi et al. 2013). Genetic ablation of LH glutamatergic neurons in mice increased the consumption of high-fat palatable food without affecting their general locomotor activity (Stamatakis, Van Swieten et al. 2016). LH_{Vglut2} neurons receive inhibitory axonal projections from GABAergic neurons in the BNST. Inhibition of these LH_{Vglut2} cells via optogenetic activation of BNST GABAergic projections induced feeding and self-stimulation. Interestingly, these effects varied according to the nutritional state of the animals (Jennings, Rizzi et al. 2013). LH glutamatergic neurons project to neurons in the lateral habenula (LHb) that in turn innervate the ventral tegmental area (VTA) and the rostromedial tegmental nucleus (RTMg) (Poller, Madai et al. 2013). Optogenetic inhibition of these LH_{Glu}-LHb projections increased the intake of a caloric palatable liquid reward and increased the time spent in the stimulation-paired chamber during a real time place-preference task (Stamatakis, Van Swieten et al. 2016). There is also a small glutamatergic population in LH, defined by the co-expression of the calcium binding protein parvalbumin (PV). These PV+ glutamatergic neurons are located within the ventrolateral division of the medial forebrain bundle (Meszar, Girard et al. 2012).

1.2.2 GABAergic neurons

The lateral hypothalamus also contains a large neuronal population of GABAergic nature. These GABAergic neurons can be molecularly defined by the presence of

components required for the synthesis of GABA: the glutamate decarboxylase gene GAD 67/65, or for its release: vesicular GABA transporter (Vgat) (Bonnavion, Mickelsen et al. 2016). The whole LH GABAergic population includes cells expressing Vgat, GAD 65/67, the long form of the leptin receptor (LepRB) or the MCH peptide (see next section and section 1.2.4). It's known that LH_{Vgat} do not coexpress MCH (Jennings, Ung et al. 2015), and that most of MCH are GAD^+, while it is not known how many LH_{Vgat} are positive for GAD. The later could be due to the fact that Vgat-Cre and Gad-Cre lines do not completely target the whole GABAergic population, and therefore a complete overlap of the two markers cannot be seen. To the present date, the exact co-expression of each of these markers within LH GABAergic population is not fully elucidated (Herrera, Ponomarenko et al. 2017). Juxtacellular recordings in head-fixed rats showed that subsets of LH GABA neurons (which were MCH-) were predominantly active during wakefulness or REM sleep (Hassani, Henny et al. 2010), states that are associated with cortical activation. Through increasing evidence during the last decades the neurotransmitter GABA has emerged also as an important candidate in regulating food intake in the LH. Classical studies showed that local injections of the GABA agonist muscimol in LH mediated a decrease in feeding (Kelly, Rothstein et al. 1979), while injections of the GABA antagonist bicuculline in LH induced food intake (reviewed in (Bernardis and Bellinger 1996).

LepRb neurons may comprise a unique cell population within LH, which modulates the function and activity of other LH neuronal types (Bonnavion, Mickelsen et al. 2016). Leptin is a hormone secreted from the adipose tissue, which circulates in proportion to body fat stores, crosses the brain-blood barrier and acts on key neurons that control energy balance, therefore acting as a satiety signal (Morton, Meek et al. 2014; Bonnavion, Mickelsen et al. 2016). About 60% of the LepRb population co-expresses neurotensin (see section 1.2.5), and these cells strongly innervate the dorsal raphe and the ventral tegmental area (Leinninger, Opland et al. 2011). LH LepRb neurons seem to directly innervate a subset of local Hcrt/Orx cells (Louis, Leinninger et al. 2010) and optogenetic stimulation of LH LepRb cells in brain slices elicited $GABA_AR$ mediated synaptic inputs in approximately 27.5% of identified Hcrt/Orx cells (Bonnavion, Jackson et al. 2015).

1.2.3 Hypocretin/Orexin expressing neurons

Orexins (Ox), also known as hypocretins (Hcrt), were simultaneously discovered by two independent groups in 1998. Sakurai and colleagues named them orexins because of the orexinergic effect observed (Sakurai, Amemiya et al. 1998). The name hypocretins references to their hypothalamic origin and to the similarities they present in their amino

acid composition with the hormone secretin (de Lecea, Kilduff et al. 1998). The somata of the Hcrt/Ox-producing neurons are exclusively located in the lateral hypothalamus, particularly concentrated around the perifornical area (Bonnavion, Mickelsen et al. 2016). However, Hcrt/Ox neurons send axonal projections to the entire brain (Mahler, Moorman et al. 2014). There are two types of Hcrt/Ox peptides (Hcrt/Ox A and B), produced from the same pre-pro-orexin precursor, and two receptor subtypes: Hcrt/Ox R1, which binds Hcrt/Ox A with higher affinity, and Hcrt/Ox R2, which has equal affinity for both neuropeptides (Sakurai, Amemiya et al. 1998). Besides Hcrt/Ox, these neurons can also express other neuropeptides: the majority of them co-express the neuropeptide dynorphin (Dyn) and recent data suggest that they also co-express neurotensin (Nts) reviewed in (Bonnavion, Mickelsen et al. 2016). One important feature of HCrt/Ox neurons is the fact that they have a glutamatergic phenotype: they express vesicular glutamate transporters Vglut1 or Vglut2, and are capable of fast glutamate release (Rosin, Weston et al. 2003), which can signal independently from orexin (Schone and Burdakov 2012). Since their discovery, Hcrt/Ox have been associated with numerous functions, including arousal and sleep/wake transitions, food intake and reward seeking. Administration of Hcrt/Ox causes food intake, and food deprivation increases Hcrt/Ox mRNA (de Lecea, Kilduff et al. 1998; Sakurai, Amemiya et al. 1998). Interestingly, Hcrt/Ox activity decreases within milliseconds after the eating onset, remaining low during eating, both in fasted and satiated mice. This rapid inactivation occurred with different types of food: standard, palatable and calorie-free food (Gonzalez, Jensen et al. 2016).

Deficit of Hcrt/Ox neurons or their receptors is linked with the sleep disorder narcolepsy in rodents, dogs and humans (Siegel 1999). Hcrt/Ox fire maximally during active waking, decrease firing rate during quiet waking, and present lowest discharge during NREM sleep and REM sleep, becoming active again before the end of REM sleep, preceding wakefulness (Lee, Hassani et al. 2005). Consequently, optogenetic stimulation of Hcrt/Ox neurons increases the probability of transition to wakefullness from either NREM sleep or REM sleep (Adamantidis, Zhang et al. 2007).

1.2.4 MCH expressing neurons

Intermingled with Hcrt/Ox and Vgat neurons, a separate population of LH neurons synthesizes and releases the neuropeptide melanin-concentrating hormone (MCH) (Broberger, De Lecea et al. 1998; van den Pol, Acuna-Goycolea et al. 2004). This neuropeptide was originally isolated from the pituitary of teleosts, in which it is involved in regulating adaptive changes in pigmentation (Kawauchi, Kawazoe et al. 1983). Similarly to the Hcrt/Ox cells, MCH neurons project extensively throughout the central

nervous system (Bittencourt, Presse et al. 1992). These neurons also co-express other neuropeptides such as nesfatin-1, and approximately 50% of MCH neurons co-express cocaine- and amphetamine-regulated transcript (CART) (reviewed in (Bonnavion, Mickelsen et al. 2016). As mentioned in section 1.2.2**,** MCH neurons are generally considered to have a GABAergic phenotype, due to their colocalization with GAD65 and GAD67 (Elias, Lee et al. 2001; Sapin, Berod et al. 2010). In vitro, optogenetic stimulation of MCH neurons resulted in GABA release onto histaminergic neurons in the tubero mammillary nucleus (TMN) (Jego, Glasgow et al. 2013). However, studies using Vgat-Cre transgenic mice revealed that they do not overlap with the LH_{Vgat} neuronal population (Jennings, Ung et al. 2015). However some studies have shown that a part of the MCH neurons express the vglut1 and vglut2 transporters (Del Cid-Pellitero and Jones 2012) and recent work suggests that MCH cells that project to the lateral septum co-express vglut2, and photostimulation of their axons induced a monosynaptic release of glutamate in the septum (Chee, Arrigoni et al. 2015). MCH neurons display an opposite to Hcrt/Ox cells discharge profile: they fire maximally during REM sleep, low during NREM sleep and minimally during wakefulness (Hassani, Lee et al. 2009). Experiments performed in rats have shown that intracerebroventricular (icv) infusion of MCH induces hypersomnia which was dose-dependent (Verret, Goutagny et al. 2003). Consequently, acute optogenetic stimulation of MCH neurons at the onset of REM sleep prolonged the duration of REM, but not of NREM episodes (Jego, Glasgow et al. 2013).

MCH neurons also play a role in the hypothalamic control of metabolism. In the rat, intracerebroventricular injections of MCH caused an increase in food intake, and after fasting MCH mRNA levels are increased (Herrera, Ponomarenko et al. 2017). MCH neurons can modulate the cerebrospinal fluid flow, by controlling the cilia beat frequency of ependymal cells of the third ventricle (Conductier, Martin et al. 2013). This modulation has been proposed as a mechanism for MCH neurons in controlling metabolism (reviewed in (Herrera, Ponomarenko et al. 2017).

1.2.5 Neurotensin

Neurotensin (Nts) is a 13 amino acid neuropeptide, which was first isolated from bovine hypothalamus by Carraway and Leeman in 1973, and owes its name to its hypotensive properties (Carraway and Leeman 1973). The majority of Nts is actually expressed in the intestines, while the brain contains approximately 10% of the body's Nts. Within the nervous system, Nts can be identified in the spinal cord, hindbrain, midbrain, limbic system, forebrain, thalamus and hypothalamus (particularly in the PVN and LH) reviewed in (Kalivas, Jennes et al. 1982; Brown, Woodworth et al. 2015). Nts receptors are expressed within the cingulate cortex, midbrain, subiculum and the hindbrain. Within the

LH, there seem to be subpopulations of Nts-expressing neurons, based on their co-expression with different molecular markers, although these have not been thoroughly characterized yet. Studies in Nts Cre mice revealed that LH Nts neurons do not overlap with those expressing MCH or Hcrt/Ox (Leinninger, Opland et al. 2011). They have a similar distribution pattern to LepRb-expressing neurons in the LH area (Kalivas, Jennes et al. 1982; Leinninger, Jo et al. 2009), and in fact a large proportion of LH Nts neurons also co-express LepRb and can be activated by leptin (Leinninger, Opland et al. 2011). In addition, some LH Nts neurons co-express the neurotransmitters glutamate (Kempadoo, Tourino et al. 2013), and many of them are GABAergic (Leinninger, Jo et al. 2009; Leinninger, Opland et al. 2011). Although to the present date there are no direct studies concerning the role of LH Nts neurons in sleep/wake, it is known that central administration of Nts promotes arousal and prolongs the latency from wake to sleep stages (Castel, Stutzmann et al. 1989).

Likewise, the precise role of LH Nts in feeding and metabolism remains unknown to date, although literature suggests that central Nts can play a role in regulating energy balance. LH Nts neurons innervate Hcrt/Ox neurons, and VTA dopaminergic neurons (DA). By controlling these neuronal populations, LH Nts could influence feeding, drinking and locomotor activity (Leinninger, Opland et al. 2011; Kempadoo, Tourino et al. 2013). LH Nts neurons might also modulate food intake through their interaction with leptin. Deletion of LepRb specifically from LH Nts neurons induces mild hyperphagia and obesity in mice (Leinninger, Opland et al. 2011).

Another important consideration to take into account regarding the heterogeneity of LH neuronal population, is the possibility that their neurochemical identity may change over time, depending on the behavioral state and metabolic and environmental conditions (Bonnavion, Mickelsen et al. 2016). This kind of neurotransmitter respecification or switching has been described in other hypothalamic nuclei: in the paraventricular and periventricular nuclei of adult brain and ventral suprachiasmatic nucleus in the developing nervous system (Spitzer 2015). These processes seem to aim to the circuit homeostasis, and to date it is not fully elucidated to which degree they occur in LH neurons.

1.3 Anatomical connections of the lateral hypothalamus

The LH is extensively interconnected with multiple brain regions, which reflects its role in integrating a wide range of innate behaviors (Bonnavion, Mickelsen et al. 2016). Anatomical studies using anterograde tracers, identified multiple brain regions and other hypothalamic nuclei, which are targeted prominently by the LH, including the dorsal

premammillary nucleus, nuclei in the anterior hypothalamus and in the medial preoptic area, the periaqueductal gray (PAG, mostly the dorsal and especially ventrolateral divisions) and the rostral lateral septal nuclei. Projections from LH to the thalamus were also identified, including a strong projection to the paratenial and reuniens nuclei, and more moderate projections to additional midline thalamic nuclei; a projection to the epithalamic lateral habenula was also visible in these studies (Hahn and Swanson 2012). Ascending fibers originated in LH also innervate the prefrontal cortex (Hahn and Swanson 2012; Bonnavion, Mickelsen et al. 2016).

Many of the structures targeted by the LH provide in turn feedback projections to the LH (Figure 1.1). Studies with retrograde labelling have identified major forebrain afferents to the LH originated in the polymodal association cortex (anterior cingulate and prelimbic areas) and visceral sensory-motor areas (infralimbic area), the lateral septal nuclei, the nucleus accumbens (NAc), bed nucleus of the stria terminalis (BNST), basolateral amygdala (BLA), and the lateral habenula (LHb) (Hahn and Swanson 2012; Bonnavion, Mickelsen et al. 2016). The hippocampal formation, specifically an intermediate region of field CA1 and the subiculum, send very prominent inputs to the LH as well (Hahn and Swanson 2012). Midbrain and brainstem afferents are also considerable, particularly from the mesencephalic and central grey areas, ventral tegmental area, dorsal raphe, locus coeruleus, and lateral parabrachial area (PB) (Bonnavion, Mickelsen et al. 2016). It should be also noted, that the lateral hypothalamic area is transversed by the medial forebrain bundle, one of the most complex fiber system in the mammalian brain, which represents the central longitudinal pathway of the limbic forebrain-midbrain continuum (Nieuwenhuys, Geeraedts et al. 1982; Simerly 2015). The medial forebrain bundle comprises ascending and descending fibers originating from more than 50 different cell groups, which extend from the prefrontal cortex, through the hypothalamus and ventral brainstem reticular formation, to sacral levels of the spinal cord. As they transverse the area, many of these projections seem to contribute with inputs to the LH neurons (reviewed in (Simerly 2015).

Thus, given the strong connections from the telencephalic regions to the LH, which are more prominent than to other hypothalamic nuclei, e.g. the paraventricular nucleus, the LH is in a good position to mediate more volitional aspects of feeding behavior, as well as to coordinate the emotional and motivational aspects of behavior with visceromotor responses (Canteras 2012; Simerly 2015).

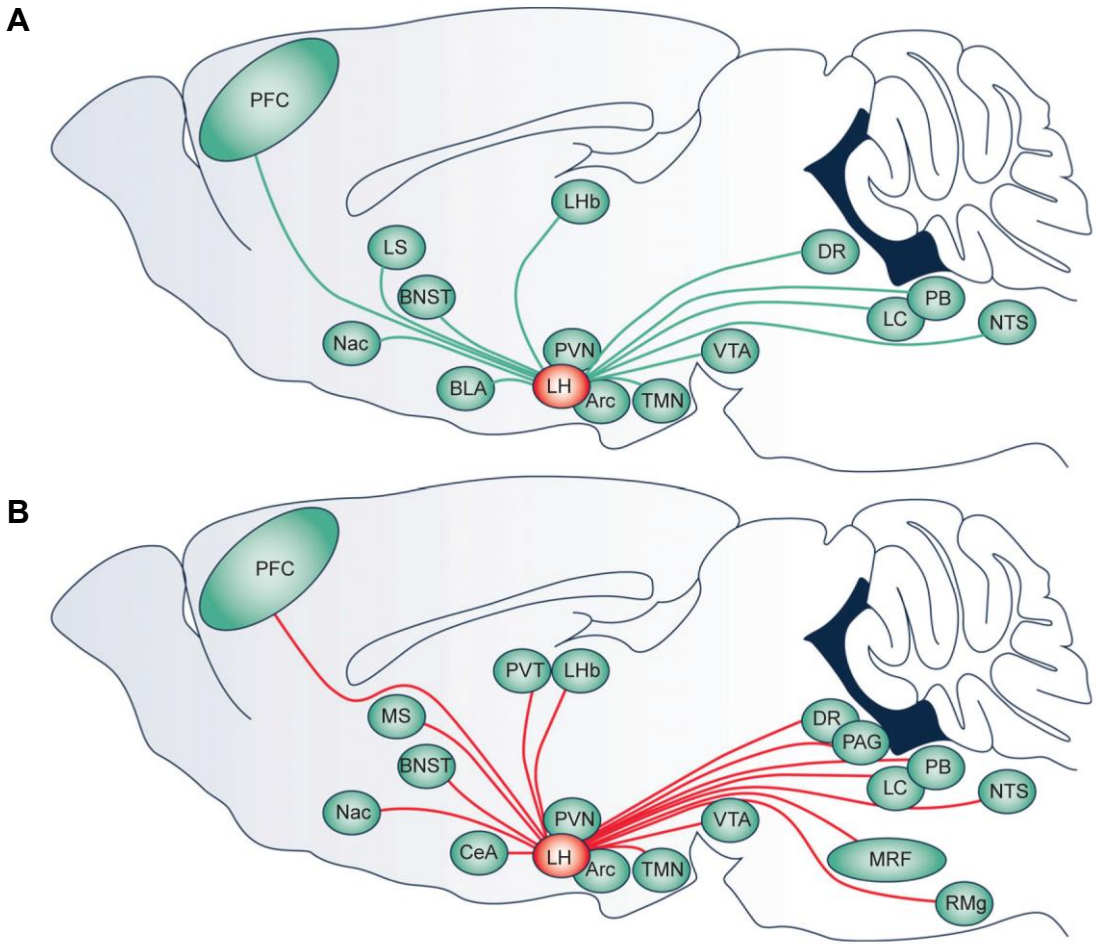

Figure 1.1 Schemes showing main anatomical connections of LH. **A** Parasagital rodent brain section displaying long-range inputs to the LH. **B** Parasagital brain section showing main long-range outputs of the LH. Abbreviations: Arc, arcuate nucleus; BLA, basolateral amygdala; BNST, bed nucleus of the stria terminalis; CeA, central nucleus of the amygdala; DR, dorsal raphe; Fx, fornix; LC, locus coeruleus;LH, lateral hypothalamus; LHb, lateral habenula; LS, lateral septal nuclei; MRF, midbrain reticular formation; MT, mammillothalamic tract; NAc, nucleus accumbens; NTS, nucleus of the solitary tract; PAG, periaqueductal grey; PB, parabrachial nucleus; PFC, prefrontal cortex; PVN, paraventricular nucleus of the hypothalamus; PVT, paraventricular nucleus of the thalamus; RMg, nucleus raphe magnus; TMN, tuberomammillary nucleus; VTA, ventral tegmental area.
Modified from (Bonnavion, Mickelsen et al. 2016).

1.4 Septum

The septum is a brain region that comprises two subdivisions: the lateral septum (LS) and the medial septum (MS). The septum is a part of the limbic system. Through broad and reciprocal connections with telencephalic and diencephalic areas it is involved in the regulation of numerous physiological functions, linking higher cognitive processes with emotions and innate behaviors (Jakab, Leranth et al. 1995). The septum is positioned in

the subcortical forebrain, rostrodorsal to the hypothalamus and the decussation of the anterior commissure, and to some extent dorsocaudal to the nucleus accumbens (Sheehan, Chambers et al. 2004). Its spatial location relative to the lateral ventricles differs to some extent between humans and rodents. In humans, the neural somata of the septal nuclei constitute ‘the septum verum', which is located ventral to the lateral ventricles. In turn, the lateral ventricles are separated by the ‘septum pellucidum' (or lucidum), comprised of fiber tracts and glia that connect the dorsal part of the septum verum to the base of the corpus callosum (Ramón y Cajal 1902; Sheehan, Chambers et al. 2004). However in rodents, the septum lies directly between the lateral ventricles. The septum is highly interconnected with the hippocampus: the medial septum provides ascending inputs to the hippocampus, while the lateral septum receives descending outputs from the hippocampus via the fimbria and fornix (Risold and Swanson 1996). These structures are commonly referred as septohippocampal formation. However, the MS and the LS differ in many aspects, including their neurochemical content and anatomical connections with other brain regions. The MS is functionally related to the ventrally situated nucleus of the diagonal band of Broca (DB), and is also referred to as the medial septum-diagonal band (MSDB). The ascending projections from MSDB to the hippocampus are predominantly GABAergic (PV+), cholinergic and glutamatergic, and are involved in the regulation of hippocampal theta rhythm (Jakab, Leranth et al. 1995; Sheehan, Chambers et al. 2004; Brown, Basheer et al. 2012). There are also PV-lacking GABAergic cells in the MS that are suggested to be local circuit neurons. In rats the MS and LS are also reciprocally interconnected with each other, although these projections are rather sparse (Jakab, Leranth et al. 1995).

1.4.1 Lateral septum

Although GABA is the major neurotransmitter in the LS, there is heterogeneity within this nucleus as well. The region was historically divided into three major parts, based on the cytoarchitecture and connections of these regions: dorsal, intermediate and ventral (Swanson and Cowan 1979). Subsequent studies by Risold and Swanson combining in situ hybridization with anterograde and retrograde tracers, redefined the LS subdivisions (Figure 1.2), based on the neurochemical identity of LS neurons and on a more detailed analysis of their anatomical connections with the hippocampus and hypothalamus. The LS was then divided into rostral, caudal and ventral parts. These parts can in turn be divided into about 20 zones, regions and domains, based on differential terminal fields and expression patterns of neuropeptides and steroid hormone receptors (Risold and Swanson 1997).

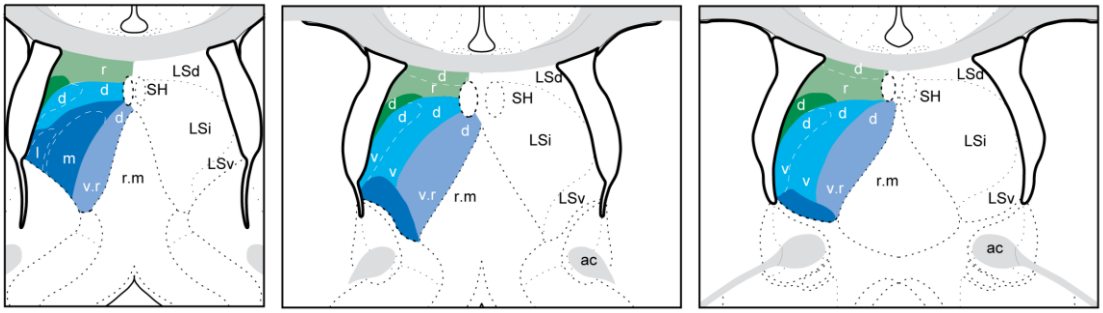

Figure 1.2 Series of coronal sections showing divisions of the lateral septum. Sections are arranged in anatomical order, from rostral (left) to caudal (right). The right side of each drawing illustrates the former historic cytoarchitectonic division of the LS, while the new subdivisions are displayed on the left. The blue areas indicate the rostral part and, within it, light blue designates the medial zone, dark blue indicates the ventrolateral zone, and sky blue shows the dorsolateral zone; areas in green color correspond to the caudal part, and within it dark green depicts the ventral zone and light green the dorsal zone. Modified from (Risold and Swanson 1997).

The rostral LS contains enkephalin-expressing and neurotensin-expressing GABAergic neurons, receives projections from the CA1 region of the hippocampus and subiculum, and in turn is highly interconnected with the medial hypothalamic nuclei. The caudal LS contains somatostatin-expressing (Sst) GABAergic neurons, but does not express mRNA for neurotensin or enkephalin. It receives input from the CA3 hippocampal region, and is strongly interconnected with the lateral hypothalamus. The ventral LS is positioned ventrally to the posterior part of the caudal LS, and is composed of GABAergic neurons that co-express estrogen receptors, but not somatostain, neurotensin or encephalin. It receives projections from the ventral tip of CA1 and subiculum, and is highly interconnected with the medial preoptic area of the hypothalamus (Risold and Swanson 1997; Risold and Swanson 1997b). Some studies in rats suggest that there may be also a population of glutamatergic neurons in the ventral part of the LS, which innervate the medial preoptic area (Kocsis, Kiss et al. 2003; Lin, McKinney et al. 2003). Therefore, there is a strict topographically organized mapping between the three structures, consisting of unidirectional hippocampo-lateral septal projection, and then by bidirectional lateral septo-hypothalamic projections. These connections provide evidence for behavioral control columns (see section 1.1.3), routing information processed in different hippocampal regions through the lateral septum, to diverse hypothalamic regions, involved in the control of different innate behaviors. The LS GABAergic neuronal population comprises predominantly spiny projection neurons, and it seems to lack the ‘classical’ interneurons. Besides to their projections to specific regions outside the septum, it should also be noted that these cells also send collateral

fibers to other LS neurons, which mainly terminate on their dendrites, although occasionally they can form axoaxonal synapses (Risold and Swanson 1997b; Sheehan, Chambers et al. 2004). This, together with electrophysiological data, supports the idea that LS neurons modulate not only extraseptal targets but also coordinate firing patterns within LS, through intraseptal autoinhibition (Sheehan, Chambers et al. 2004). For decades, the LS has been appointed to have a role in emotional, motivational and neuroendocrine-related responses. It was the first brain region reported to enable the acquisition of an operant, positive reinforcing, self-stimulation response in rats (Olds and Milner 1954). Consequently, projections from the rostral LS to the LH Hcrt/Ox neurons drive the expression of conditioned cocaine preference (Sartor and Aston-Jones 2012). Lesions of LS in rats changes the activity of hypothalamo-pituitary-adrenocortical (HPA) axis responses to forced swim stress test, and these animals show a more passive coping style in their behavior (Singewald, Rjabokon et al. 2011). Septal lesions have also been correlated with a potentiation of freezing behavior elicited by contextual stimuli (Sparks and LeDoux 1995), and with excessive and inappropriate sexual activity (Sheehan, Chambers et al. 2004). Projections from the caudal LS to the ventral tegmental area (VTA), when activating their upstream CA3 input, have been found to regulate goal-directed behavior according to the contextual stimuli (Sheehan, Chambers et al. 2004; Luo, Tahsili-Fahadan et al. 2011). However, the precise role of LS in the modulation of emotion-related behaviors remains unclear. This circuitry allows to adjust behavioral responses according to the environmental context, and based on previous experience (Risold and Swanson 1996; Sheehan, Chambers et al. 2004; Korotkova and Ponomarenko 2017).

1.5 Circuits involved in NREM sleep-wake control

Sleep is a homeostatic process and despite providing rest to the individual many brain regions display specific patterns of neuronal activity during its course. Therefore, sleep generation and regulation relies in the interactions between wake-promoting and sleep-promoting systems (Brown, Basheer et al. 2012; Weber and Dan 2016).

1.5.1 Wake-promoting systems

In the first half of the 20th century, Frederic Bremer found that transection of the brain of cats at the midbrain level (‘cervau isolé’ preparation) caused a sleep-like state with slow waves in the cortex, which he initially attributed to the lack of sensory inputs from the spine (Bremer 1935). However, in further experiments with transections at a lower level, at the junction of the brain stem and the spinal cord (‘encephale isole’ preparation) he

found no change in the normal cyclic alternation between sleep and wakefulness (Brown, Basheer et al. 2012). Some years later, Moruzzi and Magoun showed that electrical stimulation in anesthetized cats of the midbrain reticular formation produced the appearance of an ‘activated' desynchronized EEG, similar to the one observed during arousal and REM sleep (Moruzzi and Magoun 1949). Together these findings led to the notion of the ‘Ascending Reticular Activating Systems’ (ARAS) (Saper, Fuller et al. 2010; Brown, Basheer et al. 2012). These ascending nerve fibers from the brainstem can be subdivided into two main pathways: dorsal and ventral (Brown, Basheer et al. 2012).

The dorsal pathway of the ARAS is composed of cholinergic neurons in the mesopontine tegmental nuclei: pedunculopontine and laterodorsal (PPT/LDT) and by glutamatergic neurons from the midbrain, pontine, and medullary reticular formation, which provide innervation to the thalamic relay, intralaminar and reticular thalamic nuclei. The monoaminergic neurons mainly contribute to the ventral pathway, although cells from the locus coeruleus (LC) and from the dorsal raphe also send fibers (noradrenergic and serotonergic respectively) that target the intralaminar and reticular nuclei of the thalamus (Saper, Fuller et al. 2010; Brown, Basheer et al. 2012).

The ventral pathway of the ARAS comprises fibers originating also in the pontine/midbrain regions including glutamatergic neurons from the parabrachial nucleus, and the monoaminergic cell groups: noradrenergic neurons from the LC, serotonergic from the dorsal and median raphe nuclei and dopaminergic neurons from the periaqueductal gray. These systems project to the LH and TMN nuclei of the hypothalamus (synapsing onto glutamatergic, histaminergic and Hcrt/Orx neurons), as well as to the basal forebrain (BF) (Jones 2005). Outputs from the LH (orexinergic) and TMN (histaminergic) also ascend to the BF. In the BF, cholinergic, GABAergic and glutamatergic neurons project to the neocortex causing its activation (Saper, Fuller et al. 2010; Brown, Basheer et al. 2012).

The cortex receives also direct activating projections from the Hcrt/Orx and histaminergic neurons from the hypothalamus, together with the noradrenergic and serotonergic from the brain stem.

Many cholinergic neurons in the PPT and LDT fire with higher frequencies during wakefulness and REM sleep, and most slowly during NREM sleep, which suggests a role in contributing to cortical activation state, while monoaminergic cell groups fire most rapidly during wakefulness, decrease firing during NREM and are silent during REM sleep (Saper, Fuller et al. 2010).

1.5.2 NREM-sleep promoting systems

As revised in section 1.1.2, early work from Von Economo pointed to the anterior preoptic hypothalamic as a "sleep center". Later experimental lesions of the preoptic and the basal forebrain regions in rats and cats decreased sleep reviewed in (Saper, Fuller et al. 2010) and subsequently Sherin and colleagues identified with the use of Fos immunohistochemistry a population of neurons in the ventrolateral preoptic nucleus (VLPO) that were active during sleep but not during wakefulness (Sherin, Shiromani et al. 1996). These VLPO neurons contained the inhibitory neurotransmitters GABA and galanin, and innervated densely nuclei of the ARAS, including the LC, raphe system, periaqueductal gray matter, parabrachial nucleus, LH and especially the histaminergic TMN nucleus (Saper, Fuller et al. 2010; Brown, Basheer et al. 2012). Another large population of GABAergic sleep-active neurons was identified in the median preoptic nucleus (MnPO), placed just dorsal to the third ventricle. Like the sleep-active neurons in the VLPO, MnPO neurons innervate and inhibit wake-promoting nuclei of the ARAS, in the perifornical lateral hypothalamus, dorsal raphe and LC (de Andres, Garzon et al. 2011; Brown, Basheer et al. 2012). Experiments examining the extent of Fos expression during spontaneous sleep, sleep deprivation and following sleep deprivation indicate that MnPO neurons are active in response to sleep pressure during sleep deprivation, while VLPO neurons are mainly active during sleep and in response to increasing sleep amounts during sleep rebound. This suggests a role for MnPO neurons in responding to increased homeostatic sleep pressure, while VLPO neurons may be involved in consolidating and maintaining sleep, and regulating sleep depth (de Andres, Garzon et al. 2011; Brown, Basheer et al. 2012).

Besides the anterior preoptic hypothalamic area, the circuit composed by the thalamus and the cerebral cortex is essential for the generation of the main bioelectric and behavioral features that define NREM sleep (de Andres, Garzon et al. 2011; Brown, Basheer et al. 2012).

The Thalamocortical network and reticular thalamus

The reticular thalamic nucleus (RTN) is a relatively thin sheet of GABAergic neurons encasing the thalamus. It is a derivative of the ventral thalamus, and surrounds the rostral, lateral, and to some extent the ventral sides of the dorsal thalamus (Jakab, Leranth et al. 1995; Fuentealba and Steriade 2005). Due to its anatomical location, the RTN is transversed by practically all axons connecting the dorsal thalamus with the neocortex, which gives the nucleus its reticular appearance and name (Fuentealba and Steriade 2005). RTN neurons are relatively homogenous in their morphology, and most

of them have long dendrites that ramify within the boundaries of the nucleus. An intrinsic, GABAergic axonal network interconnects different parts of the RTN (Jakab, Leranth et al. 1995). It has been also shown that many neighbouring RTN neurons are interconnected by electrical synapses that depend on the gap-junction protein connexin 36 (Fuentealba and Steriade 2005; Huguenard and McCormick 2007). In addition to GABA, RTN cells can co-express other molecular markers such as parvalbumin, the CAT301 antigen, and some neuropeptides like somatostatin and Neuropeptide-Y (Fuentealba and Steriade 2005).

The RTN neurons send axons to the excitatory glutamatergic thalamocortical (TC) relay cells, exerting a strong inhibitory control over them. TC neurons are in turn interconnected with excitatory cells in the cerebral cortex, the corticothalamic (CT) neurons. Both TC and CT neurons send glutamatergic axon collaterals to the RTN, providing positive feedback to the nucleus (McCormick and Bal 1997; Fuentealba and Steriade 2005).

In addition to inputs from the thalamus and the cortex, afferent fibers to the RTN arise in the brainstem and basal forebrain (Jakab, Leranth et al. 1995). The brainstem main inputs originate in the cholinergic nuclei of the mesopontine tegmentum and in the monoaminergic, locus coeruleus and dorsal raphe nuclei. Inputs from the basal forebrain originate in cholinergic and GABAergic neurons, and there are also afferents from the pretectal area, which originate in the GABAergic cells of the optic tract nucleus (Fuentealba and Steriade 2005).

There is evidence for functional differences among RTN cells based on their electrophysiological properties, which to the present date are not correlated with morphological diversity. One neuronal population has a low-threshold Ca^{2+} conductance, which enables the generation of low-threshold spikes, and switching from a tonic firing mode to burst firing (Contreras, Curro Dossi et al. 1992), in a similar way as TC cells do. These Ca^{2+} conductances are voltage-gated T-type channels, $Ca_V3.2$ and $Ca_v3.3$, similar to the channels that TC cells have. However, unlike the T channels from TC neurons, the voltage dependence of RTN T channels is shifted to more positive membrane potentials, which allows burst firing at resting membrane potential (-65 mV). This particular difference is important for the generation of synchronized thalamocortical rhythms, like the spindle waves (see section 1.8.1) (McCormick and Bal 1997; Huguenard and McCormick 2007). The other neuronal population within the RTN apparently lacks this low-threshold Ca^{2+} conductance, and displays only tonic firing (Contreras, Curro Dossi et al. 1992). Alternatively, these neurons could present other voltage-dependent conductances that would mask or inhibit the low threshold Ca^{2+} current (Contreras, Curro Dossi et al. 1992; Lee, Govindaiah et al. 2007). There is also

a subgroup of RTN cells (20%) which can be functionally characterized by their intrinsic membrane bistability, probably due to the expression of a persistent Na^+ current (Fuentealba and Steriade 2005). Like in the TC neurons, the burst and tonic firing modes in RTN cells correlate with different states of vigilance. The tonic mode occurs during brain-activated states of wakefulness and REM sleep, and requires a more depolarized membrane potential. The bursting discharge takes place during slow-wave sleep, and is generated by the activation of the low-threshold Ca^{2+} current (I_T) at more hyperpolarized membrane potentials. However, the burst of action potentials generated in RTN neurons displays longer duration and contains more spikes than those generated in TC cells (Fuentealba and Steriade 2005).

Based on their previous work (Adamantidis, Zhang et al. 2007; Jego, Glasgow et al. 2013), Adamantidis and colleagues identified LH_{Vgat} monosynaptic projections to the RTN, both to the anterior and posterior parts. These connections were confirmed using ChR2-assisted circuit mapping and retrograde tracing experiments (Herrera, Carus Cadavieco et al. 2016).

1.6 Circuits involved in control of feeding

Feeding is a multifaceted behavior that goes beyond the act of swallowing food, it requires a long, complex behavioral sequence that relies on hierarchical processes which integrate motivation, reward, memory, current emotional state, and which are influenced and triggered by the metabolic needs (Schneider, Wise et al. 2013; Berland, Cansell et al. 2016; Korotkova and Ponomarenko 2017). The correct performance of these behaviors determines the survival of the individual, given that eating too much, not enough or at the wrong moment can have very negative consequences. Therefore it requires a precise regulation that depends on short-term feedback from the gut, long-term feedback from the adipose tissue and by environmental cues that can promote feeding, according to the availability of food (Andermann and Lowell 2017).

Therefore its regulation can be studied from different points of view, and to date is not fully understood how all the neuronal circuits, metabolic and hormonal signals interact to correctly control food intake.

1.6.1 Intrahypothalamic regulation of energy balance

As revised in sections 1.1.2 and 1.2, different neuronal populations from several hypothalamic nuclei, including the lateral hypothalamus, are responsible for regulating food intake and maintaining homeostasis. The melanocortin system in the arcuate nucleus of the hypothalamus and its circuitry is important for regulating food intake

according to the energy balance (Waterson and Horvath 2015). The arcuate nucleus contains neurons that express Pro-opiomelanocortin (POMC neurons), and also co-express cocaine- and amphetamine-related transcripts (CART), together with neurons that co-express NPY and agouti-related protein (AgRP neurons) (Waterson and Horvath 2015). Several studies including neuronal ablation (Luquet, Perez et al. 2005) and optogenetic manipulations (Aponte, Atasoy et al. 2011; Atasoy, Betley et al. 2012) have established the general notion that POMC neurons decrease food intake, while AgRP cells promote feeding. Both AgRP/NPY and POMC neurons express receptors that bind the hormones leptin (satiety signal) and ghrelin, which is produced in the gastrointestinal tract and constitutes a hunger signal. Thus, these cells from the arcuate nucleus are proposed to be 'first order' neurons, responsible for energy-sensing (Morton, Meek et al. 2014; Herrera, Ponomarenko et al. 2017). Leptin stimulates POMC neurons and inhibits the activity of AgRP/NPY neurons, leading to a decrease in food intake, while ghrelin activates AgRP/NPY cells, and inhibits POMC neurons (Morton, Meek et al. 2014; Waterson and Horvath 2015). In addition, AgRP/NPY neurons are able of directly inhibiting POMC cells themselves, by the release of NPY and GABA (Waterson and Horvath 2015). 'First order' neurons project to 'second order' neurons in the paraventricular nucleus (PVN) and in the LH, the latter include Hcrt/Orx, MCH, Neurotensin, LH_{GABA}, LH_{Glu}. Within LH, cues from the environment as well as rewarding/hedonic signals from extrahypothalamic afferents are integrated, together with the homeostatic component of the initial signal coming from the 'first order' neurons, leading to a coordinated directed behavioral response reviewed in (Morton, Meek et al. 2014; Herrera, Ponomarenko et al. 2017). It is important to mention that 'second order' LH neurons have sensing capacity as well, which may enable them to overcome the metabolic control from the arcuate nucleus (Herrera, Ponomarenko et al. 2017).

1.6.2 Extrahypothalamic regulation

In the caudal hindbrain, the nucleus of the solitary tract (NTS) receives inputs from the gut through afferent fibers of the vagus nerve. Internal satiety signals are conveyed there, such as leptin, cholecystokinin (CCK) and GLP1, the last two being secreted from the gastrointestinal tract in response to food ingestion (Morton, Meek et al. 2014). Neural signals generated by gastric distension are transmitted there too. The NTS also receives projections from hypothalamic nuclei: the PVN, the arcuate nucleus and the LH. The interaction of satiety signals in the NTS promotes the termination of a meal, and this response is especially amplified by the action of leptin, directly in the NTS and indirectly in hypothalamic nuclei (Morton, Meek et al. 2014).

The palatability of food is a crucial determinant for the decision of whether to eat or not, even if there is no current nutritional need. The hedonic aspects of feeding are processed through interactions with the hypothalamus and brain circuits that integrate information related to reward. These reward circuits include mesolimbic dopaminergic neurons in the ventral tegmental area (VTA), that project to the nucleus accumbens (NAc) and other forebrain areas (Morton, Meek et al. 2014; Korotkova and Ponomarenko 2017). The NAc sends inputs to the LH, and, in turn, neuronal populations from LH project to the VTA, where they modulate the activity of dopaminergic neurons (Nieh, Vander Weele et al. 2016; Korotkova and Ponomarenko 2017). Thus, due to its intra- and extra-hypothalamic connections, LH is proposed to integrate reward-related inputs with homeostatic and metabolic signals (Morton, Meek et al. 2014). It should be noted that hunger, food deprivation or caloric deficiency change the perception of the hedonic value of the food within the central nervous system (CNS), increasing its rewarding properties (Andermann and Lowell 2017; Cassidy and Tong 2017).

As described in section 1.2.1 the bed nucleus of the stria terminalis (BNST), a region known to regulate several components of anxiety (Kim, Adhikari et al. 2013), sends inhibitory projections onto the Vglut2-expressing LH neurons. Activation of this pathway increases feeding behavior (Jennings, Rizzi et al. 2013).

1.6.3 Appetitive and consummatory aspects of feeding

Most of the innate behaviors, including feeding, involve the realization of a complex sequence of actions. These responses were historically classified in appetitive or precurrent and consummatory (Sherrington 1906; Craig 1917). Appetitive behaviors bring individuals closer to their goals (e.g. food or a potential partner), they are partially separable in time and space from consummatory behaviors, and can provide a visible expression of the internal motivation (Schneider, Wise et al. 2013). The consummatory phase follows only when the goal is actually acquired, and normally involves stereotyped and species-typical pattern of movements, which result in the termination of the whole behavioral sequence (Berridge 2004; Ball and Balthazart 2008). Though in the present study this classification can be applied to ingestive behavior (which involves consumption of food), it should be noted that the word consummatory does not refer to consumption, but rather to consummation. Hence is also applied to other non-ingestive innate behaviors, like mating or aggression (Berridge 2004). Appetitive behaviors constitute the more variable, searching phase of the behavioral sequence, and some appetitive ingestive behaviors ensure that nutrients might be available during possible future energetic challenges, in the form of a food hoard (Schneider, Wise et al. 2013).

This appetitive-consummatory dichotomy is important because different aspects of ingestive behavior are controlled by different neural circuits, through different chemical transmitters, although their precise distinction at the neural level is not fully elucidated yet. One obvious example is that consummatory, but not appetitive, aspects of ingestive behavior are regulated in the caudal hindbrain; metabolic control of food intake remains unaltered in chronic decerebrate animals, although they do not approach a food location (reviewed in (Schneider, Wise et al. 2013).

This division of innate behaviors in appetitive and consummatory sometime has been criticised during the past decades (Sachs 2007), because the transition between the two categories is not always clear. However, this classification provides a substrate of behavioral organization for many goal-directed behavioral systems (Ball and Balthazart 2008).

1.7 Neuronal coding

As reviewed in the previous sections, different neuronal populations release diverse transmitters, which in turn will induce changes in the excitability of their target neurons that can lead to the generation of action potentials/spikes. Therefore, from a basic point of view, the brain uses a combination of chemical (neurotransmitters/neuropeptides) and electrical signalling to transmit information between different regions and elicit diverse behavioral responses (Schone and Burdakov 2012).

1.7.1 Rate code

The frequency at which action potentials are generated is defined as firing rate, neurons increase or decrease their firing rate, thus regulating release of neurotransmitters/neuropeptides. It has been described that firing at regular rates releases classical neurotransmitters, such as GABA or glutamate, whereas spiking of the same neurons at high firing rates or bursting can lead to the release of neuropeptides, (Leng and Ludwig 2008; van den Pol 2012), which can promote a different response in the downstream circuit. Hence, this constitutes information encoding based on the firing rate. Further, it is has been shown that hippocampal pyramidal cells exhibit spatial rate coding, increasing their firing rate in a particular location of the environment (the place field) (O'Keefe 1976).

1.7.2 Temporal code

Temporal code is provided by network oscillations, and can occur at many time scales (Buzsaki 2006). Different spikes can have a different phase relationship to the current

cycle of the ongoing oscillation. Both coding mechanisms are not exclusive, and can be separable. It has been shown that same hippocampal neurons can encode the animal's position within the place field based on their time of firing relative to the concurrent cycle of the hippocampal theta oscillation (temporal coding) and encode the animal's speed of movement within the place field based on their firing rate (rate code) (Huxter, Burgess et al. 2003).
Further implications of temporal coding are described in section 1.8.2.

1.8 Network oscillations

Brain oscillations are periodic fluctuations of electrical activity that reflect underlying synchronization between groups of neurons, and are a common hallmark of many neuronal networks (Contreras and Steriade 1995; Buzsaki 2006). Coherent variations in the membrane potential of neurons result in an extracellular current that can be measured by electrical recordings, intracranially in specific brain regions or from the brain scalp (like the EEG) (Buzsaki and Watson 2012). Neuronal networks in the forebrain exhibit oscillations in multiple frequency bands, spanning from 0.05 Hz to 500 Hz, which are very preserved across vertebrate taxons (Buzsaki and Watson 2012; Shein-Idelson, Ondracek et al. 2016). The better studied oscillatory activities, in humans and in rodents, are classified according to the following frequency bands: delta (0.5-4 Hz), theta (5-10 Hz), gamma (30-140 Hz) and high-frequency (>140 Hz) 'ripples' in hippocampus (Buzsaki and Draguhn 2004).
Although the precise mechanism that generates oscillations at different frequencies varies depending on the properties and connections of the underlying neural circuit, the majority of brain rhythms are inhibition-based. In short, opposing forces and positive feedback are required for a system to oscillate. If the system lacks the feedback, it could only maintain a transient oscillation, due to the opposing forces, but its amplitude would decrease. This phenomenon is called resonance. Voltage-gated ion channel with opposite properties (see next sections for example) depolarize and hyperpolarize the membrane of single neurons, enabling them to oscillate. Different combinations and distributions of ion channels in different neuronal types provide them with diverse oscillatory and resonance properties, and neuronal networks preferentially treat inputs, frequency of which matches their own resonance (Buzsaki 2006). It has been proposed then that 'pacemaker' neurons, endowed with intrinsic oscillatory activity, are connected and send inputs to a population with specific resonant characteristics, which in turn may provide feedback, and thus rhythmicity arises (Contreras and Steriade 1995). However, this particular "pacemaker" model can be difficult to generalize for the different networks

and rhythms, particularly fast oscillations normally do not have pacemakers, although the feedback remains essential for their generation (Buzsaki and Wang 2012).
In the next sections, the oscillatory activities of relevance for this study are reviewed.

1.8.1 Oscillatory patterns of sleep

Spindles

Sleep spindles are one of the defining features that can be observed in the EEG of the early stages of NREM sleep. Spindles are waxing and waning waves, at frequencies of 7-15 Hz, that recur periodically, usually every 2-5 seconds (Fuentealba and Steriade 2005). Experimental evidence supports the idea that spindles are generated in the GABAergic reticular and perigeniculate nuclei of the thalamus. During early NREM sleep, monoaminergic excitatory inputs from the brainstem to the RTN are slowly withdrawn, which allows the activation of the low-threshold T-type Ca2+ channels and the generation of burst firing at resting membrane potential (Brown, Basheer et al. 2012). These bursts from the GABAergic RTN neurons at spindle frequencies lead to inhibitory postsynaptic potentials (IPSPs) in TC relay cells, hyperpolarizing their membrane, which activates their T-type Ca2+ channel ($Ca_V3.1$) (I_T current). Calcium enters the neuron, which results in a low-threshold Ca2+ spike crowned by a burst of Na+ dependent action potentials. Because TC relay neurons are glutamatergic, their bursts lead to EPSPs and to action potentials in cortical neurons, which together constitute the spindle recorded in the EEG (reviewed in (Brown, Basheer et al. 2012). Spindles are synchronized within the RTN via recurrent inhibitory and electrical synaptic connections between RTN neurons, but experiments following decortication showed that for a widespread synchrony of spindles over the thalamus and cortex the intact cortex is required (Fuentealba and Steriade 2005). Spindles decline during deeper stages of NREM sleep, due to the high hyperpolarization of the TC neurons, which favours the generation of slower rhythms (see next section). The density of sleep spindles is correlated with memory performance and general intelligence of an individual, and their occurrence and duration is enhanced after learning, and reduced as the individual ages. Therefore, a precise regulation of spindle density and duration is essential for a proper brain function (Bartho, Slezia et al. 2014).

Delta oscillations (1-4 Hz) and slow-wave activity

Delta oscillations in the cortex and thalamus are typical during deep NREM sleep stages, and can be recorded in the EEG. As NREM sleep deepens, the withdrawal of excitatory cholinergic and monoaminergic inputs from the brainstem to the TC rely cells is increased, which results in a very hyperpolarized membrane potential. This high level of

hyperpolarization inactivates the I_T current, but leads to the activation of a cationic current I_H. This slowly activating current depolarizes the membrane towards the threshold of the action potential. Once the membrane reaches less negative potentials, the I_T becomes active again, which results in a low-threshold Ca^{2+} spike and a burst of action potentials. These bursts from TC cells lead to prominent burst firing in large numbers of CT neurons, which provide excitation through axon collaterals to the RTN neurons. In turn, the activation of RTN neurons leads to rhythmic hyperpolarization of TC cells, creating increased network synchronization and re-starting the cycle. Thus, the capability of TC neurons to burst within the delta frequency range, is due to their intrinsic membrane properties, resulting from the interaction between the I_H and the LTS Ca^{2+} spike, the I_H is the major contributor to the interburst interval reviewed in (Brown, Basheer et al. 2012). Another consequence of TC cells voltage-gated conductances, is that their membrane potentials determine which rhythmic activity will be transmitted to the cortex. During sleep spindles their membrane potentials are between -55 mV and -65 mV, while during delta waves they display potentials between -68 mV and -90 mV. Therefore, the progressive hyperpolarization of TC neurons during the course of sleep explains the predominance of sleep spindles in the early stages, and delta oscillations in the deep stages (Nunez, Curro Dossi et al. 1992).

The power of the delta band within the high voltage slow-wave activity (SWA), is considered to be a hallmark of sleep homeostasis, reflecting the intensity of NREM sleep (de Andres, Garzon et al. 2011; Brown, Basheer et al. 2012). SWA (0.5-4 Hz) in the EEG reflects the slow (<1 Hz) oscillations and delta oscillations during NREM sleep. The slow oscillation is a phenomenon, discovered by Steriade and colleagues (Steriade, Contreras et al. 1993), which is generated in the cortex, although it strongly influences the thalamus through corticothalamic connexions, and can be observed in the TC and RTN neurons as well. It is composed of prolonged depolarizations (UP states), close to the spike threshold, separated by prolonged hyperpolarizations (DOWN states) in the membrane potential of pyramidal cortical neurons (Buzsaki 2006; Brown, Basheer et al. 2012). The UP state is due to excitatory synaptic inputs, and is associated with extracellular gamma frequency activity. Fast inhibitory potentials also occur simultaneously during the UP state due to GABAergic input from interneurons that are activated by the firing of the glutamatergic pyramidal neurons. The DOWN state corresponds to the phase where cortical neurons become silent, due to the withdrawal of excitatory inputs. The slow oscillation occurs throughout all NREM sleep stages, and in fact binds together the other electrographic signs of NREM sleep, such as sleep spindles and the delta waves. The cortical depolarization during the UP state can, through the excitatory axon collaterals of the CT cells, activate the RTN neurons which

fire then bursts at the spindle frequency. The combination of one cycle of the slow oscillation followed by a sleep spindle, constitutes the so-called K-complex, and can be observed in the EEG during early NREM sleep in humans (de Andres, Garzon et al. 2011; Brown, Basheer et al. 2012). The K complexes can be spontaneously triggered by sensory stimuli that activate cortical neurons, and could serve as a mechanism of 'protection' of sleep continuity. If the UP shift neurons can bring about enough depolarization in cortical neurons, transient gamma oscillatory activity may be evoked instead of a spindle. These transient gamma-frequency events during sleep constitute the clinically described 'microarousals' (Buzsaki 2006).

The SWA is increased during sleep epochs that follow sleep deprivation in both animals and humans; and it is highest at the start of the sleep period, displaying a progressive decrease during the ongoing sleep (Brown, Basheer et al. 2012). Further, experimental work has shown that delta power within SWA reflects the duration of the prior wakefulness independently of the circadian time, and it can be particularly increased in the cortical areas that have been more active during the day (revised in (de Andres, Garzon et al. 2011).

1.8.2 Gamma oscillations

Gamma oscillations comprise rhythmic events in brain networks in the 30-120 Hz band (although the precise frequency band that corresponds to gamma oscillations is still a matter of opinion, the upper limit can be also defined as 140 Hz) (Colgin, Denninger et al. 2009; Buzsaki and Wang 2012; Sohal 2016). Gamma frequency rhythms can be observed throughout the cerebral cortex under a wide range of conditions, which are normally related to the cortex 'being active', and in fact are one of the prominent features of the EEG during wakefulness (Brown, Basheer et al. 2012; Sohal 2016). Gamma oscillations can be observed at multiple spatial scales in electrical recordings. The lowest levels at which gamma oscillatory activity can be detected are in subthreshold fluctuations within intracellular recordings and the firing pattern of neurons (in single- or multi-unit recordings) - a spiking discharge pattern that repeats every 10-30 ms. The latter can be easily characterized by simple analysis methods such as auto- and cross-correlograms (Jensen, Kaiser et al. 2007; Sohal 2016). Gamma frequency rhythms are also observed as a periodic fluctuation of the ongoing intracranially recorded extracellular LFP.

It is well established that gamma oscillations are based on the rhythmic firing of inhibitory interneurons (Cardin, Carlen et al. 2009; Buzsaki and Wang 2012; Sohal 2016). The mechanisms that generate gamma oscillations are proposed to reflect the interactions between excitatory and inhibitory neurons (E-I model) or the interactions between

inhibitory neurons themselves (I-I model) (Buhl, Halasy et al. 1994; Whittington, Traub et al. 1995; Traub, Whittington et al. 1996; Ermentrout and Kopell 1998; Borgers and Kopell 2003; Buzsaki and Wang 2012; Sohal 2016). In the E-I model, firing of excitatory neurons triggers the synchronized spiking of many inhibitory interneurons, which provides feedback inhibition, transiently silencing the excitatory neurons. When this inhibition declines, the excitatory neurons fire again, starting a new cycle, thus leading to coherent oscillations in the gamma range (Buzsaki and Wang 2012; Sohal 2016). In the I-I model, subsets of interneurons start discharging together, leading to generation of synchronous IPSPs in the partner neurons. The duration of the IPSP is determined by the subunit composition of the $GABA_A$ receptor, and when the $GABA_A$ receptor-mediated hyperpolarization declines in the inhibited neuron, the cell can discharge again, re-starting the cycle. Therefore, in the I-I model the frequency of the gamma oscillation is determined mainly by the kinetics of the IPSPs and the net excitation of interneurons (Buzsaki and Wang 2012). It remains unclear to which extent both models cooperate or compete in the brain to generate gamma frequency oscillations (Buzsaki and Wang 2012; Sohal 2016).

From a functional point of view, synchronization in the gamma frequency band provides an important mechanism for neuronal communication (Gray and Singer 1989; Fries, Nikolic et al. 2007; Jensen, Kaiser et al. 2007; Buzsaki and Wang 2012; Sohal 2016). If the firing of a group of neurons is synchronized, their spikes are coincident, which enables the postsynaptic potentials to integrate, and therefore their impact on the receiving neuron increases. In particular, oscillations at gamma frequency allow synchronizing inputs with high temporal precision, relative to the course of postsynaptic potentials (PSPs). The duration of an excitatory postsynaptic potential is approximately 10 ms, which defines the timeframe of temporal integration. Since gamma oscillations have a period of 10-30 ms, they provide ‘tighter’ synchronization than oscillations in lower frequency bands (Jensen, Kaiser et al. 2007).

Despite gamma oscillations typically emerge locally, they can be synchronized across long distances, in ways that correlate with behavior and successful encoding of information (Buzsaki and Wang 2012; Sohal 2016).

It’s proposed that gamma oscillations can dynamically and transiently organize cell assemblies, i.e. neuronal partnerships, which are processing related information, both from external sensory input and internal cognitive processes (Singer 1993; Harris, Csicsvari et al. 2003). Gamma oscillations are typically observed in the presence of sensory stimulation (Gray and Singer 1989), and provide temporal binding to neurons that code for the same sensory representation, thus organizing functional assemblies of neurons through distributed sensorimotor networks (Singer 1993; Engel, Fries et al.

2001). Neurons that participate in the same assembly should fire in temporal synchrony on a millisecond timescale, making their responses clearly demarcated from those participating in a different assembly (Singer 1993; Engel, Fries et al. 2001). This temporal mechanism provides the advantage that various assemblies can be simultaneously active in the same area, and even if at a lower (sec) time scale the activity of neurons overlap, they remain recognizable as constituents of a particular assembly without becoming confused with the others, given that their responses are correlated at a millisecond timescale (Singer 1993). Further, this temporal binding mechanism can provide coordination between neuronal networks that are more distant, integrating information from specialized processing areas, which are anatomically separated (Engel, Fries et al. 2001).

Further, gamma oscillations are implicated in cognitive processing: recent studies have shown that the power of gamma oscillations is increased in frontal regions during working memory tasks (Yamamoto, Suh et al. 2014), gamma oscillations can constitute a physiological mechanism for directed attention (Kim, Ahrlund-Richter et al. 2016), and gamma frequency activity of prefrontal interneurons mediate cognitive flexibility (Cho, Hoch et al. 2015).

1.8.3 Alterations of network oscillations

Alterations in brain oscillations can be observed in the majority of psychiatric diseases and, in some cases, perturbations of network rhythmicity by itself can trigger symptoms of pathology (Buzsaki and Watson 2012). For example, in absence epilepsy the thalamocortical network generates hypersynchronous discharges that are associated with the absence seizures (Huguenard and McCormick 2007). Increasing number of recent studies also report perturbations in gamma oscillations in patients with schizophrenia, including decreased gamma power and altered gamma synchronization also across hemispheres (Maharajh, Teale et al. 2010; Mulert, Kirsch et al. 2012). Reduced gamma synchronization has been observed in patients with Alzheimer's disease (AD), and consequently several mouse models of AD exhibit a reduction in gamma power (Stam, van Cappellen van Walsum et al. 2002; Palop, Chin et al. 2007). Interestingly, a recent study showed that entrainment of gamma rhythms using optogenetics and non-invasive light flashes decreased the amyloid load associated with AD and modified glial responses (Iaccarino, Singer et al. 2016).

Brain oscillations can constitute a measurable phenotype, recordings from different individuals during sleep or active tasks are a way of characterizing neurological and mental disorders from the point of view of brain activity since they can reflect abnormal functioning of the network. Hence, these alterations are often referred to as

‘rhythmopathies’, ‘oscillopathies’ or ‘dysrhythmias’ (Buzsaki and Watson 2012). Different psychotropic drugs can selectively and differentially affect network dynamics (Agid, Buzsaki et al. 2007), therefore making their pharmacological profiles useful for early screening and diagnosis (Buzsaki and Watson 2012). Further, while pharmacological agents induce diverse responses across several measures between humans and animal models, the induced modifications of network oscillations are identical in all mammalian species (Buzsaki and Watson 2012).

Therefore, understanding how network rhythms coordinate neuronal groups across brain structures to regulate behavior in healthy conditions can provide valuable information about mechanisms that lead to pathological conditions.

1.9 In vivo electrophysiology

Technical progress through the last decades has enable the development of numerous recording methods that acquire brain electrical signals with high temporal resolution. As a result of neuronal activity, changes in transmembrane currents take place generating and electric field, and this can be measured by extracellular electrodes with millisecond time resolution (Buzsaki, Anastassiou et al. 2012). This can provide very useful information to analyze communication between neurons. Thus, the recorded local field potential (LFP) represents the summation of various overlapping fields produced by current sources (from the intracellular space to the extracellular space) and sinks (from the extracellular space to the intracellular), happening in the proximity of the implanted extracellular electrode. The properties of the LFP waveform, such as frequency and amplitude, can vary and depend on characteristics of the tissue and on the relative contribution of the multiple current sources (Buzsaki 2006; Buzsaki, Anastassiou et al. 2012).

Neurons generate action potentials that cause large transmembrane potentials in the proximity of the cell body, therefore they can also be measured extracellularly, e.g. by extracellular glass pipettes, single etched (sharp) electrodes, or multiple-site probes. This is known as ‘unit’ or ‘spike’ activity. The size of extracellularly recorded spikes depends on the proximity of the electrode to the soma of the neuron (Harris, Henze et al. 2000; Buzsaki 2006). Neurons of the same type generate essentially identical action potentials, which in principle can make difficult the task of identifying a given neuron from the total of extracellularly recorded spikes. However positioning the electrode tip closer to a given neuron body than to any other cell enables recording a much larger spike from the closest neuron, relative to the spikes generated by more distant cells, which should be sufficient to monitor the output of a single neuron (Buzsaki 2006). The development

of silicon-based electrodes enabled high density recordings while minimizing tissue injury. Further, multishank silicon probes recording sites are geometrically distributed in such a precise way that it is possible to determine the activity from isolated single neurons (Csicsvari, Henze et al. 2003; Buzsaki 2006).

1.10 Optogenetics

Optogenetics is a recently developed technique, which, as its name indicates, combines genetic and optical methods to precisely manipulate the activity of specific cell types of living tissue (for example, neurons) in behaving animals (Yizhar, Fenno et al. 2011; Deisseroth 2015). This technology employs light-sensitive membrane proteins that are present in microbial organisms, such as algae and archaebacteria, called opsins, which in response to light transport ions into the cells, thus eliciting electrical currents across the cellular membranes (Oesterhelt and Stoeckenius 1971; Oesterhelt and Stoeckenius 1973; Matsuno-Yagi and Mukohata 1977; Hegemann, Oesterbelt et al. 1985; Harz and Hegemann 1991; Nagel, Ollig et al. 2002; Deisseroth 2015).

Opsins are in fact present not only in microbial organisms, but also through all kingdoms of life, participating in a wide range of functions. The structure of the opsin protein consists of 7 transmembrane α-helices that form an internal pocket; in which retinal, a vitamin A-related light absorbing chromophore, needs to be covalently bound in order to confer them light sensitivity (Spudich, Yang et al. 2000; Yizhar, Fenno et al. 2011; Zhang, Vierock et al. 2011; Ernst, Lodowski et al. 2014). This opsin-retinal complex is designated as rhodopsin. Absorption of a photon leads to isomerization of the retinal chromophore, inducing a series of structural changes, which can promote ion transport, channel opening, or interaction with signaling transducer proteins (Zhang, Vierock et al. 2011). Rhodopsins can be divided in two classes, in agreement with the classification of opsin genes in two superfamilies (Spudich, Yang et al. 2000). Microbial opsins or type I opsins, are found in prokaryotes, algae and fungi, where they control diverse functions (energy storage, phototaxis, retinal biosynthesis). Animal opsins or type II opsins, are G-protein coupled receptors found in eukaryotes, where they are primarily responsible for vision. Despite the fact that both opsin gene families encode for 7 transmembrane helices structures, there is barely sequence homology between the two superfamilies. There is however a high degree of sequence similarity within the families. Type I rhodopsins bind the all-*trans* isomer of retinal, while type II rhodopsins bind to the 11-*cis* isomer of retinal (reviewed in Zhang, Vierock et al. 2011).

The development of optogenetics over the last decades enabled the readout of the activity of genetically defined neuronal populations, as well as of the behavioral outcome

associated with the activation/inhibition of these populations (Carter and de Lecea 2011; Tye and Deisseroth 2012; Korotkova and Ponomarenko 2017). Prior to the development and establishment of this tool, classical stimulation methods (electrical or magnetic stimulation) were used to activate neural circuits. Electrical currents applied to neurons lead to the depolarization of their membrane, opening of voltage-gated sodium channels and consequent generation of action potential. Similarly, application of a transcranial magnetic field induces electrical currents in the tissue, leading to spike firing (reviewed in (Rajasethupathy, Ferenczi et al. 2016). Both of these methods allowed regional targeting, and led to important discoveries regarding behavioral outcomes associated with activation of a particular area. However they lacked neuronal specificity since all the neurons within the receiving area would respond to the stimulation, without cell-type specific discrimination.

In the late 1970s Francis Crick noted that a major challenge facing neuroscience was the need to precisely control activity in one neuronal type, while leaving the others unaltered. He later suggested in lectures that light would be the ideal control tool, although he did not specify how this could be achieved (reviewed in Yizhar, Fenno et al. 2011; Deisseroth and Hegemann 2017). Pioneer work in making neurons sensitive to light was performed by Zemelman and colleagues. They expressed components of photoreceptors from *Drosophila*'s eye in genetically designated neurons, enabling them to fire action potentials in response to light (Zemelman, Lee et al. 2002). This approach was denominated multicomponent, because it requires the presence of a cascade of proteins, to generate light-sensitive responses. A caveat of this method was that its multicomponent nature, contributed to difficulties in targeting the neurons, and there was some delay in the response of the cells to light (Yizhar, Fenno et al. 2011).

Currently, most optogenetic tools are based on the use of microbial rhodopsin proteins (type I opsins), which represent a single-component approach, since one single protein is able of both detecting light and generating an ion flow reviewed in (Yizhar, Fenno et al. 2011). Type I opsins use the all-trans isomer of retinal, which as a result of photon absorption isomerizes to the 13-cis configuration. The activated retinal molecule remains associated with its opsin partner and thermally reverts to the all-trans configuration. Because this reversible reaction occurs rapidly, it allows the use of microbial rhodopsins as optogenetic tools, enabling modulation of neuronal activity at high frequencies (Zhang, Vierock et al. 2011). From this family of molecules, three members have found use in optogenetics: the bacteriorhodopsins, the halorhodopsins and the channelrhodopsins reviewed in (Deisseroth 2015).

Bacteriorhodopsin (BR), which is a haloarchaeal proton pump, was the first discovered opsin, described in (Oesterhelt and Stoeckenius 1971; Oesterhelt and Stoeckenius

1973). Under low-oxygen conditions, bacteriorhodopsin is highly expressed in the cell membrane, where it pumps protons from the cytoplasm to the extracellular medium, to generate a proton-motive force to drive ATP synthesis (reviewed in (Yizhar, Fenno et al. 2011). Halorhodopsin (HR), is a light-driven chloride pump, and it was first discovered (Matsuno-Yagi and Mukohata 1977) and characterized (Hegemann, Oesterbelt et al. 1985) in archaebacteria. Halorhodopsin pumps chloride ions from the extracellular medium to the inside of the cell. The family was soon expanded by the identification of a halorhodopsin from Natromonas pharaonis (NpHR) (Lanyi and Oesterhelt 1982), action spectrum of which displays a maximum at ~580 nm (Zhang, Wang et al. 2007). Channelrhodopsin (ChR) is a light-gated channel that was identified in the green algae Chlamydomonas reinhardtii (ChR1) (Nagel, Ollig et al. 2002). Unlike BR and HR, in response to light channelrhodopsin opens an effective cation channel pore in the membrane, instead of pumping one ion at a time. This implies that the ion flux depends then on the kinetics of the channel closure, rather than on the retinal isomerization. A second ChR, channelrhodopsin-2 (ChR2) was later characterized from the same organism (Nagel, Szellas et al. 2003) and soon used to control neural excitability (Li, Gutierrez et al. 2005). Like ChR1, ChR2 also conducts cations (monovalent and divalent), and both ChRs have fast on and off kinetics, although ChR2 is expressed at higher levels than ChR1 in mammalian systems (Zhang, Vierock et al. 2011). The action spectrum of ChR2 displays a maximum at ~460 nm (Nagel, Szellas et al. 2003; Ernst, Lodowski et al. 2014).
In the next sections the opsins used in this study are described.

1.10.1 ChETA

ChETA is an engineered channelrhodopsin with ultrafast kinectics, designed and validated in (Gunaydin, Yizhar et al. 2010), which allows ultrafast neuronal excitation.
Wild-type ChR2 displays a deactivation time constant of ~10 ms after switching the light off, and thus can efficiently drive neuronal firing up to 40-50 Hz. However the ChRs were not shown to evoke reliable spiking at high rates, and many neuronal types (e.g. fast inhibitory neurons) and physiological processes (like gamma rhythms) implicate, or require high frequency spike trains (>40 Hz) (Gunaydin, Yizhar et al. 2010; Yizhar, Fenno et al. 2011; Deisseroth and Hegemann 2017). In addition extra spikes (e.g. spike doublets) can be generated in response to a single light pulse, when ChR2 is expressed at high levels (this effect was also initially reported at relatively lower expression levels), which can have potential implications in neuronal coding. Further, fast spike trains driven with ChR2 can result in plateau potentials of 10 mV or more, probably related to the interaction of ChR2 deactivation time constant with endogenous neuronal active

conductances. Plateau potentials can cause accidental up-states, which per se have intrinsic significance in information processing (Gunaydin, Yizhar et al. 2010). Therefore, due to the lack of precision in generating high-rate spikes, and to the possible creation of spurious signalling, the use of ChR2 may limit or obscure the study of certain neuronal codes (in the frequency domain above 40 Hz), with high temporal resolution techniques. Removal of the ChR2 residue glutamate (E) in the position 123, and its substitution by threonine or alanine(T/A) resulted in the acceleration of channel closure kinetics from 10 ms to 4 ms, which enables ultrafast optic control of spiking, up to 200 Hz (Gunaydin, Yizhar et al. 2010). These fast kinetic mutants were designated as ChETA variants (from ChR2-E123T accelerated), category in which E123A and combinations with other modifications are also comprised (Gunaydin, Yizhar et al. 2010). The ChETA induced photocurrent is slightly smaller than wild-type ChR2 due to the faster deactivation, which can be compensated with more intense or longer pulses (Mattis, Tye et al. 2011; Zhang, Vierock et al. 2011). Besides optically induced precise fast spiking, ChETA also reduced the occurrence of extra spikes, along with reduced spurious prolonged depolarizations of the membrane. Thus, ChETA may not only be useful to target fast inhibitory neurons, but also can enhance the fidelity of the optogenetic response to the evoked neural codes in non fast spiking cells (Yizhar, Fenno et al. 2011).

1.10.2 eNpac

eNPAC2.0 is a bicistronic viral vector that encodes both for ChR2 and NpHR, allowing then for bidirectional optogenetic control in a particular neuron (Carus-Cadavieco, Gorbati et al. 2017). NpHR and ChR2 are compatible, in terms or requiring similar light powers for their functioning while having considerably separable action spectra (see previous sections). Hence they could be separately targeted into the same cells and tested together in cultured neurons as well as in vivo in Caenorhabditis elegans (Zhang, Wang et al. 2007). A first version of eNPAC was later described and validated in vitro in (Gradinaru 2010), in which eNpHR3.0 and ChR2 were combined into the same construct using the P2A linker (Ryan and Drew 1994; Gradinaru, Zhang et al. 2010). The version eNPAC2.0 used in the present study provides the advantage that the eYFP reporter is fused to ChR2, while NpHR is not fused to either eYFP or ChR2. This can potentially improve the NpHR membrane trafficking, given that NpHR-YFP expression can lead to the generation of intracellular blebs, arising from NpHR-YFP obstruction in the endoplasmic reticulum (Gradinaru, Thompson et al. 2008; Zhao, Cunha et al. 2008).

1.10.3 Strategies for targeting selective neuronal circuits

Currently, there are several strategies for in vivo delivery and targeting of the optogenetic tools, which can be combined in order to gain specificity (Yizhar, Fenno et al. 2011; Tye and Deisseroth 2012). A very widely used strategy is viral transduction, which provides relative speed and flexibility for experimental application, as well as potency associated with high gene copy number (Yizhar, Fenno et al. 2011). Although this approach initially limits opsin expression to the injection site (somatic expression), sufficient incubation time allows for anterograde trafficking of the protein, which in turn enables axonal expression of the opsins and, therefore, optogenetic manipulation of the downstream circuitry. The most commonly employed viral vectors are lentivirus (LV) and adeno-associated viruses (AAV) (Tye and Deisseroth 2012). AAV-based vectors display high stability during periods of 1-2 years, have low immunogenicity and provide the advantage of viral titers that result in larger volumes of transduced tissue, compared to LV. Further, it is rated with the Biosafety level 1 (BSL1) while LV require BSL2+ (Yizhar, Fenno et al. 2011). The recombinant AAV2 (rAAV2) vectors are among the most commonly used AAV vectors, which can be pseudotyped with several serotype packaging systems (e.g. rAAV2/2 or rAAV2/5, normally designated as AAV2 or AAV5 respectively) (Yizhar, Fenno et al. 2011). Other viruses such as rabies or herpes simplex viruses (HSVs) offer the possibility of retrograde targeting, however the level of toxicity associated with them is much higher.

The use of Cre-recombinase-driver lines (Nagy 2000; Vong, Ye et al. 2011) combined with the use of Cre-dependent opsin-expressing viral vectors considerably improves selective targeting of the neuronal population of interest. Further, it allows the expression of larger genes, given that the genome size, that can be contained in AAV-based vectors, is normally restricted to 4.7 kb (Yizhar, Fenno et al. 2011).

There are also several possibilities for delivering light to the desired neuronal population. Optic fibers can be used acutely, by implanting a cannula, which serves as a guide, in a target region, so a bare fiber, that is itself a patch cable, can be connected through it before each experimental session. This method enables the combination of pharmacological studies with optogenetics, since chemical agents can be delivered through the cannula in the same region where the neurons are optostimulated. However, this approach increases the risk of breaking the fibers in the guide cannula. Optic fibers can also be implanted chronically in the brain region of interest, and they can be connected to a patch cable outside the brain, normally through a ceramic ferrule, which considerably increases their durability across multiple experimental sessions (Tye and Deisseroth 2012). Although this method does not allow the use of pharmacological

agents, the increased durability makes it more suitable for its combination with high density electrophysiological recordings, which require a stable chronical implant. The combination of optogenetics and electrophysiology enables the identification of molecularly defined neuronal types, enabling the characterization of their activity in spontaneous recordings.

2 Project Aims

The lateral hypothalamus has been appointed through the last decades to play a key role in the regulation of innate behaviors. However, due to its anatomical location and complex reticular structure composed of a heterogenous neuronal populations, it has been difficult to investigate LH circuitry; especially from an electrophysiological point of view, with high temporal resolution and neuronal specificity. Furthermore, LH is highly interconnected with multiple brain regions, which reflects its importance in integrating a variety of behavioral states, and probably transitions between them. Interestingly, LH receives more inputs (direct and indirect) from telencephalic regions than other hypothalamic nuclei, suggesting a possible role in integrating more volitional and cognitive aspects of innate behaviors, a role which to the present date is not fully elucidated.

By combining high density electrophysiological recordings in behaving mice with optogenetics, this project had the following specific aims:

- Investigate patterns of activity of LH neurons, including molecularly defined and photoidentified LH_{Vgat} neurons, across sleep/wake states.
- Determine the role of LH_{Vgat} projections to the RTN on the signaling of RTN neurons, and the behavioral outcomes associated with optogenetic manipulations of this circuit across sleep/wake states.
- Characterize the activity of LH neurons, including molecularly defined LH_{Vgat} cells, during active locomotion and during different aspects of feeding behaviors, as a mouse freely explores a free-choice innate behaviors setup.
- Investigate neural oscillations in the LH and in the LS, their relationship with LH neuronal activity and their possible correlation with different innate behaviors.
- Determine the effect of optogenetic manipulation of LS-LH circuit on the signaling of LH neurons and the subsequent behavioral outcome.

3 Methods

3.1 Animals

Vgat-ires-Cre (Vong, Ye et al. 2011), Sst-Cre (Madisen, Zwingman et al. 2010) and C57BL/6 male mice, 10–25 weeks old, were used in this study. All mice were housed under standard conditions in the animal facility and kept on a 12 h light/dark cycle. All procedures were performed in accordance with national and international guidelines, and were approved by the local health authority (Landesamt für Gesundheit und Soziales, Berlin). All efforts were made to avoid or minimize pain, distress and discomfort of the experimental animals.

3.2 Strategies for probing functions of neuronal circuits

Injections were performed according to (Zhang et al 2010). Mice were anaesthetized with isoflurane (1.5 – 3% isoflurane in oxygen) via a gas vaporizer, and placed in a stereotaxic head frame (David Kopf Instruments). Animal's eyes were protected from drying using eye gel. The head was shaved and disinfected using ethanol solution. The skin was cut along the midline, so that bregma and lambda were exposed. The skull was then cleaned with NaCl solution and dried using an air puff. Bregma and lambda were aligned to the same dorsal-ventral (or Z) coordinates. Stereotaxic coordinates were relative from bregma and based on Paxinos and Franklin's mouse brain atlas (Paxinos 2013).

A 34-gauge beveled metal needle connected via a tube and a 5 µl Nanofil Hamilton Syringe with a microsyringe pump (PhD Ultra, Harvard Apparatus, Holliston, MA, USA) was used. The viral vector was withdrawn in the needle using the microsyringe pump; the needle was positioned then above the craniotomy and then slowly moved in the brain according to stereotaxic coordinates. The viruses were infused at a rate of 100-150 nl/min (depending on the viscosity of the viral construct). After the injection the needle was left for 10 min at the injection site to allow the virus to difuse within the targeted region, and then removed from the brain very slowly.

For manipulation of LH_{Vgat} cells, Vgat-Cre mice were injected billaterally in the LH (AP -1.5, ML±1, DV 5.4 mm) with 0.3 µl per injection site of AAV2/5-Ef1a-DIO-ChETA(E123T/H13R)-eYFP-WPRE-hGH (Penn Vector Core) or 0.3 µl per injection site of AAVdj-nEF-DIO-NpHR-TS-p2A-hChR2(H134R)-eYFP (eNPAC2.0, titre 6.1 × 1012vg ml−1) or 0.3 µ l per injection site of AAV2-EF1a-DIO-eYFP-WPRE-hGH (Penn Vector Core, titre 2 × 1012vg ml−1).

Sst-Cre mice were injected bilaterally in the LS (right: AP 0.38, ML 0.4, DV 3.0, 2.5 mm) with 0.125-0.25 µl per injection site of per injection site of AAV2/5-Ef1a-DIO-ChETA(E123T/H13R)-eYFP-WPRE-hGH, titre 1.75 × 1012vg ml−1(Penn Vector Core) or 0.2 µ l per injection site of AAVdj-nEF-DIO-NpHR-TS-p2A-hChR2(H134R)-eYFP (eNPAC2.0, titre 6.1 × 1012vg ml−1) or 0.125–0.2 µ l per injection site of AAV2-EF1a-DIO-eYFP-WPRE-hGH (Penn Vector Core, titre 2 × 1012vg ml−1).

3.3 Optic fibers

Preparation of optic fibers was adapted from (Zhang, Gradinaru et al. 2010; Ung and Arenkiel 2012). Multimode optic fiber of 100 µM-diameter (Thorlabs, Dachau, Germany) were used. A fiber stripping tool was used to remove the fiber cladding. Afterwards, the fiber core was cut using a diamond scribe. The bare fiber core was inserted into a ceramic stick ferrule (Precision Fiber Products, Milpitas, CA, USA), in a way that the edge of the fiber would protrude beyond the convex end of the ferrule. Cyanocrylate glue or epoxy resin were applied to both edges of the ferrule. After this had hardened, the convex end of the ferrule was polished using Aluminum Oxide Lapping (Polishing) Sheets (Thorlabs). In order to make the fibers more resistant within the implant, the base of the ferrules was protected by inserting them into the insulating support material of contact pin strips (Bürklin), and applying some glue and dental acrylic. This prevents separation of the ferrule from the fiber, after several connections and disconnections throughout experimental sessions. Final length of the fiber is adjusted according to the target brain region, using the diamond scribe.

For bilateral implantations of optic fibers in LH, the fibers were glued together, so that both fibers would be perfectly parallel, and the distance between their tips would be 2 mm. This approach shortened the surgery time and facilitated the implantation of bilateral fibers in deep brain structures (such as LH).

3.4 Implantations

3.4.1 Implantations of silicon probes

For silicon probes implantations only animals weighting at least 27 gr were used, to ensure fast recovery and unaltered behavior. The weight of the complete implant should not exceed 4 gr. A total of three Vgat-Cre mice, expressing ChETA in LH, were implanted with silicon probes in the RTN. Coordinates were set at AP. 1, ML 1.2, DV 3.9 mm, to implant the electrodes above RTN (Herrera, Carus Cadavieco et al. 2016), so that it could be gradually advanced to maximize yield of recorded units, and then moved to LH

(DV 5mm). Four holes were drilled in the skull and four miniature stainless-steel screws (Bilaney) were positioned in the skull. Copper wires were soldered to the screws above the cerebellum before the surgery, so they could be used as reference and ground electrodes (see Figure 3.1). In addition, at least one copper wire was soldered to one or both of the frontal screws, in order to collect cortical EEG signal. Muscles next to the cerebellum were carefully pushed aside, to avoid noise artefacts introduced by muscle movements in the recorded signal. Each screw was completely covered by dental acrylic, and then connected to the other screws with dental acrylic, so that a 'cement ring' was built on the skull (Korotkova and Ponomarenko 2017). Four sheets of copper mesh were fixed to the cement ring using dental acrylic and cyanoacrylate glue. This mesh protects the implant and serves as an electrical shield. A craniotomy slightly bigger than the size of the probe was performed and dura was carefully removed using a small forceps and/or miniature hooks. Saline was constantly applied to the brain surface to prevent drying. Probes were positioned above the craniotomy using a stereotaxic device (Kopf instruments) and gradually immersed into the brain in a slightly orthogonal fashion so that the first shank of the probe would enter at AP -1, and the fourth shank would enter the brain at AP -1.5 to get maximal coverage of the RTN and later LH neurons. This was done under continuous visual inspection using a surgical binocular (Zeiss) to prevent any bending of the shanks and to avoid blood vessels. A melted mixture of wax/paraffin oil (50/50) was applied to cover the craniotomy after implantation of the electrode. The microdrive legs were then cemented to the cement ring, taking care about leaving the screw of the microdrive free to turn, and avoiding any leaking of the dental acrylic onto the probe. The copper mesh sheets were elevated, soldered together at the corners and grounded to one of the ground screw wires. The connector of the silicon probe was cemented to the posterior sheet of the copper mesh. Likewise, the edges of the upper board of the microdrive were carefully cemented to the copper mesh, in order to provide more stability to the implant. Ground and reference wires of the probe were soldered to the wires of reference and ground screws. Those soldering points were covered with a small coat of varnish (Loctite) for tamper-proofing. A nanoconnector (pin male nano dual row conecor, Omnetics Connector Corporation, Minneapolis, USA) was attached from the outside to the posterior sheet of the copper mesh, using a small amount of dental acrylic. The EEG and EMG wires were then soldered to the pins of the nanoconnector, and several leyers of cement were applied on top of these connections. A thin layer of half-liquid dental acrylic followed by cyanoacrylate glue was applied from outside to the copper mesh sheets. Right after the implantation, the screw of the microdrive was turned

60' anticlockwise, causing the probe to move downwards, and confirming that the silicon probe can move freely.
Three Vgat-Cre mice expressing ChETA in LH were implanted with silicon probes in LH at coordinates AP − 1.6, ML 1, DV 4.7 mm, the procedure was performed as described above.
One Vgat-Cre mouse expressing ChETA in LS was implanted with a B64 silicon probe in LH, so that central shanks of the probe would target coordinates AP -1.6, ML -1.0, DV 4.70 mm, following the same procedure previously described (implantation and recordings of this mouse were performed together with Suzanne van der Veldt).
LS units from fig Figure 4.14 and Figure 4.18 were recorded from 3 mice implanted with CM32 linear probes in LS at coordinates LS: AP 0-0.5, ML 0.2-0.45, DV 2.3-3.4 mm (these recordings were performed by Natalia Denisova).

3.4.2 Implantations of wire arrays

A total of 3 C57BL/6 mice were implanted with wire arrays in LH at coordinates AP -1.50, ML 1.00, DV 5.00. The procedure followed was very similar to the one described in the previous section. For this implantation, only one wire is soldered to the ground screw (two, in the case that two wire arrays would be simultaneously implanted), and no reference wire is required. Since the craniotomy is smaller than for a silicon probe implantation, very little amount of wax or even none (if it's very small) is needed, and fixation of the electrode to the headset with dental acrylic can be done right afterwards. No copper mesh should be added to the headset.
Three Sst-Cre mice expressing ChETA in LS were implanted with a wire array in LH, at coordinates AP -1.50, ML 1.00, DV 5.00. An optic fiber was glued to this wire array before the implantation, so that its final position would be at coordinates AP -1.60, ML -1.00, DV 4.7. An optic fiber was implanted in these mice in LS: AP 0.5, ML 0.3, DV 2.7 (implantation and recordings of these mice were performed together with Suzanne van der Veldt).

3.4.3 Silicon probes and wire array co-implantations

From the total of 7 Vgat-Cre mice implanted with probes in LH, 2 of them had in addition wire arrays implanted in lateral septum (LS), for simultaneous recording of LS LFP together with LH units and LFP. These arrays were implanted at coordinates: AP 0.7, ML 0.38, DV 3.2 mm. One of these mice was recorded across sleep/wake cycle as well, hence the EEG and EMG wires were soldered to free pins of the frontal wire array.
After completion of implantations, wounds were sued and lidocaine was applied onto wound edges. An antibiotic (erythromycin) and a painkiller (Carprofen), were injected

daily 3 days after the surgery. Weight was controlled daily during the first week after surgery. Wet food and condensed milk facilitated mice's recovery.

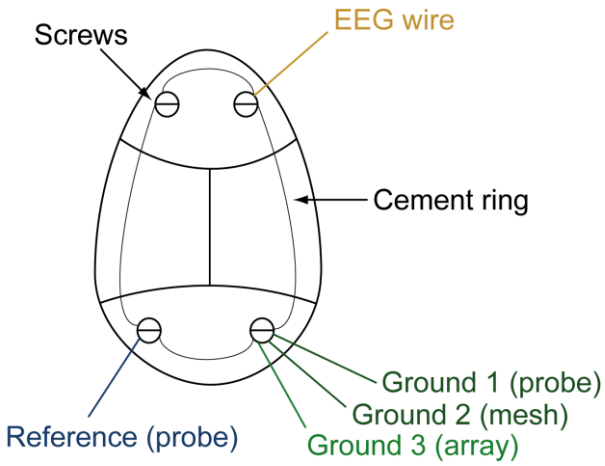

Figure 3.1 Scheme of headset connections for silicon probe and wire array co-implantations

3.4.4 Optic fibers implantations

These were performed following the same procedure previously described. For optogenetic manipulations of LH_{Vgat} projections in the RTN within silicon probe preparations, single optic fibers were implanted above this nucleus with an angle, following coordinates AP −0.8, ML 3, DV 3.4 mm, α 28° (3 mice). For somatic optogenetic stimulation of LH_{Vgat} neurons within silicon probe preparations, a single optic fiber was implanted with an angle in the LH at coordinates AP .80, ML -1.00, DV 5.00 mm, α 22° (7 mice). For optogenetic stimulation or optogenetic inhibition in the LH (optegenetic manipulation of LS_{Sst}-LH or LH_{Vgat}), optic fibers were bilaterally implanted above LH at coordinates AP − 1.6, ML 1, DV 4.8 mm (28 mice). For somatic stimulation of LS_{Sst} neurons, optic fibers were implanted unilateraly in the LS at coordinates AP 0.5, ML 0.3, DV 2.7 mm in 6 mice (these mice were implanted and recorded together with Suzanne van der Veldt).

3.5 Behavioral setups

Innate behaviors setup

A custom-built enclosure (30x50x20 cm), similar to that described previously (Jennings, Rizzi et al. 2013) consisted of two interconnected chambers, which contained food and water in designated areas, each zone 10x10 cm (Figure 3.2). All walls of the setup were

painted in matt-black color. This avoided any possible reflection of the LED tracking lamp and of the light emitted by the laser during optostimulation epochs and thus facilitated accurate video recording of mice’s position. Food (Dustless Precision Pellets, 20 mg, Rodent Purified Diet, Bio Serv) was provided either in a food cup or in a pellet feeder (Coulbourn Instruments Pellet Feeder H14-23M); one nose poke led to the delivery of one food pellet to the feeder. Water was presented in a standard drinking tube, placed on an optical lickometer (Coulbourn Instruments Optical Lickometer H24-01M). A small custom-made pulley was fixed over the behavioral enclosure and two small crocodile clips were attached to both of the pulley's string ends. One of the crocodiles held the laser patchcords and electrode cables, while the other held a counterweight object (this object would change depending on the size of the implant). This system alleviated the mice from carrying additional weight of patchcords or cables, allowing animals to freely explore the setup.

Home cage-like setup

A custom-built enclosure (30x22x22) that replicated the dimensions of the mice's homecage, containing soft paper tissues as bedding, some of which were also placed inside the homecage of the corresponding mouse, several days before the start of the experimental sessions.

Self-stimulation setup

This consisted of a custom-built two chambers enclosure that exactly replicated the innate behaviors setup, but contained no food or water, but instead an active nosepoke port (Coulbourn Instruments, nose poke operandum H21-09M).

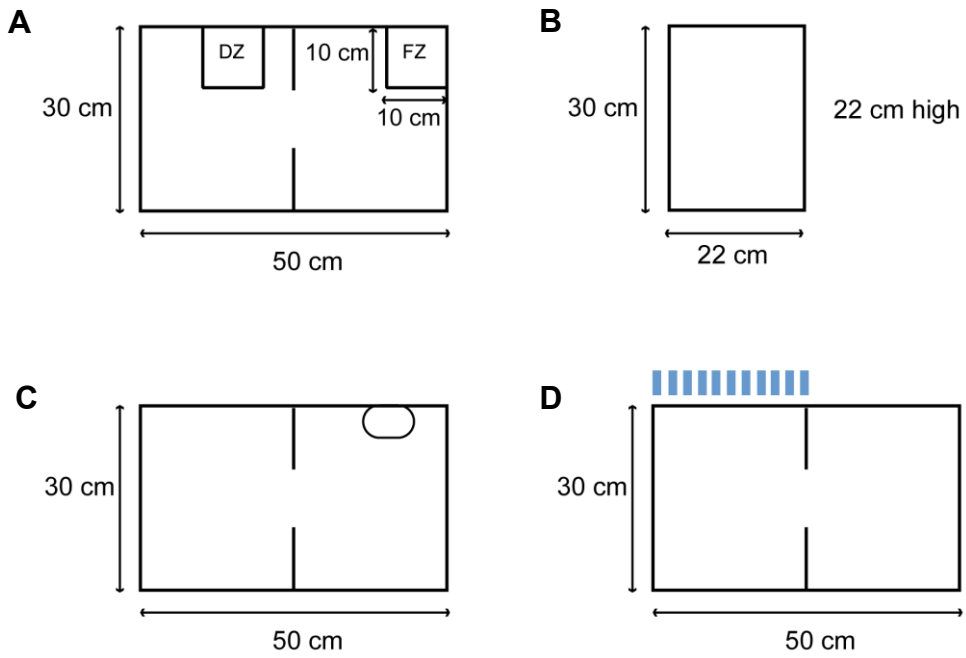

Figure 3.2 Shemes showing designs and dimensions of experimental setups. **A** Innate behaviors setup, including food zone (FZ) and drinking zone (DZ). **B** Homecage-like setup. **C** Self-stimulation setup, with a nosepoke port. **D** Place preference setup, blue pulses represent photostimulation-paired chamber

3.5.1 Optogenetic stimulation

For optogenetic stimulation, a 3 m long patch cord with protective tubing (Thorlabs) was connected to the implanted optical fiber with a zirconia sleeve (Precision Fiber Products), which allowed the mice to freely explore an enclosure or sleep in the home cage-like enclosure during optogenetic manipulations. For optogenetic stimulation, the patch cord was connected to a 473 nm diode-pumped solid-state laser (F471005FX, Laserglow Technologies) with an FC/PC adaptor. The laser output for the different stimulation protocols was controlled using a stimulus generator (Multichannel systems, STG 4004) and MC Stimulus software (Multichannel Systems, Reutlingen, Germany). Light power output was measured before recordings using a power meter (PM100D, Thorlabs), with an average output of 10-25 mW from the tip of the patch cord (during light-on parts of illumination cycles). For bilateral optogenetic inhibition, the implanted fibers were connected to a 593-nm diode-pumped solid-state laser (R591005FX, Laserglow Technologies) using a multimode fiber optic coupler (FCMM50-50A-FC, Thorlabs). Continuous yellow light, with approximately 15-20 mW power output from the tip of each patch cord was delivered into the targeted brain region. For within animal comparisons (described in sections 4.3.1, 4.3.2, 4.7.1, 4.7.2 and 4.7.3), the patch cords were

connected to dummy ferrules, attached to the headset, and light of the same wavelength and power as during opsin-activating stimulation was delivered at the same stimulation frequency.

3.6 Behavioral assays

Free-access feeding model.

These experiments were performed in the innate behaviors setup. Before experimental sessions, mice were habituated to the behavioral setup for at least 3 days, and received the same kind of pellets (20 mg Dustless Precision Pellets, Bio Serv) in the homecage for at least 2 days. Mice freely explored the enclosure. Duration of experimental sessions and optogenetic manipulations are described below

Optogenetic activation of LS_{sst}-LH projections. The recording sessions consisted of 30 minutes: 10 minutes of baseline before stimulation, 10 minutes of optogenetic stimulation, 10 minutes after stimulation. Blue light (473 nm) was bilaterally delivered over LS-LH projections, at 67Hz in 5 ms pulses (Carus-Cadavieco, Gorbati et al. 2017), at 5 Hz in 5 ms pulses or using a control, non-gamma (theta) frequency stimulation, which matched in amount and intensity of the delivered light (167 Hz bursts of 4ms pulses repeated at 9 Hz).

Optogenetic activation of LS_{Sst}–LH projections during free-access to high-fat food. The recording sessions consisted of 20 min in which mice could freely explore the enclosure. Blue light (473 nm) was bilaterally delivered over LS-LH projections, at 67 Hz in 5 ms pulses. High-fat food pellets (Testdiet, 60% energy from fat) were weighted before and after the experiment, to calculate the amount of food consumed per session (Carus-Cadavieco, Gorbati et al. 2017), sessions where mice ate at least 5 mg were analyzed.

Optogenetic stimulation of LH_{Vgat} cells. The recording sessions consisted of 30 or 60 minutes: 10 or 20 minutes baseline before stimulation, 10 or 20 minutes of optogenetic or control light stimulation, 10 or 20 minutes after stimulation. Blue light (473 nm) was delivered bilaterally over LH at 20 Hz in 5 ms pulses. Dustless Precision Pellets (Bio Serv) were counted to measure the amount of food consumed per session, sessions where mice consumed at least 1 pellet were analyzed.

Optogenetic inhibition of LH_{Vgat} cells in food-deprived mice. The recording sessions consisted of four epochs: 10 minutes light-on (optogenetic or control stimulation), 10 minutes light-off, 10 minutes light-on, and 10 minutes light-off. Yellow light (593 nm) was bilaterally delivered over LH. All food-deprived mice received approximately 2.5-3 gr of

standard chow daily, and their weight was controlled so that weight loss did not exceed 10% (Carus-Cadavieco, Gorbati et al. 2017).

Real time place preference

Optogenetic activation of LS_{Sst}-LH projections in a stimulation-paired chamber This was performed in a custom two-chamber enclosure similar to the one used for the free-feeding model (30x50x20 cm). One of the chambers was paired with optogenetic stimulation (Jennings, Rizzi et al. 2013). Recording sessions consisted of 30 minutes, every time the mouse crossed to the photostimulation-paired side, blue light (473 nm) was bilaterally delivered over LS-LH projections, at 67Hz in 5 ms pulses. Stimulation side was assigned in a counterbalanced way.

Self-Stimulation

Optical self-stimulation of LS_{Sst}-LH projections This was performed in a custom two-chamber self-stimulation enclosure. Mice were trained daily in 30 min sessions for at least 3 days to nose poke for optical self-stimulation of LS_{Sst}-LH projections. Recording sessions were performed daily, and consisted of 30 minutes, in which mice could freely explore the enclosure. Every active nose poke resulted in a train of blue light (473 nm) 5ms pulses during 3 seconds at 67 Hz.

Polisomnographic recordings

Mice were habituated to the homecage-like enclosure several days before the start of experiments, as well as 45 minutes before the initiation of each session, in order to allow the animals to relax and acquire more sleep episodes. All sleep-related experimental recordings took place between 9:00 and 15:00. No more than two sessions were recorded within one day, having at least one hour break between the two of them.

To characterize LH neurons response to stimulation of LH_{Vgat} cell bodies, blue light (473 nm) of 5 ms pulses was delivered at 20 Hz during 2 minutes or in 100 ms, 200 ms and 1 second pulses (40 seconds each) during 2 minutes.

To characterize RTN neurons response to stimulation of LH_{Vgat}-RTN projections, blue light (473 nm) was delivered at various frequencies: 1, 5 or 20 Hz for 40 seconds each, or 20 Hz during 2 minutes followed by at least 10 minutes break and stimulation in 2 second pulses during 2 minutes.

3.7 Electrophysiology

3.7.1 Preparation of electrodes

Wire arrays

In order to record LFP signals, custom-made wire arrays were prepared according to a protocol (Knoche, Yokoyama et al. 2003; Korotkova and Ponomarenko 2017). Rows of tungsten wires (40 µm, California Fine Wire Company) were formed by inserting the wires through 70 µm silica tube guides (Polymicro technologies) assembled in parallel using tape. Enamel-insulated copper bonding wires and a longer grounding wire were cleared from the insulation on both sides and soldered to the pins of a nanoconnector (Omnetics). Tips of the tungsten wires were deinsulated and bended in the shape of a hook, this hook was then connected to the bonding wires, using conductive and afterwards insulating varnish. The impedance of each tungsten wire and potential cross-talks between different wires were measured before implantation, using an Impedance Conditioning Module (FHC, USA). Wire Arrays with crosstalks (<5 Mohm) were discarded. Final length of the tungsten wire was adjusted according to the brain region of interest.

For co-implantations of silicon probes and wire arrays, the following modification was applied, in order to reduce weight of the implant: the hooks of the tungsten wires were directly attached to the nanoconnector, using golden pins extracted from a versadrive (Neuralynx) as interface between the wires and the pins of the connector.

Silicon probes

Movable probes (B32, NeuroNexus Technologies), were used. Preparation of the implant and surgical procedure were adapted from (Vandecasteele, M et al. 2012). Probes were mounted on a custom-made microdrive, which allowed to move the implanted silicon probe over the course of chronic recordings. Microdrives were prepared with two printed circuit boards (Sigmann Electronik) and a three-pole strip with a middle pole replaced by a 10 mm long screw (DigiKey). One complete turn (60') of the screw moves the probe approximately by 300 µm. Turning the screw in an anticlockwise fashion, causes the probe to move downwards, whereas a clockwise turn will make the probe to move upwards. By using a micromanipulator (Narishige), the probe was aligned with the microdrive, so that the shanks are perfectly parallel with the screw. The probe was then fixed to the microdrive with dental acrylic and cyanoacrylate glue. An assembled microdrive and mounted silicon probe are shown in fig (Figure 3.3). Prior to the implantation, thin layers of DiI solution (diluted in ethanol) were applied to the back

of the probe shanks, close to the tip, in order to visualize the tracks of the probe in brain slices after experiments (Korotkova and Ponomarenko 2017).

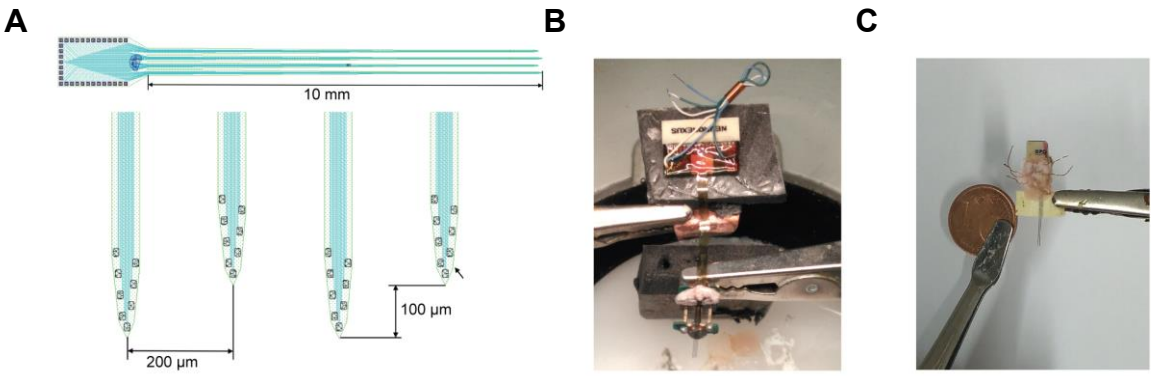

Figure 3.3 Images of electrodes layout. **A** Scheme of a B32 silicon probe, used in this study, lower panel shows the tips of the 4 shanks, with the distribution of the active recording channels (modified from Neuronexus). **B** Silicon probe mounted on a microdrive. **C** Custom-made wire array.

3.7.2 Data acquisition and analysis

Electrodes were connected to a 128-channel acquisition system (Digital Lynx, Neuralynx, USA) via operational amplifiers (HS-8, Neuralynx, Bozeman, Montana USA or Noted B.T., Pecs, Hungary) to eliminate cable movement artefacts. Electrophysiological signals were differentially amplified, band-pass filtered (1 Hz-10 kHz) and acquired continuously at 32 kHz (Digital Lynx, Neuralynx). Time stamps of laser pulses were simultaneously recorded with electrophysiological signals. A light-emitting diode was attached to the headset to track the animal's position within the behavioral setup (at 25 Hz).

Data preprocessing

Processing of electrophysiological signals and position tracking data was done using Neurophysiological Data Manager (NDManager (Hazan, Zugaro et al. 2006), (http://neurosuite.sourceforge.net). When necessary, recordings were concatenated and visually inspected in Neuroscope. After pre-processing all data were uploaded into a MySQL database to be analyzed. Analysis was performed together with Alexey Ponomarenko and Maria Gorbati.

Unitary data

Action potentials (spikes) were detected in the band-pass (0.8 Hz-5 kHz) filtered signal and extracted, by thresholding the signal. Thus, voltage waveforms with a magnitude

exceeding 3 s.d. above mean (Herrera, Carus Cadavieco et al. 2016) and which were in a time-window of a spike with at least 1 ms of refractory period were detected. Spike waveforms were then represented by the first three principal components. Spike sorting was performed automatically using KlustaKwik (Harris, Henze et al. 2000) (http://klusta-team.github.io/klustakwik/). This resulted in grouping spikes which were presumably fired by the same individual neurons in different 'clusters' (Buzsaki 2006). Manual cluster adjustment was performed using Klusters (Hazan, Zugaro et al. 2006), in order to improve the outcome of automatic clustering, by visually inspecting auto-correlograms of clustered units and further discarding of signals created by noise and artifacts. Isolation distance (Harris, Henze et al. 2000) was computed for sorted units. Single units with a clear refractory period (2 ms) and multiunits were used in further analysis. Computation of firing rates, interspike intervals and detection of timestamps of laser pulses and of stimulation epochs were done in MATLAB (MathWorks, Ismaning DL) using custom-written algorithms as described elsewhere (Wulff, Ponomarenko et al. 2009; Korotkova, Fuchs et al. 2010).

Putative LH_{Vgat} neurons recorded across sleep/wake cycle (section 4.2) were phototagged based on their rapid (<10 ms) significant increase of the firing rate in cross-correlograms of the unit firing triggered by laser pulse onset, compared to a pre-pulse baseline (Herrera, Carus Cadavieco et al. 2016).

Putative LH_{Vgat} cells recorded within the free feeding paradigm were photoidentified, based on their rapid (<10 ms) significant increase of the firing rate in cross-correlations triggered by the laser pulse onset. Reliability of the light triggered responses was assessed as a probability of the maximal light induced spike count in a Poisson distribution calculated for the cross-correlogram times in the pre-pulse baseline (Carus-Cadavieco, Gorbati et al. 2017).

Firing maps of LH neurons were computed by dividing the number of spikes in a given spatial pixel (2x2 cm) by the time spent in this pixel during the baseline (excluding periods of immobility). The peak firing rate for each neuron was determined as the maximum firing rate over all pixels in the environment.

Local Field Potentials

LFP was obtained by low-pass filtering and down-sampling of the wide-band signal to 1250 Hz (Wulff, Ponomarenko et al. 2009) and were further analyzed using Spike2 (Cambridge Electronic Design, Cambridge) and MATLAB. Gamma oscillations were detected at 30–60 Hz, 60–90 Hz. Events with amplitudes passing 2 s.d. above mean for at least 25ms were detected (Csicsvari, Jamieson et al. 2003). The beginning and the end of oscillatory epochs were designated at points at which the amplitude fell below 1 s.d.

Phases of the gamma oscillations were analyzed for signal epochs within the detected gamma episodes, as previously described in (Wulff, Ponomarenko et al. 2009; Korotkova, Fuchs et al. 2010). In short, zero degree and 360° were designated to the troughs of each gamma cycle and 180° to the cycle peak. Phases for each data sample between these points were calculated using linear interpolation (Csicsvari, Jamieson et al. 2003; Igarashi, Lu et al. 2014).

For data analyzed in Figure 4.14 A and B, gamma phases were computed for data samples when action potentials fired for each recorded neuron and firing phase histograms were calculated. Because a possible asymmetry of oscillation cycles can lead to a different number of phase samples that compose the ascending and descending parts of the cycle, and therefore bias firing phase histograms (Sirota, Montgomery et al. 2008), the uniformity of grand gamma phase distributions for each recording was tested using Rayleigh test. If it resulted significantly non-uniform, a deviation of a grand phase histogram from uniformity was computed by dividing by the average across all bins. In those recordings firing histograms were normalized by the corrected grand phase histogram (Korotkova, Fuchs et al. 2010). Each firing phase histogram was normalized by its total number of spikes. Circular uniformity, mean phase and the resultant vector length were computed for each histogram and before averaging, individual histograms were convolved with the Gaussian kernel of size 0.65 SD (Csicsvari, Hirase et al. 1999).

For analysis of data in Figure 4.17, trough activation of a cell was defined based on firing probability, as described in (Carus-Cadavieco, Gorbati et al. 2017) -spontaneous gamma (60-90 Hz) phase histograms, as the median firing probability bin within 20° around the trough. Units that did not meet this requirement were classified as non-trough. Fractions of non-responsive and responsive neurons, in the response range 5 to 40, bin width 5, were calculated, subtracted between non-trough and trough populations and then correlated with the magnitude of the response to the stimulation.

Figure 4.18 E was computed with a polynomial model fit: $y = x^2 + 0.5471$, R^2=0.21, where x is the trough phase inhibition and y is FZ-match index.

Position tracking data

Mice positions data were also preprocessed using NDManager. Positions were smoothed by Gaussian Kernel (SD 6) in a one second window to omit noise created by head movements of the mice. For analysis in sections 4.3 and 4.7, the enclosure was divided in equally sized quadrants (10 cm x 10 cm), in a way that one would correspond with the food zone and one with the drinking zone (Figure 3.4). Control zones were assignated in the non food compartment.

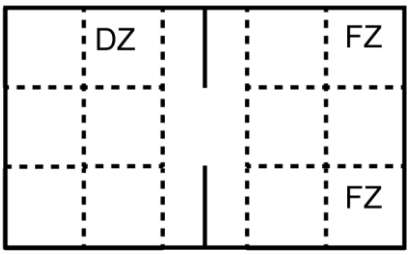

Figure 3.4 Scheme of setup divisions in 12 zones for analysis. FZ represents zones that were food was positioned (food zone) during different stages of the study. DZ represents drinking zone.

3.7.3 Elimination of optoelectrical artifacts

Direct laser light pulses on metal electrodes can be associated with optoelectrical artifacts (Korotkova and Ponomarenko 2017). These result from the photoelectricochemical effect upon exposure of the uninsulated metal from the recording sites of the implanted electrode to the laser beam, and could obscure LFP signals. The size of optoelectric artifacts varies between experimental preparations depending on the amount of exposed metal, the electrode material, distance and orientation between the electrode and the tip of the optic fiber and the laser power. In contrast to the optogenetic evoked neural activity, their onset exactly corresponds with the light onset, instead of displaying a delay of several miliseconds (Cardin, Carlen et al. 2010).

Tungsten wire electrodes are not very sensitive to optoelectrical artifacts. However, silicon probes used in this study had recording sites made of a platinum-iridium alloy, which are quite sensitive to optoelectric artifacts. On the ongoing recording these artifacts can be easily identified since they display one upward and one downward component that corresponds to the onset and offset, respectively, of the laser pulse. Due to their conservative waveform and consistent profiles across channels, they are typically sorted in a separate cluster during automatic clustering, distinct from optogenetically excited neurons. (Figure 4.2) (Korotkova and Ponomarenko 2017). Hence, autocorrelograms of these clusters belonging to artifacts are completely different from those belonging to neurons, which facilitates their identification and removal (see Figure 4.2). Note that discarded spikes are not actually deleted from the data file when performing manual cluster adjustment with Klusters (Hazan, Zugaro et al. 2006). Because movable silicon probes were used, the presence and extent of light artifacts could be used to estimate the anatomical location of the probe (i.e neurons are recorded in the same area that is stimulated) veryfing the position calculated by the turning of the

microdrive's screw. In general, optoelectrical artifacts could be prevented or reduced by implanting optic fibers with such an angle, that the light would not hit directly the recording sites.

3.7.4 Polysomnographic recordings and characterization of different brain states

The EEG, EMG and RTN LFP signals recorded from each sleep session were plotted (sampling rate 1250 Hz) and visually scored in 10 seconds epochs in Spike 2 (Cambridge Electronic Design, CED), using the Sleepscore v1.01 script. Scoring of each epoch was based on the visual signature of the EEG and EMG waveforms, the spectral analysis of the EEG signal (Hamming window, fast Fourier transform (FFT) size= 2048) as well as the video monitoring of each mouse during the corresponding session, as described previously (Franken, Chollet et al. 2001; Adamantidis, Zhang et al. 2007). Wakefulness was defined as desynchronized low-amplitude cortical EEG and high tonic EMG activity with phasic bursts, associated to movement (Figure 3.5 A). NREM sleep was defined as syncronized high-amplitude low frequency (0.5-4 Hz) EEG waves with a predominant delta power and highly reduced EMG activity, with no phasic bursts (Figure 3.5 B). REM sleep was defined by the desyncronized EEG with a pronounced theta rhythm (6-9 Hz) and a flat EMG. However, tethered, implanted with silicon probe mice did not have sufficient amount of REM sleep episodes to perform statistical assessment of neuronal activity during that state, therefore they were not analyzed in this study.

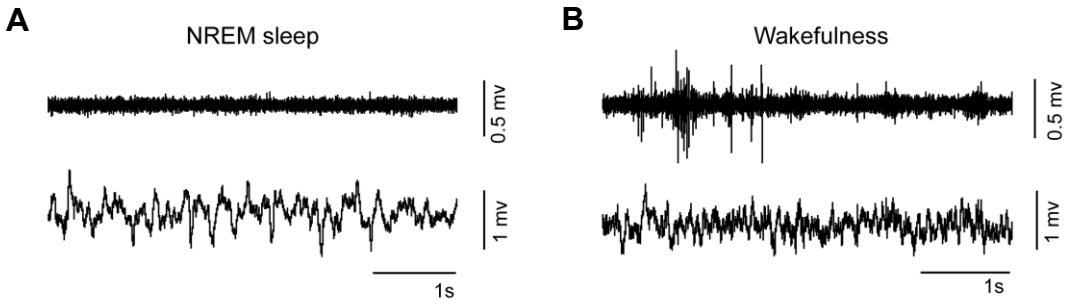

Figure 3.5 Representative EEG and EMG traces during different behavioral states. **A** NREM sleep. **B** Active wakefulness.

3.8 Statistical analysis

Each statistical test used in this study was employed according to the design of the experiment and the structure of the acquired data. The size of the sampled data was determined according to the accepted practice for the applied assays, no statistical methods were used to predetermine sample size. Conditions of the behavioral

experiments were taking into account during the design of analysis algorithms. The computations during analysis of the data were performed blindly using automatic selection of data from the database in MySQL.

Two-group comparisons were performed using t-test, or the non-parametric Mann-Whitney or Wilcoxon matched pair tests, depending on whether the analyzed data were normally distributed. To test the normality of the dataset, Kolmogorov-Smirnov or D'Agostino-Pearson tests were used. To evaluate experimental effects in experiments involving several conditions ANOVA was used, followed, when appropriate, by Bonferroni (for preselected contrasts) or Tukey tests, adjusting for multiple comparisons. Likewise, ANCOVA with a fixed factor and a covariate was used followed by post-hoc test when required. Grubbs test was employed to exclude outlier points from the behavioral datasets.

A more detailed description of the statistics for each dataset is provided in the results section. Descriptive statistics are reported as mean ± standard error of the mean.

3.9 Histology and microscopy

After completion of experiments, histological analysis was performed in order to verify expression of the viral vector and/or to confirm position of the electrode. Mice were deeply anaesthetized with isoflurane and electrolytic lesions were done at selected recording sites, according to the mapping of the B32 probe connector, using a DS3 Constant Current Isolated Stimulator (Digitimer). Afterwards, animals were perfused intracardially with saline followed by 4% paraformaldehyde in PBS (PFA) (Santa Cruz Biotechnology) and decapitated. In the case of mice implanted with silicon probes, the complete head (without removal of the headset) was fixed in PFA for 2-6 days for better later visualization of probes tracks. In all other cases, brains were removed immediately after the perfusion, fixed for 24-48h in 4% PFA and subsequently equilibrated in 1% Phosphate-buffered saline (PBS) (Bio Rad) for at least 24h. Then, 50-60 µm slices were prepared using an oscillating tissue slicer (EMS 4500, Electron Microscopy Science).and mounted (Flouromount Aqueous Mounting Medium, Sigma-Aldrich). Because eYFP endogenous fluorescence of the opsin constructs used in this study was good and slices were analyzed shortly after perfusion, no additional immunohistochemistry to enhance fluorescence was performed.

In slices containing presumable tracks and electrolytic lesions from silicon probes shanks, Nissl staining was performed for better visualization of the tracks (see Table 3.1 for the protocol).

Reagent	Time
Demyelination	
95% Ethanol	5 min
100% Ethanol	5 min
95% Ethanol	5 min
70% Ethanol	10 min
50% Ethanol	3 min
Stain	
Cresyl viotlet	6/7 min
Destain	
70% Ethanol+Acetic Acid (~1%)	3 min
95% Ethanol	5 min
100% Ethanol	5 min
100% Ethanol	5 min
Cover	
Xylene	2 min

Table 3.1 Nissl Staining protocol.

DiI labeling surrounding the shanks was viewed under fluorescence microscope. Images were taken using an Olympus BX 61 microscope (x2/0.06 numerical aperture (NA), x10/0.3 NA and x20/0.5 NA, dry)) coupled to a mono-fluorescence camera (Qimaging, Surrey, BC) or using a Leica DMI 6000 microscope (x20/0.7 NA, x63/1.4 NA; oil-immersion objectives).

4 Results

4.1 Targeting GABA neurons in LH

4.1.1 Histology

Vgat-Cre Ires mice (mice expressing the Cre recombinase in cells expressing the vesicular GABA transporter, Vgat, also known as Slc32a1 gene) (Vong, Ye et al. 2011) were injected in LH with Cre dependent viral constructs, encoding the opsin ChETA or the opsin eNPAC. Opsin expression in LH neurons and their projections, as well as silicon probe tracks and/or lesions, were confirmed in all animals before the statistical analysis. This method allowed selective targeting of LH_{Vgat} neurons (Figure 4.1 A, Figure 8.1).

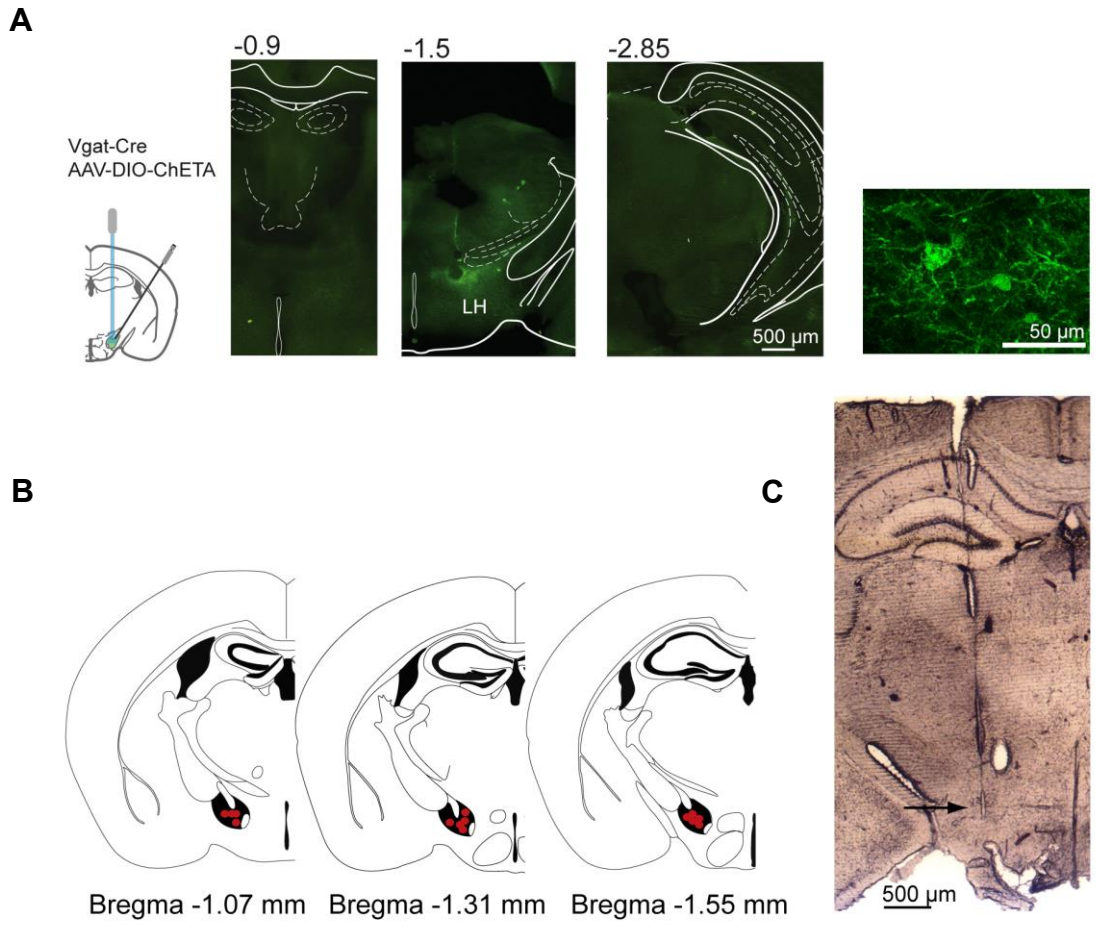

Figure 4.1 Histological confirmation of opsin expression and recording sites in LH. **A** Scheme of injections in LH and representative photomicrograph of coronal brain slices from a Vgat Cre mouse expressing ChETA in LH. Note that the expression is confined to the LH. Right: high magnification (63x) of a coronal slice showing LH_{Vgat} ChETA-expressing neuronal bodies. **B** Schemes of coronal sections showing reconstructions of electrodes positions in LH, in which

units were recorded, from all recorded mice (N=7). **C** Photomicrograph of a coronal brain hemisection from a Vgat Cre mouse, showing the track left by one of the shanks of the silicon probe (the shank located in the most medial position) and the lesion in the LH. Modified from (Herrera, Carus Cadavieco et al. 2016; Carus-Cadavieco, Gorbati et al. 2017)

Distance between consecutive shanks of the silicon probe is 200 µm, and the total size of the B32 probe is approximately 800 µm (including the 4 shanks), therefore, positions of the four electrodes at the termination of experiments can be reconstructed based on the lesion, tracks and fluorescence of the DiI. Further, by calculating the movement of the probe within the brain after each turn of the microdrive, it is possible to estimate the locations in which neurons were recorded (Figure 4.1 B).

4.1.2 Optogenetic identification and control of LH_{Vgat} Neurons

Implantation of movable silicon probes in LH enabled the recording of a statistically representative fraction of neurons of the investigated circuits in behaving animals with a high temporal resolution (Csicsvari, Henze et al. 2003). A total of 56 LH units were recorded during sleep/wake experiments, and 291 LH units across the free feeding paradigm and included for analysis in this study. The combination of optogenetics with in vivo electrophysiological recordings allowed identification of LH_{Vgat} cells (Figure 4.2) since they responded to the laser pulses with a short latency (<10 ms, Figure 4.2 E). In order to identify them, cross correlograms of the spike trains and laser pulses time stamps were calculated by computing the histogram of the firing probability of a given neuron as a function of time relative to the laser pulses (see methods 3.7.2). In addition, targeting of LH_{Vgat} cells with ChETA enabled optical control of their activity over a wide range of frequencies in vivo, within fast timescales, and with the magnitude of the response being proportional to the stimulus: (Figure 4.2 H). LH_{Vgat} neurons increased progressively their firing rate over the baseline in response to pulses of different length, showing the biggest increased upon the longest pulses (n=18 cells, N=1 mouse, Wilcoxon signed rank test, 1 sec $P<0.0001$, 200 ms $P=0.0023$, 100 ms $P=0.0104$) The waveform of spikes triggered by optogenetic stimulation did not differ from the waveform of spontaneous spikes fired during the baseline (Figure 4.2 D). Putative Vgat neurons expressing ChETA were able to follow repetitive stimulation (see Figure 4.2 A and G). Photoidentified LH_{Vgat} neurons were recorded from the four shanks of the silicon probes, indicating that they are located from medial to lateral aspects of the LH, in agreement with the histological verifications of opsins expression and the literature (Jennings, Ung et al. 2015). Number of photoidentified LH_{Vgat} neurons, out of the total number of recorded neurons in the different paradigms is given in the next sections.

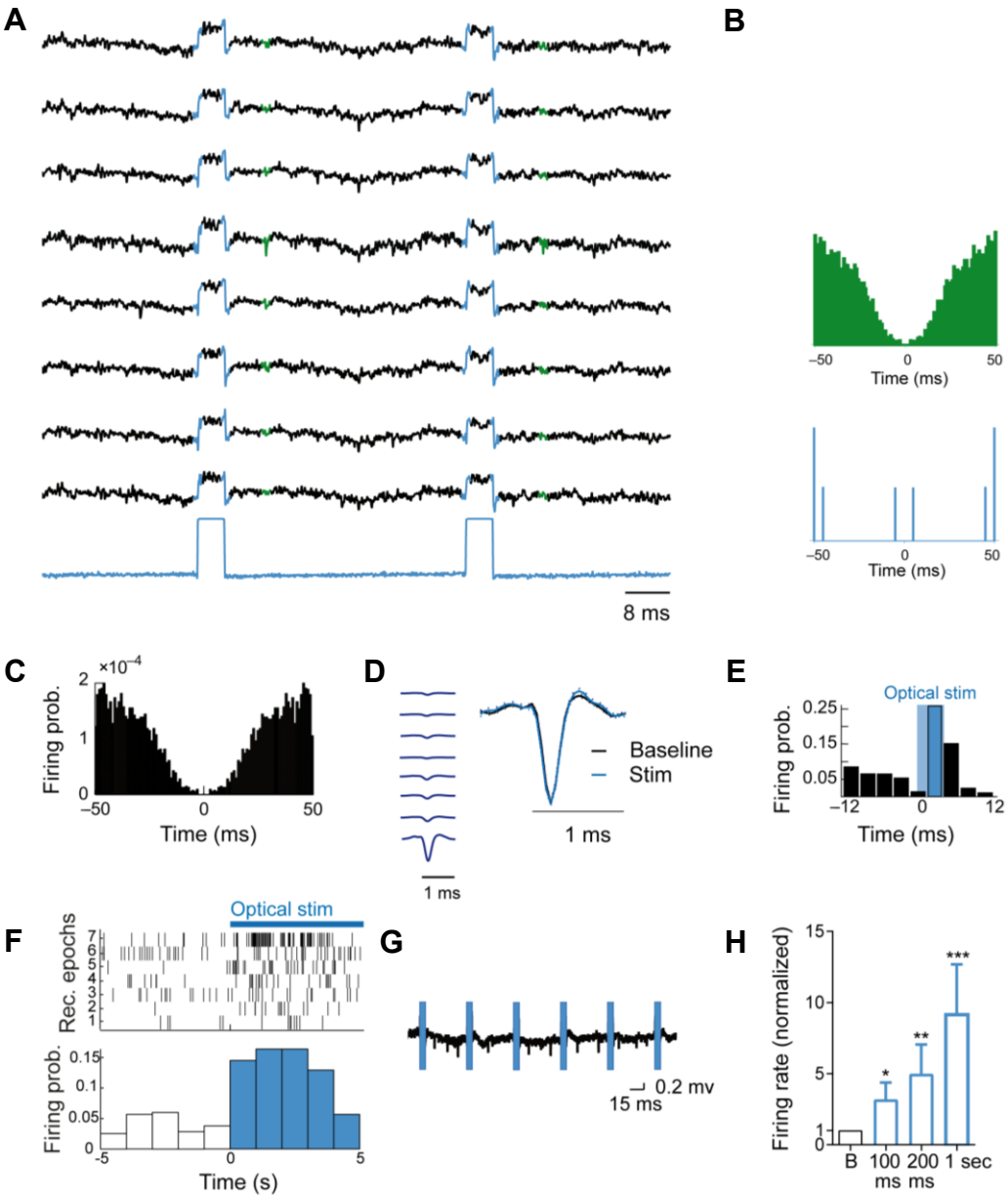

Figure 4.2 Optogenetic identification and control of LH_{Vgat} neurons. **A** Wide-band signal traces of 8 probe channels belonging to the same shank, and of the channel containing laser pulses during optogenetic stimulation, with simultaneous display of the activity of a clustered single unit (green) and of the optoelectrical artifacts created by the laser pulses (blue). Note that in contrast with the optogenetically evoked spikes, artifact signals are exactly aligned with the onset and offset of the laser pulses. **B** Autocorrelogram of the presumable LH_{Vgat} cell (up) shown in (A) and of the artifacts created by laser pulses at 20 Hz (down), shown in (A), which were separated in different clusters during automatic clustering. **C** Autocorrelogram of the single unit shown in (A). **D** Example of average spike waveforms of a putative LH GABA cell, recorded from different probe channels (left) and average spike waveforms of the same representative presumable ChETA-expressing LH GABA cell before (black) and during optogenetic stimulation at 20 Hz (blue, right). **E** Cross-correlogram of a representative presumed ChETA-expressing LH_{Vgat} cell firing probability triggered by laser pulses. Cross-correlation bin width: 3 ms. **F** Examples of optogenetic stimulation onset-triggered rastergrams of representative seven LH cells (n=3 recordings, N=2 mice; of 31 recorded presumable LH_{Vgat} cells, N=4 mice), and their firing probability before and after the optostimulation onset, showing a fast change in the discharge (5 Hz). **G** Representative wide band trace showing firing of a putative ChETA-expressing LH_{Vgat} cell following the laser pulses (blue lines) during a

photostimulation experiment (20 Hz). **H** Normalized average firing rate +- SEM of LH units during baseline and following optostimulation with pulses of different length (*** P<0.0001, ** P=0.0023, * P=0.0104), α corrected for multiple comparisons.
C-G Modified from (Herrera, Carus Cadavieco et al. 2016).

4.2 LH_{Vgat} cells across the sleep/wake cycle

4.2.1 LH_{Vgat} cells and arousal

To characterize the activity of LH_{Vgat} neuronal population in vivo across the sleep/wake cycle, 3 Vgat-cre mice expressing ChETA in LH were recorded with a silicon probe and stimulated in LH, while simultaneously registering cortical EEG and EMG in the homecage-like enclosure. A total of 56 LH units were obtained from these recordings and 22 out of the 56 significantly increased their firing rate with a short latency (<10 ms) following optostimulation at 20 Hz, and therefore were classified as presumable Vgat neurons. Then, the spontaneous activity of these putative Vgat neurons was studied during active wakefulness and NREM sleep epochs (Figure 4.3). Average firing rates and interspike intervals (ISIs) were not significantly different between wakefulness and NREM periods (Figure 4.3) (5.78 ±0.93 Hz and 6.71 ±1.17 Hz respectively, P= 0.20, P= 0.20; coefficient of variation, CV: 1.00 ±0.07 versus 0.83 ±0.05, P= 0.10; Wilcoxon signed rank test, N=3 mice, n= 22 cells).

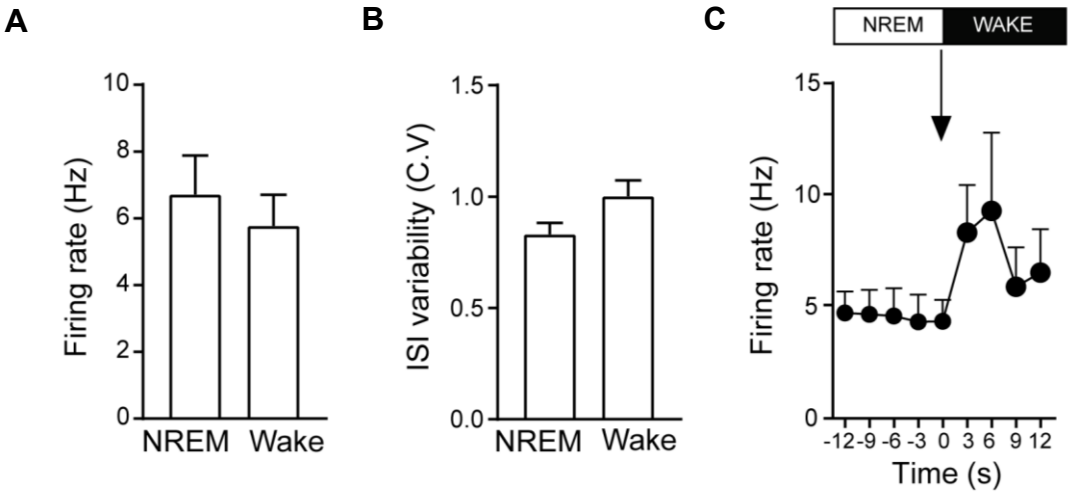

Figure 4.3 LH_{Vgat} cells activity across sleep/wake cycle. **A** Average firing rate ± sem of LH_{Vgat} cells during NREM and wakefulness epochs. **B** Coefficient of ISIs variation (CV) of LH Vgat cells across NREM sleep and wake states. **C** Firing rates of LH_{Vgat} cells before and after wakening (P < 0.05, binomial test, 3 s. around NREM sleep-to-Wake transitions).
Modified from (Herrera, Carus Cadavieco et al. 2016).

However, when their activity was analyzed during fast transitions between NREM to active wakefulness (Figure 4.3 C), LH_{Vgat} cells showed a temporary increase in firing rate during the first 3 s after NREM sleep-to-wake transitions (11 of 13 cells, 3 mice, P= 0.02, binomial test), but not during the following waking epochs, suggesting that this increase is transient and limited to the behavioral change.

Accordingly with this finding, when LH Vgat cells were stimulated during NREM sleep, a fast awakening of the animals was observed. This behavioral outcome was confirmed by our collaborators (Antoine Adamatidis & Carolina Gutierrez-Herrera) who quantified the latency from NREM to wake, and found a significant decrease upon optostimulation of ChETA expressing LH_{Vgat} cells, compared with YFP-expressing control mice (Herrera, Carus Cadavieco et al. 2016). Altogether these results suggest that LH_{Vgat} cells mediate rapid arousal from NREM by transiently increasing their activity.

4.2.2 LH_{Vgat} cells projections to RTN mediate arousal

Given the role of LH_{Vgat} cells in promoting fast transitions from sleep to arousal and the involvement of the RTN in the generation of sleep-related brain states, *we hypothesized* that this LH GABA-RTN projection would exert direct hypothalamic control over RTN neurons, and therefore indirect control the thalamocortical network during NREM-wake transitions. To investigate this, 3 Vgat-Cre mice expressing ChETA in LH were implanted with silicon probes and optical fibers in RTN (Figure 4.4), both for simultaneous recordings and optogenetic manipulation of LH_{Vgat} terminals across sleep/wake cycle.

A total of 72 units were recorded, 70 out of these cells recorded in RTN displayed a typical narrow spike waveform (half-trough time, <0.2 ms; n= 70 cells, N=3 mice), consistent with previous reports (Halassa, Chen et al. 2014), and therefore were used for further analysis.

The majority of RTN units displayed state-dependent activity across sleep-wake cycle (Figure 4.5). The variability of their Inter-spike intervals (ISIs) also known as coefficient of variance (CV) was lower during spontaneous waking than during NREM sleep (46 of 70 cells, N=3 animals, Wilcoxon signed rank test, P = 3.523 × 10-9), which indicates that these neurons fire with a more regular pattern during wakefulness. No correlation was found between these changes in the CV of RTN neurons across states and changes in firing rates (Table 4.1) (Pearson correlation, P=0.26). Units which displayed this state-dependent activity and units which did not, had similar firing rates (NREM sleep: 6.19 ± 0.71 and 4.86 ± 1.08 Hz, respectively, P = 0.17; waking: 7.58 ± 0.81 and 5.54 ± 0.92 Hz, respectively, P = 0.22, Wilcoxon signed rank test) and mean ISIs (275.0 ± 44.83 versus 406.99 ±77.98 ms, respectively, P = 0.2, Wilcoxon signed rank test).

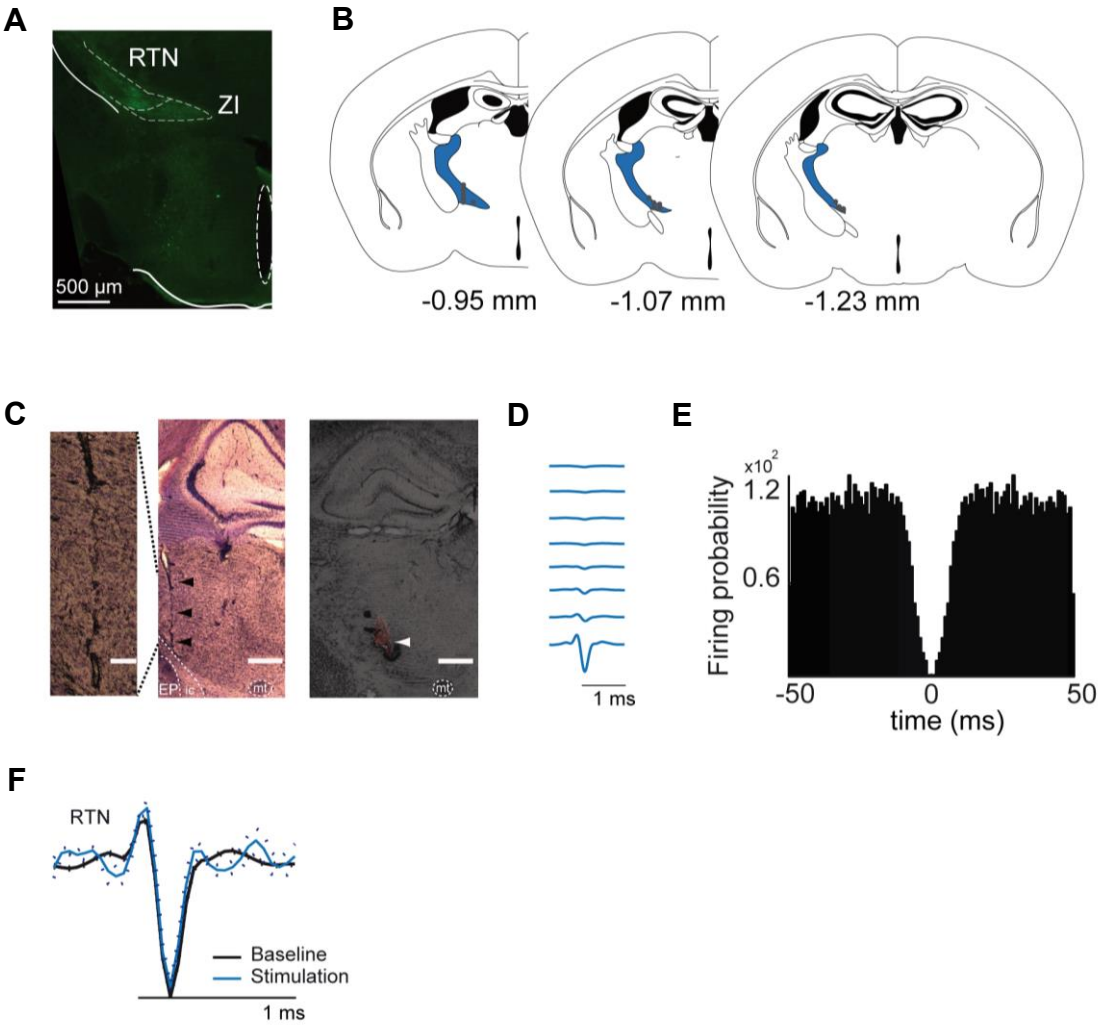

Figure 4.4 In vivo recordings of RTN neurons across sleep/wake cycle. **A** Photomicrograph of a coronal section showing fibers of LH_{Vgat}-ChETA expressing cells in the RTN. **B** Histological reconstruction of silicon probe positions in which RTN units were recorded. **C** Photomicrographs of coronal sections (Nissl staining). Left and middle: track left by the lateral silicon probe shank in the RTN at higher (left, scale bar: 100 µm) and a lower (middle, scale bar 500 µm) magnification, black arrows point to the electrode track. Right: electrolytic lession, indicated by the white arrow, performed on the medial probe shank (right to the RTN, scale bar 500 µm), overlayed with a fluorescent image from the same section, showing DiI (red), applied to this shank before the implantation. Recordings in RTN were performed from the lateral shanks of the probe. **D** Example of average spike waveforms of an RTN cell, recorded from different probe channels. **E** Autocorrelogram of an RTN cell and **F** the average spike waveform of this unit before (black) and during optogenetic stimulation of LH_{Vgat}-RTN at 20 Hz (blue). Modified from (Herrera, Carus Cadavieco et al. 2016).

Optogenetic stimulation of LH_{Vgat} projections in the RTN exerted a strong inhibitory action on RTN cell activity (Figure 4.6, n= 70 cells, N=3 mice, one-way ANOVA followed by Bonferroni post hoctest, $F_{3,3}$ = 38.2831, P= 9.42 ×10−16), compared to their spontaneous activity during the baseline. For the analysis of these effects 2 minutes of recording before optostimulation were selected as baseline, given that optogenetic stimulation epochs were not longer than 2 minutes.

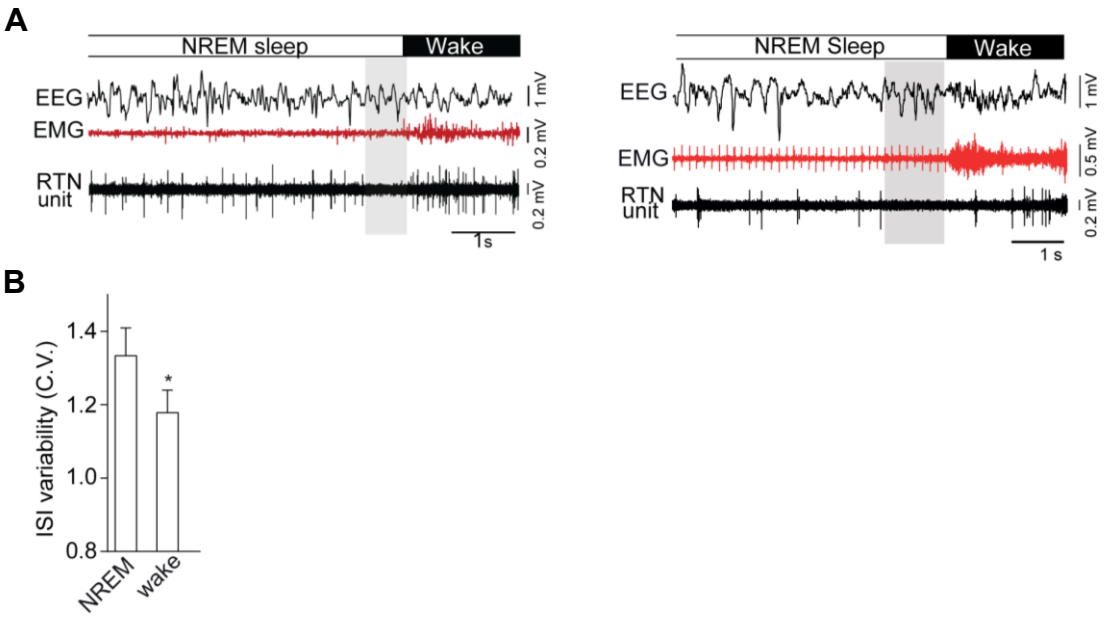

Figure 4.5 RTN neurons firing during NREM sleep and wakefulness. **A** Representative traces of EEG, EMG and RTN unit recording during a spontaneous transition from NREM sleep to wakefulness in a freely moving mouse, from two different sessions. Note the transient period of RTN cell inactivity preceding behavioral transition in both of them (grey shaded boxes). **B** Coefficient of ISIs variation (CV) of RTN cells across NREM sleep and wake states. CV is significantly lower during wake periods (* P= 3.52 × 10−9).
Modified from (Herrera, Carus Cadavieco et al. 2016).

	NREM		WAKE	
	Mean±sem firing rate (Hz)	**Number of cells**	**Mean±sem firing rate (Hz)**	**Number of cells**
Cv decrease	6.19 ± 0.71	46	7.58 ± 0.81	46
No CV decrease	4.86 ± 1.08	24	5.54 ± 0.92	24
All RTN cells	5.8±0.59	70	6.98± 0.6418	70

Table 4.1 Summary of firing rates and CV of RTN neurons during NREM sleep and wakefulness.

The firing rate of RTN neurons was decreased in a frequency-dependent manner, the cells reduced progressively their activity with increasing optical stimulation frequency or duration (Figure 4.6 B, 20 Hz: 57 of 70 cells, 3 mice, Wilcoxon signed rank test, P= 1.62 × 10−10; 2-s continuous illumination: 17 of 17 cells, N=1 mouse, un-paired two-tailed Student's t-test, $t_{32,32}$ = 5.89, P= 0.0000014).

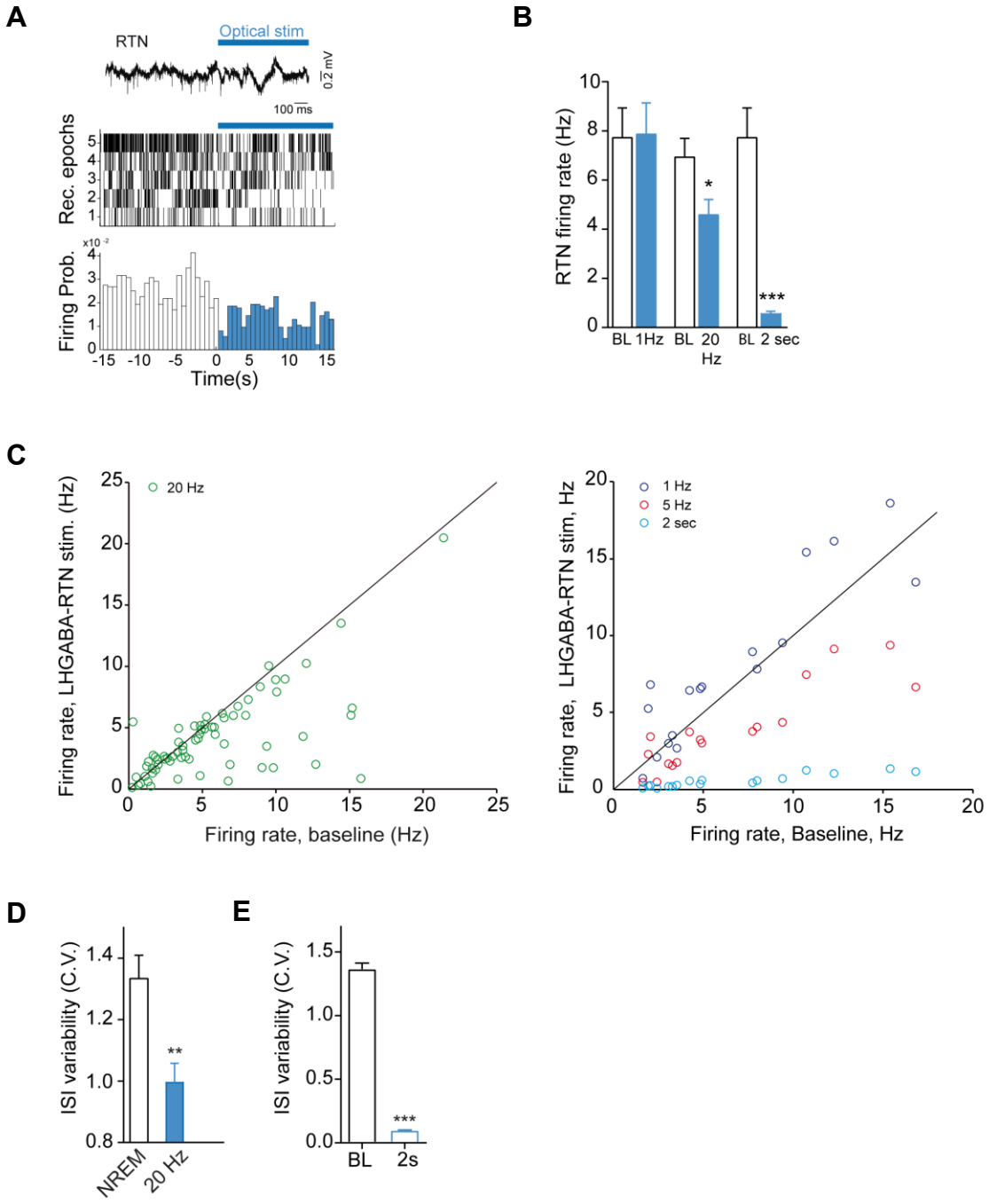

Figure 4.6 In vivo optogenetic stimulation of LH_{Vgat}-RTN circuit. **A** Representative wide-band signal trace of an RTN cell before and after optogenetic stimulation of LH_{Vgat} terminals (top), blue bar shows optical stimulation. Note the fast decrease of RTN spikes upon laser onset. Rastergrams of five representative RTN units (N=2 mice, middle) and their average firing probability (bottom) before and after the optical activation. Blue bars denote optostimulation at 20 Hz Hz. **B** Average firing rates ± s.e.m of RTN cells during baseline (BL, white bars) and after optogenetic stimulation of LH_{Vgat} axon terminals in the RTN at different frequencies (blue bars). Optogenetic stimulation decreased activity of RTN neurons, * $P<0.05$, *** $P<0.0001$, t tests with α adjusted for multiple comparisons. **C** Firing rates of individual RTN units during baseline (x-axis) and during optostimulation (y-axis) at 20 Hz (left panel) and 1 Hz, 5 Hz, and 2 sec continuous light pulses (right panel). **D** Coefficient of ISIs variation (CV) of RTN cells across NREM sleep and optogenetic stimulation of LH_{Vgat}-RTN circuit at 20 Hz. CV was significantly

decreased upon optostimulation of LH_{Vgat}-RTN terminals, ** P= 0.0086. **E** CV of RTN neurons following optogenetic stimulation of LH_{Vgat}-RTN circuit with 2 sec continuous light pulses was significantly decreased, *** P= 0.00195.
Modified from (Herrera, Carus Cadavieco et al. 2016).

Examination of the actual distribution of RTN cells' firing rates before and during the optogenetic stimulation revealed that optical activation of LH_{Vgat} terminals reduced the firing rate of both fast and slow spiking neurons (Figure 4.6 C). However, modulation by these inputs appears to be stronger on fast spiking cells than on slow spiking cells.
Optogenetic LH-induced inhibition of RTN replicated state-dependent changes in the activity of RTN neurons, (20 Hz: n= 46 cells, N=3 mice, P= 0.0086, Wilcoxon signed rank test; 2-s continuous illumination: n=10 cells, N=1 mouse, Wilcoxon signed-rank test), P= 0.00195, Figure 4.6 D,E). Thus, stimulation of LH-RTN Vgat/GABAergic projections decreased the ISI variability of RTN neurons, making their firing pattern more regular and similar to the one they have during spontaneous wakefulness.
In according with the behavioral transition observed after optostimulation of LH_{Vgat} neurons, when LH_{Vgat} projections in the RTN were optogenetically stimulated during NREM sleep, a fast transition to wake was observed in the animals (3 mice). Our collaborators (Antoine Adamatidis & Carolina Gutierrez-Herrera) further studied these effects by quantifying the latency of arousal transitions from NREM after optostimulation of LH_{Vgat} axonal projections in the RTN, and found a significant decrease of NREM sleep-to-wakefulness transition latency (Herrera, Carus Cadavieco et al. 2016).
Altogether these results support the hypothesis that the LH_{Vgat} projections to the RTN exerted an inhibitory control on the activity of RTN neurons that mediated NREM sleep to wake transitions.

4.3 LH cells and their activity in relation to feeding behavior

To further study behavior-dependent activity of LH neurons within the free feeding model, firing maps were created for each recorded LH cell during exploratory episodes (speed > 3 cm/s). Firing of LH cells was analyzed as it has been described previously for quantification of positional firing (Muller and Kubie 1989; Korotkova, Fuchs et al. 2010). Examples of LH units firing maps are shown in Fig (Figure 4.7).
As expected, different LH units displayed heterogeneous preferences for different areas of the behavioral setup. However, manual inspection of the firing maps revealed subgroups of neurons with similar firing patterns. Activity of some of the cells showed a clear preference for the food zone, whereas others exhibited preferential firing at a distance from the food zone, or fired equally in most zones of the enclosure. Based on

these differences, LH neurons were then classified according to their feeding-related activity by calculating their food-zone preference (FZ-match index). This index was computed by dividing the average firing rate of a cell in the food zone by the average firing rate in a control zone of the same size (10x10 cm), located in the non-food compartment of the setup. For further analysis, units were split in 'FZ-match' (index higher than 1) or 'FZ-mismatch' (index lower than 1) groups.

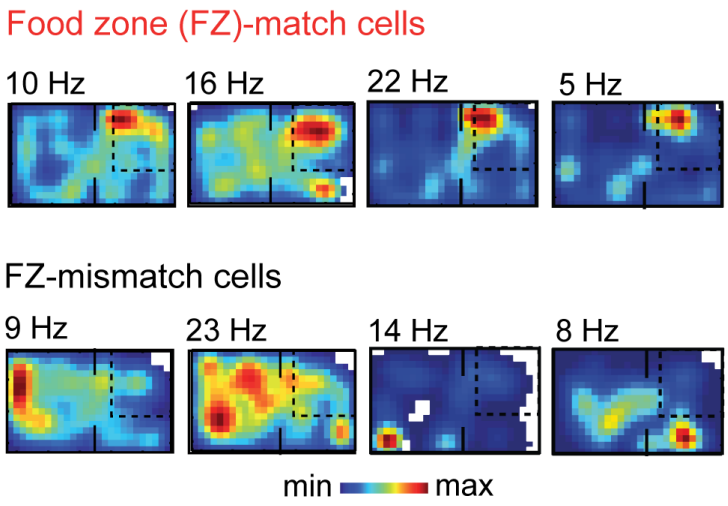

Figure 4.7 Examples of firing maps of LH neurons in the free feeding setup and their maximal firing rates. Black square in upper right corner represents the food zone. Up: neurons which fire preferentially in the food zone (FZ-match cells), bottom: neurons which are preferentially active outside the food zone (food zone mismatch cells).
Modified from (Carus-Cadavieco, Gorbati et al. 2017).

From the analyzed LH neurons, 32 were classified as FZ-match and 52 were FZ-mismatch. From the total number of units recorded in Vgat-Cre mice expressing ChETA in LH, i.e. potentially photo-identifiable LH neurons, 41% of recorded cells (60 out of 146) were identified as Vgat neurons, based on their rapid response to laser pulses during stimulation epochs (as described in section 3.7.2). Vgat neurons were preferentially active either inside or outside the food zone, which has also been corroborated by (Jennings, Ung et al. 2015). 13 of them were classified as FZ-match, and 21 were classified as FZ-mismatch (full distribution of FZ-matching indexes of Vgat cells is shown on Figure 4.18). Thus, in a free feeding context, LH_{Vgat} neurons also display behavior-dependent activity, and within their population there are functional subgroups.

4.3.1 Optogenetic stimulation of LH_{Vgat} cells significantly increases food intake

To determine a causal role of LH_{Vgat} neurons in regulating aspects of feeding behavior, food intake was compared during baseline and stimulation epochs in the free feeding

paradigm. For this purpose, Cre-dependent opsins ChETA or eNPAC 2.0 were expressed in the LH of Vgat-Cre mice, and blue light (473 nm) was delivered at 20 Hz to the LH. Because amount of food intake in spontaneous conditions is variable across different individuals, within-animal comparisons were performed for analysis in this section and the next one. Behavioral effect upon optostimulation did not differ in mice expressing ChETA compared to mice expressing eNPAC 2.0 (Mann-Whitney test, P=0.09; ChETA: n=13 exp., N=3 mice; eNPAC2.0: n=10 exp., N=2 mice), therefore both groups were analyzed together. Two-way ANOVA, with factors 'experimental subject' and 'experimental group' (control light vs opsin stimulation) revealed a significant effect of the experimental group on food intake ($F_{3,72}$= 6.5, P=0.0006). Subsequent tests revealed that number of consumed pellets was significantly increased during LH_{Vgat} stimulation compared to baseline (Wilcoxon test, P=0.0078) but not in control sessions (Figure 4.8 A) (Wilcoxon test, P=0.23). LH: n= 23 exp., N=5 mice; control: n=25 exp., N=7 mice. To investigate whether optogenetic stimulation of LH_{Vgat} cells could have a differential behavioral effect depending on the nutritional state of the animal at the beginning of the experiment, experiments were divided according to the number of pellets eaten during the baseline. Optostimulation of LH_{Vgat} neurons at 20 Hz significantly increased food intake also when the mice were satiated: consumed <3 pellets (<60 mg) during the baseline recording (Figure 4.8 B). Two-way ANOVA with factors 'experimental subject' and 'stimulation type' revealed a significant effect of the optogenetic stimulation on food intake increase over the baseline ($F_{1,32}$=12.9, P=0.0016; LH: n=16 exp., N=5 mice; control: n=17 exp., N=6 mice).

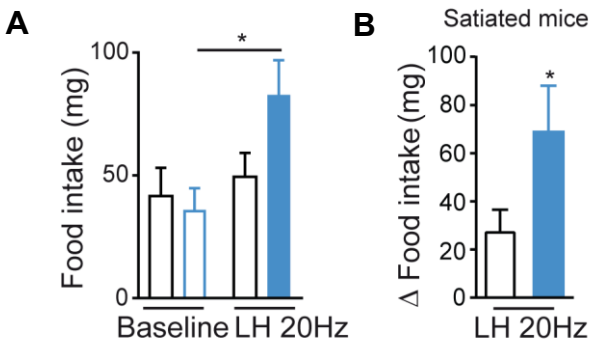

Figure 4.8 Optogenetic stimulation of LH_{Vgat} cells mediates food intake. **A** Optogenetic stimulation of LH_{Vgat} neurons at 20 Hz significantly increased amount of food intake * P= 0.0078 (LH 20 Hz versus baseline), P= 0.23 (control stimulation versus control baseline) **B** also in a subset of experiments in which the mice were satiated during the baseline, * P= 0.0016. Modified from (Carus-Cadavieco, Gorbati et al. 2017).

4.3.2 Optogenetic inhibition of LH_{Vgat} cells decreases food intake in food-deprived mice

To further confirm that the activity of LH_{Vgat} neurons is important in mediating food intake, the somata of LH_{Vgat} cells from Vgat-Cre mice expressing the opsin eNPAC 2.0 were optogenetically inhibited in the free feeding paradigm. Prior to the beginning and during the course of the experimental sessions, the mice were food deprived (see methods). To better assess the effect of hunger in this paradigm, only sessions in which mice consumed more than 3 pellets in the baseline were included for analysis. Likewise, the number of pellets consumed during inhibition epochs was averaged, and compared with the number of pellets eaten during baseline before optogenetic manipulation. N-way repeated measures ANOVA with factors 'experimental subject', 'type of optical stimulation' (inhibition vs control light) and 'experimental epoch', revealed a significant effect of the effect of 593 nm light inhibition ($F_{1,66}$=13.2, P=0.0005), and of experimental epoch ($F_{1,66}$=19.6, P=0.00004), Figure 4.9.

Subsequent Tukey test indicated that optogenetic inhibition with 593 nm light significantly reduced the number of consumed pellets compared to control light sessions (Figure 4.9, P=0.0003) and compared to the baseline (P=0.0007). LH: n = 12 experiments, N = 3 mice; baseline: n = 12 experiments, N=3 mice.

Thus optogenetic inhibition of LH_{Vgat} cells decreases food intake despite food deprivation, providing further confirmation of the role of this neuronal population in mediating food intake.

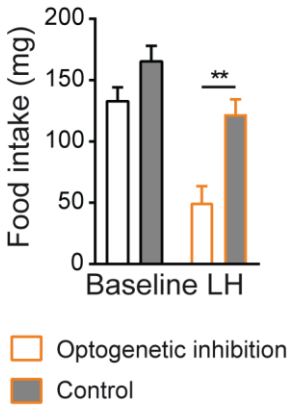

Figure 4.9 Optoinhibiton of LH_{Vgat} cells decreases food intake in food-deprived mice. Optogenetic inhibition of LH_{Vgat} neurons (orange open bar) significantly decreases food intake in food-deprived mice compared to control light and compared to the baseline, N=3 mice, ** P=0.0003, ** P=0.0007 respectively.
Modified from (Carus-Cadavieco, Gorbati et al. 2017).

4.4 Firing of LH cells displays rhythmicity at gamma frequencies

During electrophysiological recordings in behaving mice during the free feeding paradigm, spontaneous gamma oscillations could be observed (Figure 4.10). These could be seen in the raw traces of unitary recordings, as intermittent, spindle-shaped envelopes that lasted several tens of milliseconds, and were usually embedded in slower rhythmic cycles. Further inspection of autocorrelograms of sorted units from the baseline of those recordings revealed that this gamma-frequency activity could also be observed in the spiking patterns of some units (Figure 4.10).

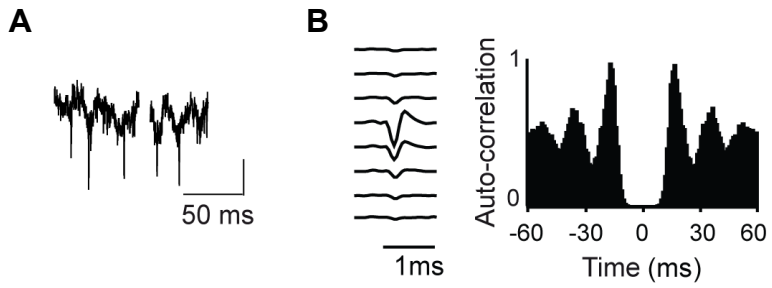

Figure 4.10 Firing of LH neurons displays rhythicity at gamma frequencies.

A Wide-band signal trace showing gamma oscillations in LH and spikes locked to troughs of gamma oscillations. Scale bar: 0.2 mV. **B** Example of a sorted LH unit. Average spike waveforms (left) and the corresponding auto-correlogram (right), during the baseline. Bin width, 1 ms, note the prominent rhythmicity of the discharge every 20 ms, which is indicative of gamma oscillatory activity at ~50 Hz.
Modified from (Carus-Cadavieco, Gorbati et al. 2017).

4.4.1 LH cells firing related to LH gamma phase

Next, the timing of LH neurons' firing during spontaneous locally recorded gamma oscillations was analyzed. Given the broad range of frequencies withinthe gamma band, and to investigate if cells would display different dynamics within the slower or the faster range, gamma oscillations were detected in 30-60 Hz, and 60-90 Hz range(Colgin, Denninger et al. 2009). 291 neurons fired during slow gamma, and 290 during fast gamma. The majority of LH cells displayed high firing probability preferentially at the trough of the spontaneous LH gamma oscillations cycle (Figure 4.11) for both 30-60 Hz and 60-90 Hz gamma. However, approximately a quarter of LH neurons were inhibited at the trough and fired during the rising phase of the LH gamma oscillation (Figure 4.11).

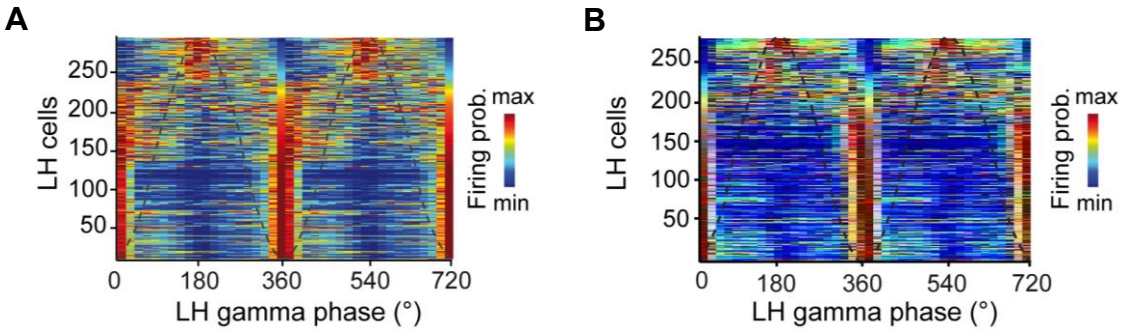

Figure 4.11 Timing of LH neurons firing during LH gamma oscillations. **A** Firing probability of individual LH neurons in behaving mice during fast LH gamma (60-90 Hz, n=290 cells). Color scale normalized firing probability for each neuron. **B** Firing probability of individual LH neurons during slow LH gamma oscillations (30-60 Hz, n=291 cells).
Modified from (Carus-Cadavieco, Gorbati et al. 2017).

Neuronal excitability at the trough is characteristic of discharge timing being controlled by local oscillatory inhibition (Csicsvari, Jamieson et al. 2003). Hence these results suggest that the activity of a subgroup of LH neurons during gamma oscillations might be organized by extra-LH inputs.

4.4.2 LH gamma oscillations during food intake and food seeking

In order to understand whether LH gamma oscillations correlate with different innate behaviors, LFP gamma power in behaving mice was analyzed in the free feeding paradigm. For this purpose gamma power was compared during food approach and during feeding itself, which represent two important sides of food intake, in mice implanted with wire array in LH. Food approach epochs were defined based on extraction of LED tracking mice's position in the setup. For a precise assessment of feeding epochs in these experiments, mice were continuously observed and trains of TTL pulses were manually sent to the recording system every time mice were actively consuming a pellet. This provides timestamps for eating behavior and helps to prevent false positives, which the food detection system could sometimes give, for example, signal from pellet removal by the mouse, without its real consumption). LFP gamma power during spontaneous oscillations in LH was decreased during feeding compared to food approach (Figure 4.12).

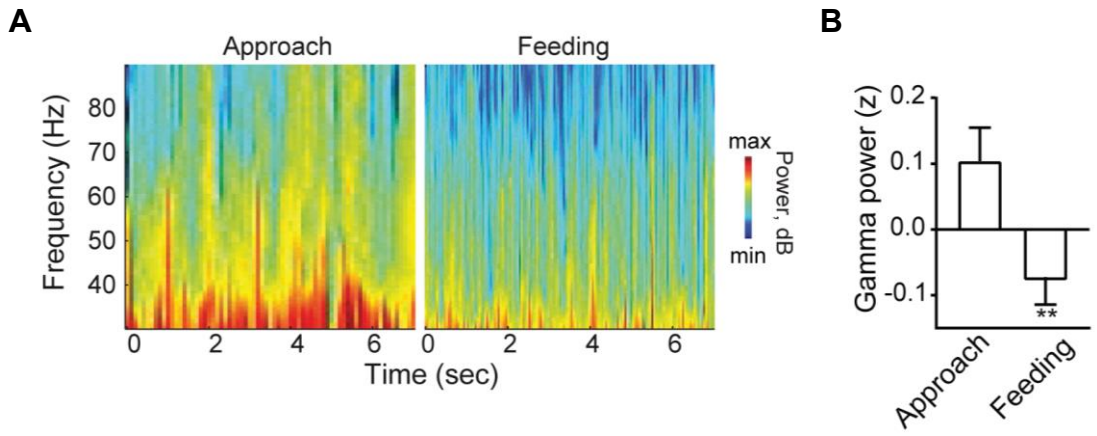

Figure 4.12 Gamma oscillations in LH during food approach and food intake.

A Example of representative spectrograms (30-90 Hz band) computed from spontaneous LFP in LH in the course of food approach and feeding in the same experimental session, power is scaled from minimum to maximum across both plots. **B** Power of LH LFP gamma oscillations (mean±sem) during feeding compared to food approach, ** P=0.0088.
Modified from (Carus-Cadavieco, Gorbati et al. 2017).

Repeated ANOVA with factors 'gamma frequency band' (30-60 Hz and 60-90 Hz) and 'state' revealed a significant reduction of gamma power during food intake compared to food seeking: N=3 mice, $F_{1,1035}$=6.9, P=0.0088.

These data suggest that changes in gamma oscillatory activity in LH are related to behavioral changes (from food seeking to feeding).

4.5 LH cells during spontaneous exploration

In order to characterize the activity of LH cells during spontaneous locomotion, their firing rates were analyzed during the baseline of silicon probe recordings within the free feeding model, in the innate behaviors setup. From 17 recorded LH cells (N=1 mouse), 11 of them (65%) displayed locomotion-dependent activity, since they increased their firing rate with the onset of locomotion, and preserved increased discharge during spontaneous running (Figure 4.13, Pearson's correlation, firing rate versus running speed, P<0.05) (Figure 4.13).

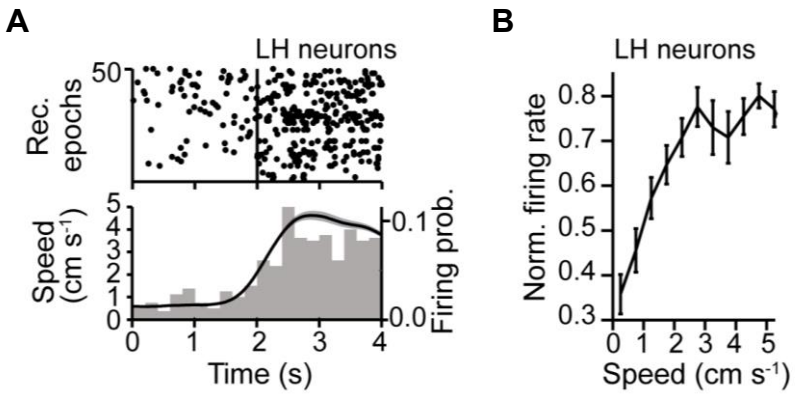

Figure 4.13 LH neurons activity during spontaneous locomotion. **A** Examples of running onset-triggered rastergrams of LH neurons (Top, 50 epochs, ordered according to firing rate) and spike count and average running speed for the same epochs (Bottom, grey bars and black line, respectively). **B** Changes in firing rate of LH neurons, according to running speed. Modified from (Bender, Gorbati et al. 2015).

4.6 LH and LS display coordinated gamma oscillations

Given that the dorsal and caudal part of the LS provides prominent inhibitory inputs to the LH, which were found to be involved in movement (Bender, Gorbati et al. 2015) and neuroendocrine functions (Singewald, Rjabokon et al. 2011) and that these represent an important connection between the hypothalamus and cortical regions, the coordination between LS and LH within the free feeding paradigm was investigated, which is described in the following section.

4.6.1 LH cells firing related to LS gamma phase

To study the coordination between the LS and LH, spontaneous neuronal firing and LFP were recorded in both regions, as mice freely explored the innate behaviors setup. As described for LH in section 4.4, LFP in LS and LH displayed prominent gamma oscillations. Figure 4.14 A shows the firing probability of LS and LH cells during the LS gamma oscillation phase (60-90 Hz). Gamma phases were computed for data samples when action potentials were emitted for each recorded cell and firing phase histograms were calculated.

Rayleigh test revealed that cells discharge in both regions significantly changed according to the gamma oscillation phase (LS: n=68 cells, N=42 recordings, N= 3mice, P=0.00005; LH: n=126 cells, n=11 recordings, N=5 mice P=0.00006). Figure 4.14 B shows firing probability of LH neurons according to the LH gamma oscillation phase (60-

90 Hz), (n=290 LH cells, n=25 recordings, N=5 mice, Rayleigh test, P<0.00001). Discharge of 57% of LH cells was phase-locked to gamma oscillations, Rayleigh test, p<0.05 for each cell.

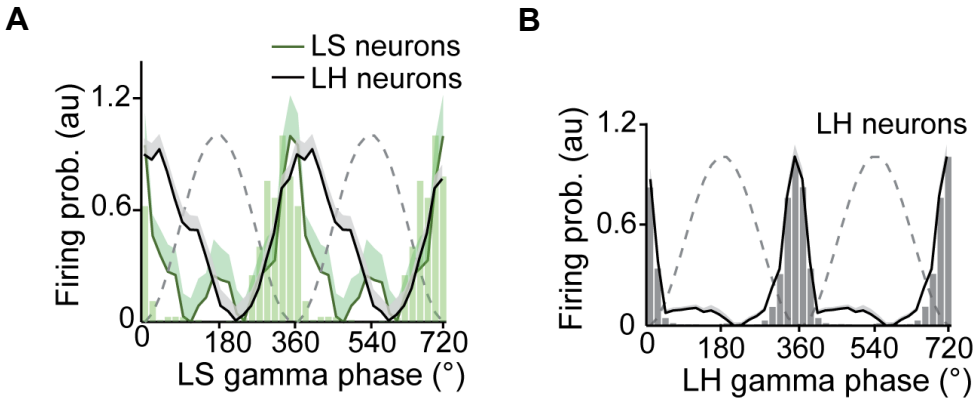

Figure 4.14 Gamma oscillations coordinated between LS and LH. **A** Coordinated firing of LS and LH cells during gamma oscillations (60-90 Hz) recorded in LS, LS cells, P=0.00005; LH cells: P=0.00006. **B** Firing of LH cells changed according to the gamma oscillations phase recorded in LH, P<0.00001, N=5 mice).
Bar histograms display firing probability of representative cells in LS and in LH.
Modified from (Carus-Cadavieco, Gorbati et al. 2017).

4.6.2 LS GABA cells projections to the LH

To visualize LS GABAergic projections in the LH, two constructs were expressed in the same Vgat-Cre mouse: ChETA-eYFP was expressed in LH to label LH_{Vgat} neurons, while ChR2-tdTomato was expressed in the caudal portion of the LS (see 3.2 for coordinates). In agreement with the literature (Risold and Swanson 1997; Risold and Swanson 1997b), strong GABAergic projections from the caudal portion of the LS were visualized in the LH, in the same area where LH_{Vgat} neurons are located (Figure 4.15).

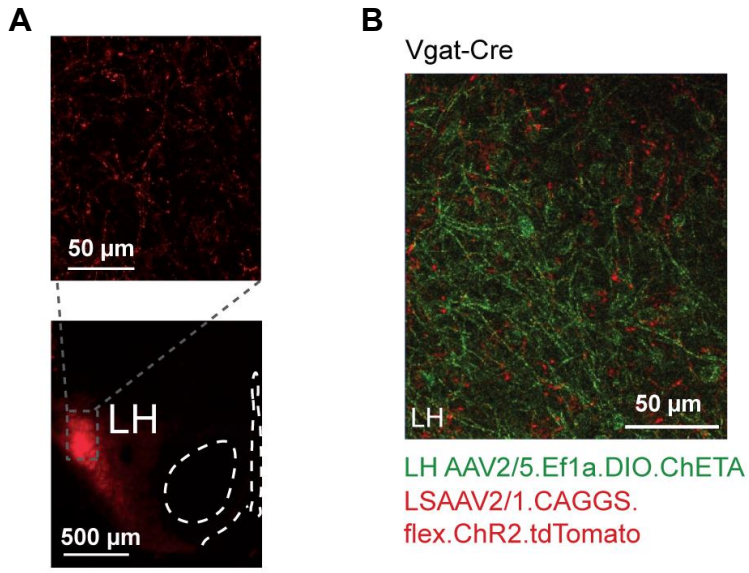

Figure 4.15 LS GABAergic projections in LH. **A** Coronal section showing LS GABAergic projections in LH. **B** Photomicrograph of the same mouse showing ChR2-tdTomato-expressing LS_{Vgat} fibers in LH (red fluorescence) and ChETA-YFP-expresing LH_{Vgat} neurons. Note that some LH neurons are not labelled (black circles) suggesting that LS GABAergic axons contact non-Vgat LH cells as well.
Modified from (Carus-Cadavieco, Gorbati et al. 2017).

4.6.3 Optogenetic stimulation of LS-LH projections

Because LS sends prominent GABAergic projections to the LH, and both regions display coordinated gamma oscillations, the possible role of these inputs in synchronizing neuronal activity in LH was investigated. To do so, ChETA was targeted to LS GABA cells in Vgat-Cre mice, or to the somatostatin-positive population of LS GABA neurons (LS_{Sst}).

Optogenetic stimulation of LS projections in LH at gamma frequency efficiently entrained the majority of the neurons (72.5%) and induced gamma oscillations in the LH (Figure 4.16).

To investigate the effect of LS gamma inputs on the oscillatory activity of LH neurons, LH neurons were recorded while stimulating LS-LH GABAergic terminals at gamma frequency. The response of each recorded LH cell to the LS-LH stimulation was then quantified by calculating CCGs for each neuron using the timestamps of light pulses as trigger. In order to avoid spurious peaks in the CCG at the stimulation frequency, only every second timestamp was included. To estimate the increase in the cell's response, a reshuffled CCG was computed using the same laser times, shifted to the baseline epoch of the recording (before stimulation, no light).

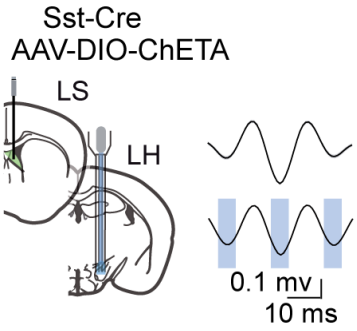

Figure 4.16 Optogenetic stimulation of LS_{Sst}-LH projections at gamma frequency elicits gamma oscillations in LH. An example of average optogenetically induced and frequency-matched spontaneous LH gamma LFP, recorded from one Sst-Cre mouse expressing ChETA in LS and implanted with wire array and optic fibers in LH.
Modified from (Carus-Cadavieco, Gorbati et al. 2017).

Then power spectra of the response of every cell were created by subtracting the power spectrum of the reshuffled-baseline CCG from the power spectrum of the stimulation CCG (Figure 4.17 B). The significance of a difference between the maximal power ±5 Hz around the stimulation frequency and the mean power for all gamma frequencies was estimated for each cell from the normal cumulative distribution function ($P<0.001$ – significant, $P\geq0.05$ – non significant).

Then the firing probability during the trough of spontaneous gamma oscillations was investigated for both ‘responsive’ and ‘non responsive’ to the LS-LH optogenetic stimulation cells. First, a whole phase histogram was calculated showing the convolved difference in firing probability between responsive and non-responsive neurons, to better visualize diversity between the two groups (Figure 4.17 C). Firing probability was normalized for each cell (to prevent a possible bias due to rate variability across the different cells) by the division of spike count in each phase bin by the total number of spikes. Two-way ANOVA, with factors ‘frequency of the spontaneous gamma' (30-60 Hz vs. 60-90 Hz) and ‘response to the LS-LH stimulation' (responding vs. non-responding) revealed that, both for slow and fast gamma ($F_{1,149}=1.7$, $P=0.19$), LH cells rhythmically responding to the optogenetic stimulation of LS-LH projections fired with a significant lower firing probability during troughs of spontaneous gamma oscillations compared to LH cells, not entrained by the LS input ($F_{1,149}=7.5$, $P=0.007$; responding cells, n=61, not responding cells, n=15) (Figure 4.17 D). Pearson correlation revealed

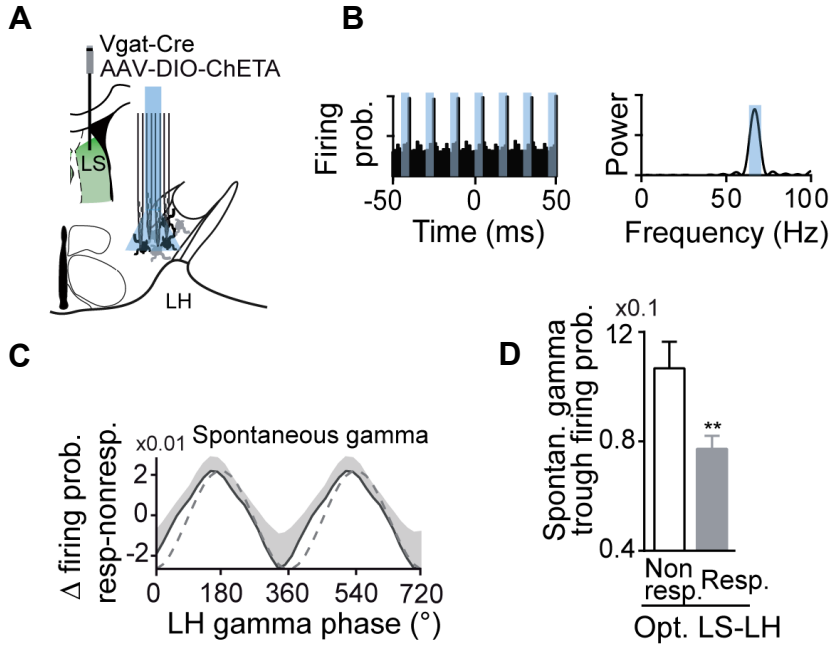

Figure 4.17 Identification of LH cells responsive to LS GABAergic inputs. **A** Optostimulation and recording scheme of LS_{Vgat}-LH projections and identified LH cells, responsive (grey) and non-responsive (black) to LS gamma-rhythmic input. **B** Example of a cell, firing of which was modulated by the LS-LH stimulation: cross-correlogram with laser pulse onsets (top) and its power spectral density. **C** Differences of firing probability between populations of responsive and non-responsive LH neurons according to gamma phase. **D** Firing during troughs of spontaneous gamma oscillations of LH cells, entrained (resp.) vs. non-entrained (non-resp.) by subsequent LS-LH optostimulation (** P=0.007).
Modified from (Carus-Cadavieco, Gorbati et al. 2017).

that the stronger an LH neuron is entrained by LS input, the less likely it displays firing preference at the trough, r=0.85, p=0.007.

These results suggest that the phase-offset that a subset of LH cells display (approx. ¼, see Figure 4.11) during spontaneous gamma oscillations, is mediated by LS inhibitory inputs.

4.6.4 LS inputs enable temporal separation of functionally defined LH neurons

In order to better understand the effect of LS inputs on LH neurons, the relationship between the different timing of neuronal discharge from LH cells during gamma oscillations and their feeding-related activity was investigated. With this purpose, the activity of the FZ-match cells and FZ-mismatch cells (section 4.3) across spontaneous gamma cycle was analyzed. Figure 4.18 A and B show the firing probability of FZ-match and FZ-mismatch cells, respectively, during spontaneous gamma oscillation in LS, as well as the firing probability of LS neurons. FZ-match cells appeared to prominently

reduce their firing during the gamma oscillation trough, when LS cells showed maximal firing, and LH is then mostly influenced by LS inhibition (Figure 4.18).

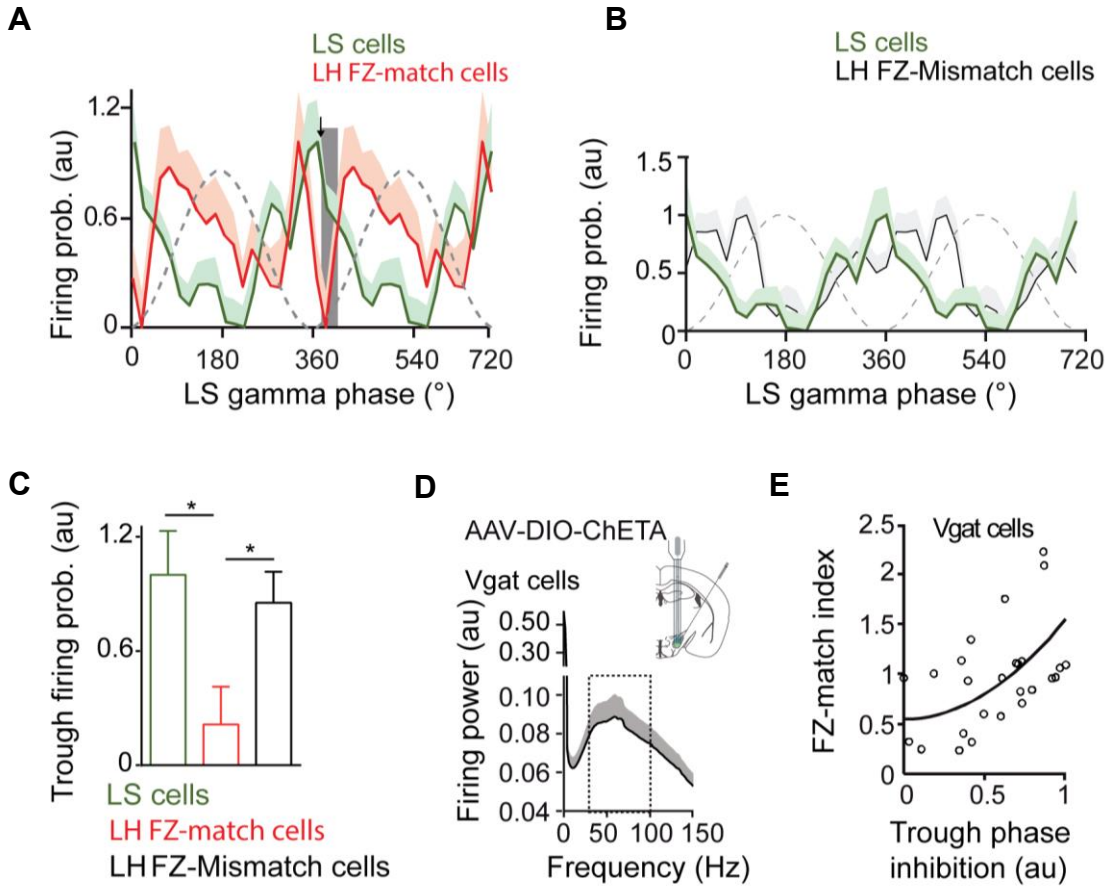

Figure 4.18 Firing of functionally identified LH neurons during gamma oscillations. **A,B** Changes of firing probability of LS and LH FZ-match cells during spontaneous LS gamma oscillations (30-60 Hz, LS: n=69 cells, LH: n=37 cells). **A** LH FZ-match cells were inhibited at the trough of spontaneous gamma oscillation. Arrow - maximal firing of LS cells, grey shade – phases corresponding to time of monosynaptic delay after LS cells discharge (<2 ms); data bins marked by the arrow (for LS cells) and the grey shade (for LH cells)_were analyzed in panel C. **B** LH FZ-mismatch cells displayed high firing probability at the trough of the spontaneous gamma oscillation 30–60 Hz, n= 55 cells. **C** Firing probability of LH FZ-match cells but not FZ-mismatch cells was significantly reduced upon maximal firing of LS cells, * P<0.05. **D** Firing of optogenetically identified LH_{Vgat} cells (n=60) displayed increased rhythmicity at gamma frequencies in behaving mice. **E** Association of inhibition during the gamma trough with FZ-match index in optogenetically identified LH_{Vgat} cells (30-60 Hz, n=26 cells, Pearson's correlation, r=0.49, P=0.012).
Modified from (Carus-Cadavieco, Gorbati et al. 2017).

FZ-match cells fired with higher probability during the following rising phase of the gamma cycle (Figure 4.18 A).

On the contrary, FZ-mismatch cells appeared to fire with high probability at the gamma trough (Figure 4.18 B), which is characteristic for control of discharge timing by local oscillatory inhibition. This temporally-separated signaling of LH FZ-match and FZ-

mismatch populations according to the LS gamma (30-60 Hz) oscillation phase is quantified in Figure 4.18. Data bins marked by the arrow (for LS cells) and the grey shade (for LH cells, trough phases corresponding to time of monosynaptic delay after the maximal LS cells discharge, <2 ms) were analyzed. To facilitate comparisons between cell groups, a relative probability of discharge across all phases in each cell was computed by normalizing individual unit phase histograms by the total number of spikes in each histogram, computing group averages and scaling them from 0 to 1. T-tests revealed that FZ-match but not FZ-mismatch cells reduced their firing during the gamma oscillation trough phases (Figure 4.18), adjusted α=0.0167, FZ-match vs. FZ-mismatch cells: t=2.5, P=0.014; FZ-match vs. LS cells: t=2.6, P=0.0102; FZ-mismatch vs. LS cells: t=0.5, P=0.60; FZ-match: n=37, FZ-mismatch: n=55, LS: n=69 cells. In previous sections it was shown that LS axons in LH innervate the same area were LH_{Vgat} neurons are found (Figure 4.15), and that the activity of these LH_{Vgat} neurons controls food intake (Figure 4.8 and Figure 4.9). To further investigate how the signaling separation during gamma phase driven by LS inputs affects the activity of LH neurons involved in feeding, the oscillatory responses of genetically defined LH_{Vgat} cells were analyzed. The firing of optogenetically identified LH_{Vgat} neurons during baseline epochs of recordings in the free feeding paradigm in behaving mice, displayed a maximum of rhythmicity at gamma frequencies (Figure 4.18 D). Interestingly, analysis of their feeding-related activity revealed that part of the Vgat neurons are FZ-match cells, whereas other Vgat cells are FZ-mismatch cells. Next, the firing of LH_{Vgat} cells during spontaneous gamma oscillations was investigated, and how their signaling in the gamma cycle related to their feeding activity (FZ-match index). Consequently with the results in Figure 4.18 C, Vgat cells that were more active outside the food zone (low FZ-match index), fired more during the trough of spontaneous gamma oscillation (Figure 4.18 D). On the contrary, Vgat cells with preferential firing inside the food zone (high FZ-match index), displayed stronger inhibition during the trough of spontaneous gamma oscillation. The inhibition is scaled from 0 to 1, computed as 1-x complement of firing probability, x, within ±18° from the trough. (n=26 cells, Pearson correlation: r=0.49, P=0.012).

These results suggest that gamma oscillatory inputs from the LS to LH, enable precise temporal separation of LH_{Vgat} cells signaling; based on their feeding-related activity, rather than on their neurochemical identity.

4.7 Behavioral effects of gamma rhythmic stimulation of LS-LH projections

In addition to local field potential and unitary data, behavioral data were recorded in order to address whether gamma oscillatory inputs from the LS to the LH could causally regulate aspects of food seeking and feeding behavior. For this purpose, the excitatory opsin ChETA or the dual opsin variant eNPAC 2.0 was expressed in the population of LS somatostatin-positive GABAergic neurons (LS_{Sst}), since this population projects strongly to the LH (Risold and Swanson 1997; Risold and Swanson 1997b), in Sst-Cre mice. Blue light (473 nm) was delivered bilaterally in LH or unilaterally in LS at 67 Hz, in order to stimulate LS_{Sst} cells and their projections in the gamma range.

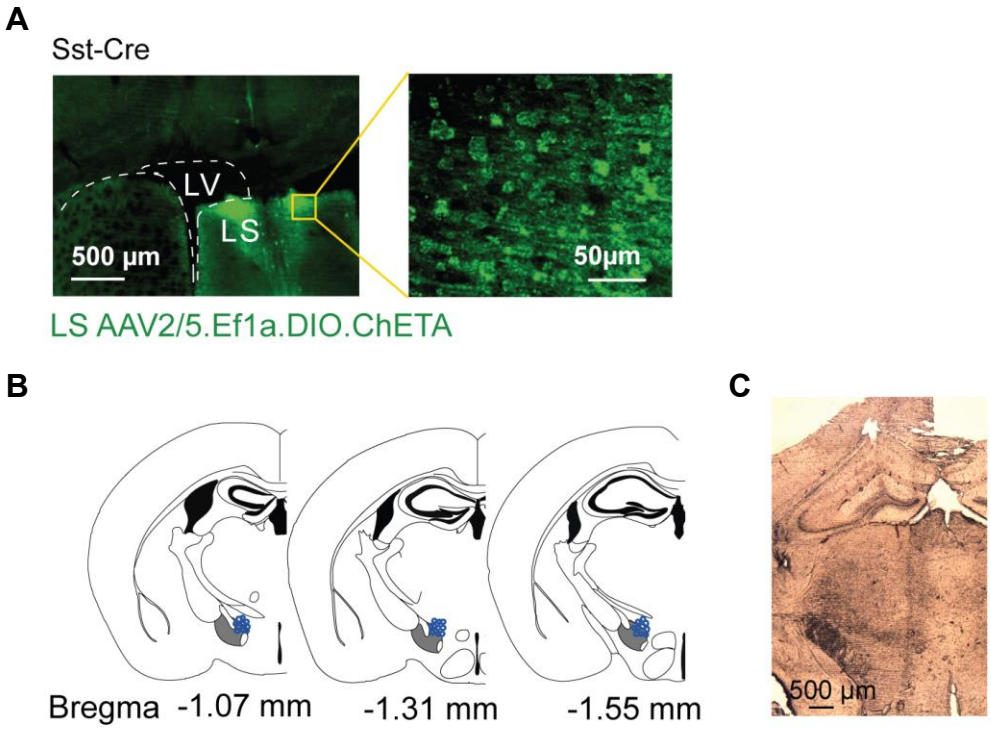

Figure 4.19 Targeting of LS_{Sst}-LH projections. **A** Photomicrograph of a coronal section showing Sst ChETA-expressing cells in the LS of a Sst-Cre mouse; right: higher magnification of the same picture **B** Hit maps of fibers termination sites (blue circles) in LH; ten representative sites for a given bregma position, representing the whole range of termination positions from the experiments described in the following sections, are shown. Reconstruction was made based on implantation coordinates and visualization of tracks left by the optic fibers. **C** Photomicrograph of a coronal brain hemisection from a Sst- Cre mouse, showing the track left by one of two bilateral fibers implanted in the LH.
Modified from (Carus-Cadavieco, Gorbati et al. 2017).

4.7.1 Gamma-rhythmic optogenetic stimulation of LS_{Sst} pathway significantly decreases latency to reach the food zone

In the initial set of experiments designed to explore the LS_{SSt} pathway described here, all opsin-expressing mice were also subjected to sham stimulation sessions (control light), to enable within-animal comparisons and ensure that the visible blue light emitted during stimulation per se was not affecting the behavior. This was done by attaching dummy ferrules to the laser patchcord, which in turn was attached beside the implant, to prevent delivery of light inside the brain but to have the same intensity of visible light than in the optogenetic experiments as described in (Goshen, Brodsky et al. 2011).

For each experiment, the first visit of the mouse to the food zone or the control zone after the stimulation onset was detected. Latency to enter each zone was defined as the time (in seconds), between the beginning of optogenetic or sham stimulation and the first entry of the mouse in a zone in which the animal stayed there for at least 1 sec. Trials in which the mouse was already in the food or the control zone at beginning of the stimulation epoch were excluded from the analysis. ANCOVA, with a fixed factor 'type of optical stimulation' (LS_{Sst}, LS_{Sst}-LH or sham stimulation) and a covariate 'distance to the food zone', revealed that optostimulation of LS_{Sst} somata and LS_{Sst}-LH projections at 67 Hz significantly decreased the time needed to reach the food zone upon stimulation onset compared with control light sessions (Figure 4.20 A) ($F_{2,68}$=7.6, P=0.001; Post-hoc Tukey tests: LS_{Sst} vs. control stimulation, P=0.0017, LS_{Sst}-LH vs. control stimulation, P=0.016; LS_{Sst}: n=18 exp., N=5 mice; LS_{Sst}-LH: n=25 exp., N=6 mice; control: n=29 exp., N=5 mice).

Gamma frequency stimulation of LS_{Sst} cells and LS_{Sst}-LH projections did not significantly change the latency to reach the control zone. ANCOVA, $F_{2,34}$=1.2, P=0.31;LS_{Sst}: n=18 exp., N=5 mice; LS_{Sst}-LH: n=25 exp., N=6 mice; control: n=29 exp., N=5 mice (Figure 4.20 B).

Interestingly, latency to enter the drinking zone during LS_{Sst} cells and LS_{Sst}-LH projections 67 Hz stimulation was not significantly changed, ANCOVA $F_{2,54}$=0.8, P=0.47; LS_{Sst}: n=16 exp., N=4 mice; LS_{Sst}-LH: n=18 exp., N=6 mice; control: n=24 exp., N=5mice (Figure 4.20 C). This result suggests that gamma oscillatory activity of this pathway might specifically regulate approach to food. Optogenetic stimulation of LS_{Sst} cells and LS_{Sst}-LH projections at 67 Hz did not change the amount of time the mice spent in food zone, ANCOVA $F_{2,69}$=2.3, P= 0.1075; LS_{Sst}: n=21 exp., N=5 mice; LS_{Sst}-LH: n=25 exp., N=6 mice; control: n=27 exp., N=5 mice (Figure 4.20). No significant

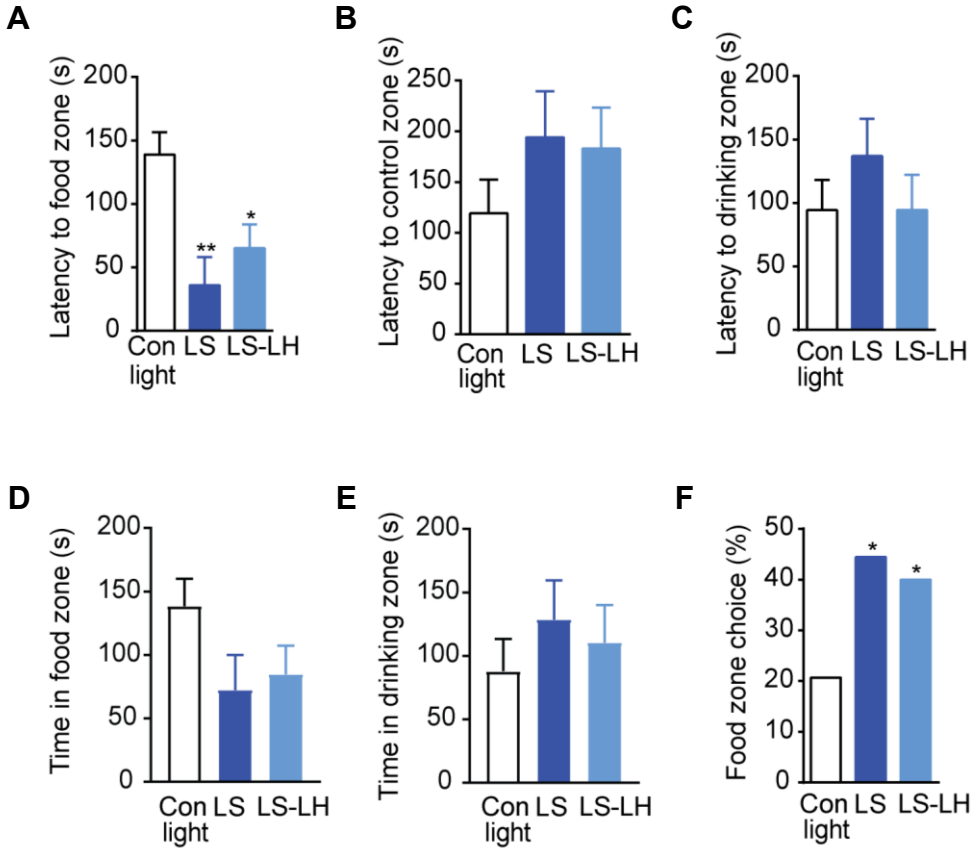

Figure 4.20 Optogenetic stimulation of LS_{Sst} and LS_{Sst}-LH at gamma frequency decreases latency to reach food zone. **A** LS_{Sst} optostimulation or LS_{Sst}-LH projections stimulation (LS_{Sst}-LH stim.) at gamma frequency (67 Hz) significantly reduced latency to enter the food zone, ** P=0.0017, * P= P=0.016, **B** but did not affect latency to enter a control zone (**C**) or the drinking zone. **D** LS_{Sst} or LS_{Sst}-LH stim. did not significantly change the time spent in the food zone (**E**) neither was changed the time inside the drinking zone. **F** LS_{Sst} or LS_{Sst}-LH stim. significantly increased fraction of trials where an animal visited food zone prior to other 3 corners of the enclosure * P<0.05.

difference was found in the amount of time spent in the drinking zone, upon stimulation of LS_{Sst} cells and LS_{Sst}-LH projections at gamma frequency, ANCOVA $F_{2,54}$= 0.5325, P= 0.59; LS_{Sst}: n=16 exp., N=4 mice; LS_{Sst}-LH: n=18 exp., N=6 mice; control: n=24 exp., N=5 mice (Figure 4.20 E). Gamma-rhythmic stimulation of LS_{Sst} cells and LS_{Sst}-LH projections also significantly increased the probability of entering the food zone prior to food-free zones located in other corners of the setup (Figure 4.20 F). Binomial test revealed that stimulation of LS_{Sst} cells and LS_{Sst}-LH projections increased the fraction of trials where an animal visited the food zone before other 3 corners of the enclosure: LS_{Sst} vs. control stimulation, P=0.0199, LS_{Sst}-LH vs. control stimulation, P=0.0248; LS_{Sst}: n=18 exp., N=5 mice; LS_{Sst}-LH: n=25 exp., N=6 mice; control: n=29 exp., N=5 mice). Together

with the previous results, this indicates a role of gamma frequency activity of LS_{Sst} pathway in mediating goal-oriented behavior, specific for food seeking.

4.7.2 Non-gamma-rhythmic optogenetic stimulation of LS_{Sst} pathway

In order to control that specifically gamma oscillations and not synchronization within other slower frequency band were responsible for these behavioral effects, experiments with 5 Hz stimulation epochs were performed, and the same parameters were analyzed. Optogenetic stimulation of LS_{Sst} cells and LS_{Sst}-LH projections at non-gamma frequency did not affect approach to the food zone (Figure 4.21 A). ANCOVA, with a fixed factor "type of optical stimulation" (LS_{Sst} somatic, LS_{Sst}-LH projections and control blue light stimulations) and a covariate "distance to the food zone" ($F_{2,28}$=0.6, P=0.56; LS_{Sst}: n=9 exp., N=5 mice; LS_{Sst}-LH: n=12 exp., N=4 mice; control: n=11 exp., N=4 mice).

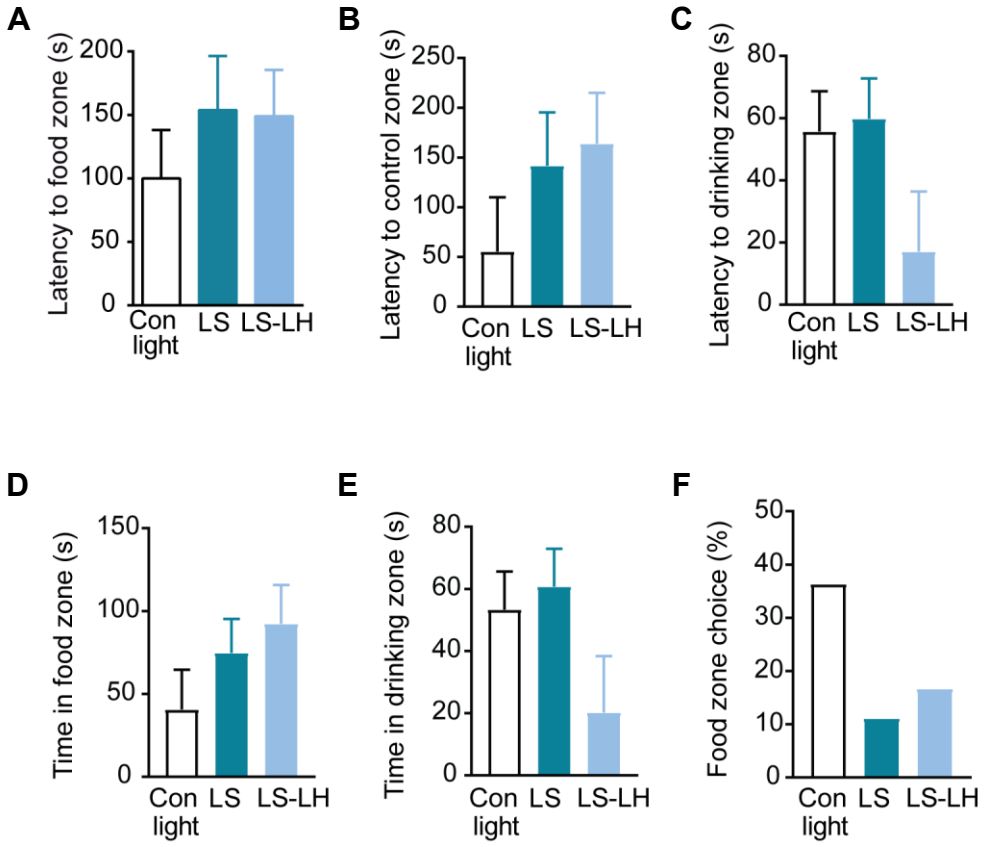

Figure 4.21 Optogenetic stimulation of LS_{Sst} and LS_{Sst}-LH at non-gamma frequency does not affect latency to reach food zone. **A** LS_{Sst} or LS_{Sst}-LH stim. at non-gamma frequency (5 Hz) did not affect latency to enter the food zone compared to control light (**B**) and did not affect latency to enter a control zone (**C**) or the latency to visit the drinking zone. **D** LS_{Sst} or LS_{Sst}-LH stim. at 5 Hz did not significantly modify the time spent in the food zone (**E**) or drinking zone. **F** LS_{Sst} or LS_{Sst}-LH stim. at non-gamma frequency (5 Hz) did not significantly changed the probability of entering the food zone before other 3 zones of the enclosure.

Latency to get to the control zone was not significantly changed during optogenetic stimulation at 5Hz of the LS_{Sst} pathway (Figure 4.21 B). ANCOVA, ($F_{2,15}$=1.12, P=0.35; LS_{Sst}: n=6 exp., N=4 mice; LS_{Sst}-LH: n=7 exp., N=6 mice; control: n=6 exp., N=3 mice). Optostimulation of LS_{Sst} cells and LS_{Sst}-LH projections at non-gamma frequency did not significantly change the latency to reach the drinking zone (Figure 4.21 C). ANCOVA, ($F_{2,23}$=1.82, P=0.18; LS_{Sst}: n=11 exp., N=4 mice; LS_{Sst}-LH: n=5 exp., N=4 mice; control: n=11 exp., N=4 mice). Optogenetic stimulation of LS_{Sst} cells and LS_{Sst}-LH projections at 5 Hz did not significantly change the amount of time the animals spent in the food zone, ANCOVA $F_{2,25}$=1.1288, P=0.3393; LS_{Sst}: n=11 exp., N=4 mice; LS_{Sst}-LH: n=9 exp., N=6 mice; control: n=9 exp., N=3 mice (Figure 4.21 D). Non-gamma frequency stimulation of LS_{Sst} cells and LS_{Sst}-LH projections did not affect the amount of time mice spent in the drinking zone, ANCOVA $F_{2,23}$=1.773, P=0.1915; LS_{Sst}: n=11 exp., N=4 mice; LS_{Sst}-LH: n=5 exp., N=4 mice; control: n=11 exp., N=4 mice (Figure 4.21 E). Consequently, stimulation of the LS_{Sst} pathway at 5Hz did not change the probability of visiting the food zone prior to other 3 food-free corners of the enclosure upon the onset of the stimulation (Figure 4.21 F). Binomial tests: LS_{Sst} vs. control stimulation, P=0.17, LS_{Sst}-LH vs. control stimulation, P=0.23; LS_{Sst}: n=9 exp., N=5 mice; LS_{Sst}-LH: n=12 exp., N=4 mice; control: n=11 exp., N=4 mice.

4.7.3 Gamma-rhythmic optogenetic stimulation of LS_{Sst} pathway does not affect feeding behavior

Together with exploratory parameters, the amount of food intake was analyzed, by comparing the number of pellets eaten during baseline and stimulation epochs. Given the wide range of projections of the LS to other brain structures (which could also be involved in locomotion or exploratory behaviors), only the effect of stimulation on feeding behavior of the specific LS_{Sst}-LH projection was analyzed here. In contrast to the promotion of food seeking, optogenetic stimulation of LS_{Sst}-LH at 67 Hz did not significantly change food intake over time (Figure 4.22 A). Two-way ANOVA with factors ‘type of optical stimulation’ and ‘time’ ($F_{1,119}$=2.3, P=0.13; LS_{Sst}-LH: n=16 exp., N=6 mice; control: n=17 exp., N=4 mice).

Food with a high content of fat is known to be more rewarding than standard food, and a high caloric diet can lead to overeating (Johnson and Kenny 2010; Berland, Cansell et al. 2016). To investigate if gamma rhythmic activity of LS_{Sst}-LH circuit could induce food consumption that is specific for palatable calorie-rich food, experiments in which the mice had free access to high-fat food were done. These experiments did not have a baseline (see methods 3.6), to exclude the possibility that mice would be satiated after eating

high-fat food in the pre-stimulation epoch, which could obscure a possible effect of the optogenetic stimulation. Two-way ANOVA, with factors 'experimental subject' and 'type of optical stimulation (optogenetic stimulation vs control blue light stimulation)', did not reveal differences in amount of high fat food consumed during the session (Figure 4.22 B) ($F_{1,19}$= 0.3, P=0.54; optogenetic stimulation: n=12 exp., N=5 mice; control: n=13 exp., N=5 mice).

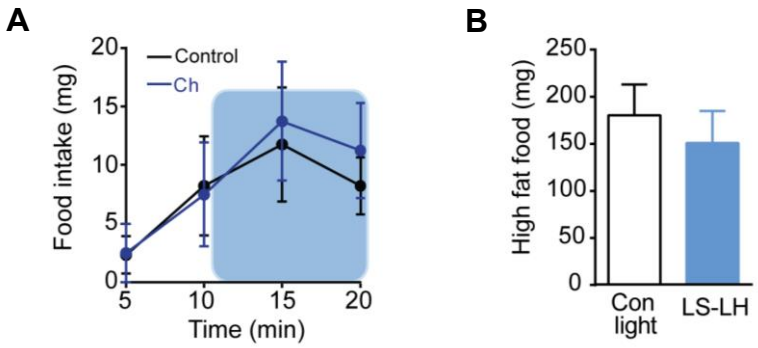

Figure 4.22 Optogenetic stimulation of LS_{Sst}-LH projections at gamma frequency does not increase food intake. **A** Food eaten (mg) during baseline and stimulation epochs of control light (black) or optogenetic stimulation of LS_{Sst}-LH at gamma frequency performed in the same animals. **B** Amount of high-fat food (60% energy from fat) consumed within 20 min upon optogenetic LS_{Sst}-LH projections at gamma frequency or control light stimulation.
A modified from (Carus-Cadavieco, Gorbati et al. 2017).

Together with the previous results, these indicate that gamma oscillatory activity of LS_{Sst}-LH projections facilitates food seeking, but does not influence food intake, neither of standard food nor of energy-dense palatable food. These findings are in accordance with the ones from the analysis of gamma power in LH during food approach and food consumption (section 4.4.2).

Driven by the interesting behavioral results obtained in the first set of experiments that explored the influence of gamma oscillatory activity of the LS_{Sst} pathway in different aspects of feeding behavior, new subsets of experiments were designed, with the aim of further confirming the role of this circuit in promoting food seeking without having a real physiological need of consuming food. These experiments were focused in the LS_{Sst}-LH projection and are described in the following section.

Controls using sham stimulation with dummy ferrules provide very useful information since they enable comparing how behavioral parameters change upon optogenetic stimulation within the same individual, while simultaneously controlling the presence of optic fibers implants. It is also very common in the field to use as a control group animals injected with fluorophore-only AAVs that are implanted with optic fibers in the same brain

regions as in the opsin-expressing mice. This allows to control the virus injection and to account for the non-specific effects of light on the tissue. Therefore, Sst-Cre mice were injected with a Cre dependent YFP-AAV in the LS (Figure 8.2), and implanted with bilateral optic fibers in LH, to be used as external controls.

In the statistical analysis of the previous section, it was taken into account that several experiments were performed in each individual (an animal was used as a factor in ANOVA, as in Tye et al 2011). Because these are dependent samples, data from this subset of experiments were averaged first within an animal, and then statistically compared between YFP and opsin groups using the t-test.

4.7.4 Gamma frequency stimulation of LS_{Sst}-LH projections promotes food seeking

Given that optogenetic stimulation started after 10 min baseline, independently of the animal's position in the behavioral enclosure at that moment, one of the objectives of this subset of experiments was to further reinforce that the facilitation of food approach was not dependent on the mice's initial location. With this purpose, in each experiment the latency to reach the food or control zone upon stimulation onset was normalized to the average latency required to enter the same zone from the same distance during the baseline.

Gamma-frequency stimulation of LS_{Sst}-LH projections significantly decreased the time to reach the food zone in ChETA-expressing but not in YFP-expressing mice (Figure 4.23 A). Opsin: N=10 mice, YFP: N=8 mice, t-test, t_{16}=4.5, P=0.0004. Repeated ANOVA revealed no influence of food intake during baseline (sated: ≤20 mg; non-sated: >20 mg) on the latency to enter the food zone during LS_{Sst}-LH stimulation: $F_{1,22}$=2.1, P=0.17, therefore indicating that stimulation of this pathway at gamma frequency induces food seeking independently of the nutritional state. Latency to enter the control zone did not significantly differ between the opsin: N=8 mice and the YFP: N=7 mice, groups: t-test, t13=-1.0, P=0.33 (Figure 4.23 B). Latency to enter the drinking zone was not significantly different between the opsin: N=9 mice and the YFP: N=6 mice, groups, t-test, t_{13}=0.5, P=0.62 (Figure 4.23 C). In according with the previous experiments, gamma optogenetic stimulation of the LS_{Sst}-LH projections significantly increased the probability of visiting the food zone before visiting other food-free zones located in other corners of the behavioral setup, opsin: n=40 exp., N=12 mice; YFP: n=33 exp., N=8 mice, binomial test, P=0.0047 (Figure 4.23 D).

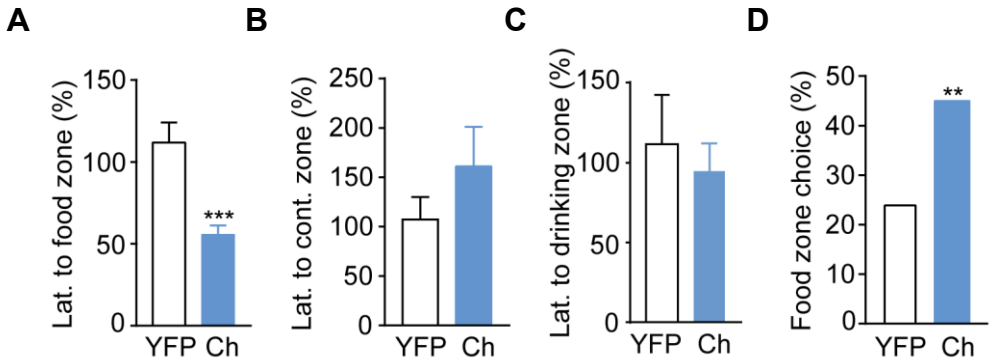

Figure 4.23 Gamma frequency stimulation of LS_{Sst}-LH projections drives food seeking. **A** LS_{Sst}-LH stim. at gamma frequency (67 Hz) with excitatory opsin ChETA (Ch) significantly reduced latency to enter the food zone compared to YFP controls, *** P=0.0004 (**B**) but did not affect the time required to enter the control zone (**C**) or the latency to visit the drinking zone. **D** LS_{Sst}-LH stimulation at 67 Hz significantly increased the probability of visiting first the food zone instead of food-free corners of the enclosure, ** P=0.0047.
Modified from (Carus-Cadavieco, Gorbati et al. 2017).

4.7.5 Non-Gamma frequency stimulation of LS_{Sst}-LH projections

Another important point here was to further demonstrate that specifically coordination between LS_{Sst}-LH through gamma oscillations and not in other frequencies, drives food seeking. In the initial experiments, 5 Hz stimulation was used as a frequency control stimulation, which did not induce any significant change in food-seeking behavior. However, stimulation with pulses of 5 ms at 5 Hz involves 13 times fewer light pulses in the brain than stimulation with pulses of 5 ms at 67 Hz. Therefore, the higher stimulation intensity rather than the frequency could be responsible for the facilitation of food approach. To control for this possibility, a new non-gamma frequency stimulation protocol was designed, that matched in light intensity the 67 Hz one. This consisted of pulses of 4 ms at 167 Hz, repeated at 9 Hz (theta frequency).

Non-gamma-frequency stimulation of LS_{Sst}-LH projections did not affect the latency to reach the food zone in ChETA-expressing mice compared to YFP-expressing mice, opsin: N=7 mice, YFP: N=8 mice, t-test, t_{13}=-0.4, P=0.70 (Figure 4.24 A). Consequently, the probability of visiting the food zone prior to food-free corners upon non-gamma optogenetic stimulation of the LS_{Sst}-LH projections was not significantly changed, opsin: n=30 trials, N=8 mice, YFP: n=33 trials, N=8 mice, binomial test, P=0.52 (Figure 4.24 B). These results further confirmed the specific importance of gamma frequency in driving food seeking.

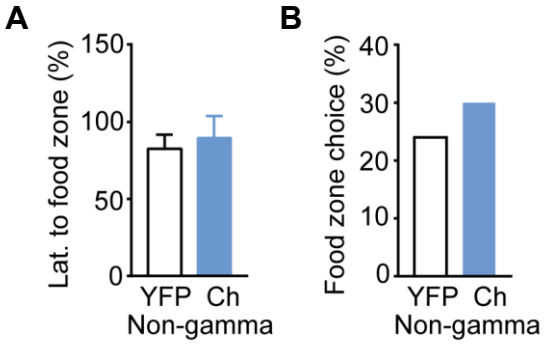

Figure 4.24 Non-gamma optogenetic stimulation of LS_{Sst}-LH projections does not affect food seeking. **A** LS_{Sst}-LH stim. at non-gamma (theta) frequency, intensity-matched protocol, did not affect the latency to reach the food zone (**B**) or change the fraction of trials in which an animal visited the food zone prior to the other three corners of the enclosure.
Modified from (Carus-Cadavieco, Gorbati et al. 2017).

4.7.6 Gamma frequency stimulation of LS_{Sst}-LH projections does not affect food intake

The amount of food consumed upon gamma-frequency optogenetic stimulation of LS_{Sst}-LH projections was also compared between ChETA-expressing mice and YFP-expressing mice. Stimulation of LS_{Sst}-LH axons at 67 Hz did not affect intake of standard food: opsin: N=9 mice, YFP: N=8 mice, t-test, t_{15}=-0.3, P=0.8, (Figure 4.25 A). Consequently with the previous experiments, the amount of high-fat food consumed during optostimulation of LS_{Sst}-LH projections at gamma frequency was not significantly different between the two groups, opsin: N=6 mice, YFP: N=7 mice, t-test, t_{11}=0.04, P=0.97 (Figure 4.25 B).

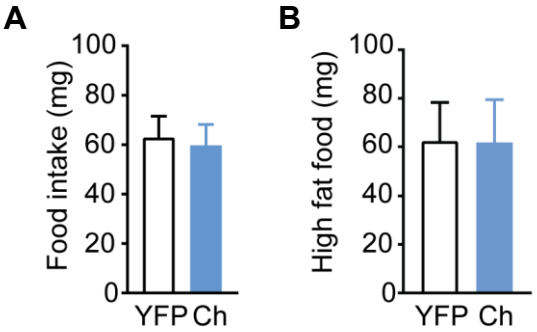

Figure 4.25 Gamma frequency optogenetic stimulation of LS_{Sst}-LH projections does not affect food intake. **A** LS_{Sst}-LH optostim. did not change food intake of standard pellets. **B** Amount of

high-fat food (60% energy from fat) in mg consumed per 10 min upon LS_{Sst}-LH stimulation at 67 Hz.
Modified from (Carus-Cadavieco, Gorbati et al. 2017).

These results corroborated the initial ones, and emphasized the role of this pathway in promoting seeking which is specific for food, but without inducing or inhibiting food intake.

4.7.7 Reinforcing properties of the LS_{Sst}–LH

Given the role found for LS_{Sst}-LH pathway in driving food seeking, and that stimulation of the LS has been reported to have rewarding properties (Olds and Milner 1954; Cazala, Galey et al. 1988), the reinforcing properties of this circuit were also investigated. To do so, Sst-Cre mice expressing ChETA in LS and YFP expressing mice were tested in an optical self-stimulation assay, in which every active nose poke of a mouse resulted in the delivery of laser pulses at gamma frequency in LH (see methods section 3.6). No significant difference was found in the number of nose pokes between the two groups, opsin: N=4 mice, YFP: N=4 mice, Mann Whitney-test, P= 0.9429, (Figure 4.26 A). However, even if photo-activation of the LS_{Sst}-LH circuit did not induce active self-stimulation, this does not completely exclude the possibility that activation of this circuit might still have rewarding properties in a different context.

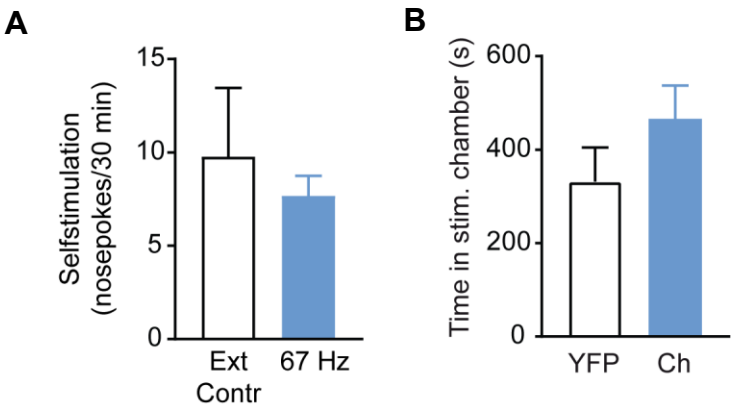

Figure 4.26 Gamma frequency optogenetic stimulation of LS_{Sst}-LH projections did not elicit self-stimulation or place preference. **A** Gamma-rhythmic optogenetic stimulation of LS_{Sst}-LH projections did not significantly change the number of responses in the self-stimulation assay. Mean±SEM number of nosepokes across the different sessions, averaged within mouse. **B** Time spent in the photo-stimulation paired chamber was not significantly different between YFP and opsin groups, upon optogenetic stimulation of LS_{Sst}-LH projections at 67 Hz.
B Modified from (Carus-Cadavieco, Gorbati et al. 2017).

To further explore reinforcing effects of these projections, mice were tested in a real-time place preference paradigm. Cre-dependent opsins ChETA or eNPAC 2.0 were

expressed in the LS of Sst-Cre mice, and blue light (473 nm) was bilaterally delivered at 67 Hz to the LH in the photostimulation-paired chamber. Behavioral effect upon optostimulation did not differ in mice expressing ChETA compared to mice expressing eNPAC 2.0 (Mann-Whitney test, P=0.38), therefore both groups were analyzed together. Optogenetic stimulation of excitatory-opsin-expressing LS_{Sst}-LH projections at 67 Hz did not result in a significant preference for the photostimulation-paired chamber of the enclosure compared with YFP-expressing controls, opsin: N=7 mice, YFP: N=7 mice, t-test, t=1.321, P=0.21 (Figure 4.26 B).

5 Discussion

5.1 Methodological considerations and limitations

This study combined the use of high density in vivo electrophysiological recordings with optogenetics in behaving mice, in order to characterize and manipulate the activity of LH neurons and their coordinated activity with other brain regions across different behaviors. This methodological combination, including recently developed opsin constructs (ChETA, eNPAC2.0) and silicon probe electrodes, represented an innovative approach to better understand the LH circuitry and its associated functions. Specific considerations and limitations are addressed in the following section

5.1.1 Experiments with ChETA

From a total of 56 recorded units in LH across the sleep/wake cycle, 22 out of them (39%) were optogenetically identified as presumable Vgat neurons. And from a total of 146 LH units recorded Vgat-Cre mice transduced with ChETA in LH during the free feeding paradigm, 60 out of them (41%) were phototagged as Vgat cells. LH_{Vgat} neurons could be phototagged using optostimulation, Vgat ChETA-expressing neurons reliably responded to the laser pulses with very short latency (<10 ms). In the same area, in addition to Vgat cells and intermingled with them, also MCH and Hcrt/Orx neurons can be found, and these three molecularly defined populations do not overlap (Jennings, Ung et al. 2015). Thus, given the neuronal heterogeneity of the region, the use of ChETA provided a good targeting of LH_{Vgat} population. Waveforms of LH_{Vgat} spikes evoked with optogenetic stimulation did not differ of waveforms of spontaneous spikes fired during the baseline. In addition, histological verifications showed that the expression of AAV DIO-ChETA-eYFP was high and restricted to the lateral hypothalamic area.

The use of ChETA efficiently enabled the use of stimulation protocols with high frequencies including: pulses of 5ms at 67 Hz for manipulation of gamma oscillations; and bursts at 167 Hz of 4 ms pulses that repeat every 9 Hz, for non-gamma control stimulation protocol. Although ChR2 can very efficiently control neuronal firing up to 40-50 Hz (Yizhar, Fenno et al. 2011; Zhang, Vierock et al. 2011), for optogenetic stimulation with such high frequencies ChETA represents a better alternative (especially if response of individual neurons to fast stimulation will be assessed), since it can reliably drive spike trains up to at least 200 Hz without the occurrence of spike doublets and plateau potentials (Gunaydin, Yizhar et al. 2010). Further, the mutation E123T makes the action spectrum of ChETA slightly more red-shifted (20-nm compared with wild type ChR2),

which can potentially improve tissue recruitment with the use of a deeper-penetrating light (Gunaydin, Yizhar et al. 2010). This could be also beneficial when evaluating responsiveness of cells to the laser pulses, since more neurons might receive light and therefore be excited, especially in a region like LH, where different neuronal types are intermingled forming a reticular-like nucleus.

It should be noted, that cells expressing opsins with faster-off kinetics (like ChETA) present less light-sensitivity within prolonged light stimulation than cells expressing opsins with slower-off kinetics, which can integrate more photons over time at low light powers, since member of the population of opsins in a neuron will accumulate in the open state as light delivery continues (Mattis, Tye et al. 2011). When using fast opsins this can be compensated by increasing the expression levels of the opsin or by increasing the light power and length of the light pulse (Gunaydin, Yizhar et al. 2010; Mattis, Tye et al. 2011).

5.1.2 Experiments with eNPAC

Upon transfection with eNPAC2.0 simultaneous expression of ChR2 and NpHR in the same neuron is achieved, which allows then by using light sources with the corresponding wavelength to excite or inhibit the same cell respectively (Carus-Cadavieco, Gorbati et al. 2017). Stimulation at 20Hz of LH_{Vgat} neurons transduced with eNPAC2.0 within the free feeding paradigm led to an increase in food intake, while inhibition of LH_{Vgat} neurons expressing eNPAC2.0 resulted in a decrease in food intake despite food deprivation. Therefore, eNPAC2.0 allows fast monitoring of behavioral outcomes from a given neuronal population or their projections, since it enables to perform stimulation and inhibition sessions within the same experimental subjects.

In the eNPAC2.0 construct the eYFP is fused to ChR2, which results in a better axonal expression of NpHR, since NpHR-eYFP levels has been reported to experience membrane trafficking problems (Gradinaru, Thompson et al. 2008; Zhao, Cunha et al. 2008), at high expression levels experiences accumulation in the endoplasmic reticulum (Gradinaru, Thompson et al. 2008). NpHR is also not fused to ChR2, which virtually ‘makes the protein smaller’ and facilitates transport to the axon terminals. Indeed, bilateral inhibition of LS_{Sst} projections expressing eNPAC2.0 in LH, reduced gamma oscillations and induced robust behavioral changes in food seeking behavior (Carus-Cadavieco, Gorbati et al. 2017).

However special attention should be paid when selecting wavelengths of light sources when using multiplexed opsins, to avoid spectral overlapping that could prevent independent control of both opsins (Wiegert, Mahn et al. 2017). The opsin NpHR action spectrum displays maximum near 580 nm (Zhang, Wang et al. 2007), while the maximum

of ChR2 is ~460 nm (Nagel, Szellas et al. 2003). Therefore, their spectral separation enables independent activation of the opsins, when using appropriate light sources (Zhang, Wang et al. 2007). Indeed, optogenetic stimulation of eNPAC2.0-expressing neurons during in vitro electrophysiological recordings demonstrated precise bidirectional control of neuronal excitability in the same cells (Carus-Cadavieco, Gorbati et al. 2017). Further, optostimulation or optoinhibition of LH_{Vgat} neurons with eNPAC2.0 elicited robust behavioral effects (increase of food intake and decrease in food intake, respectively), which are in agreement with similar experimental preparations, that used independently ChR2 and NpHR (Jennings, Ung et al. 2015).

Another important consideration is the intrinsinc light requirements and functioning mechanism of the ion pumps halorhodopsins (persistent photon flux is needed for continued ion transport). In vivo optogenetic inhibition strategies use high-power light sources providing constant illumination (Wiegert, Mahn et al. 2017). Nevertheless, the continuous delivery of high-intensity light through an optic fiber can cause heating of the targeted tissue, which by itself can change blood flow and increase firing rates in the local neurons reviewed in (Wiegert, Mahn et al. 2017). Therefore it is particularly essential to measure and adjust the light power output before each session involving optogenetic silencing and use appropriate controls. An additional consequence of the halorohodopsins functional properties is that long-lasting inhibition protocols could potentially affect the cellular ion homeostasis (Wiegert, Mahn et al. 2017). A prolonged activation of halorhopsin can lead to an increase in the intracellular chloride concentration, which can alter the intracellular pH (Wiegert, Mahn et al. 2017), and has been described to induce a depolarizing effect in $GABA_A$ receptors (Raimondo, Kay et al. 2012). Accordingly, experimental protocols need to be carefully planned and tested, in order to avoid unnecessary long inhibition epochs.

5.1.3 Experimental design

Optogenetic manipulations

It could be argued that using optogenetic stimulation of LS projections to manipulate gamma oscillations in LH, would actually result in the manipulation of additional parameters of the circuit, which would be the actual promoters of the observed behavioral effect (e.g. levels of inhibition or the firing rates of certain cells). However, spontaneous oscillations by their nature require the interaction between inhibition and excitation levels that modulate neuronal firing. Thus, it would not be possible to induce or inhibit oscillations in a neural network without manipulating other aspects of the circuit (Sohal 2016). This concern is not exclusive for oscillations or optogenetic manipulations since electrical stimulation or lesions in specific areas can evoke unintentional effects

(Otchy, Wolff et al. 2015). Because of the complex and dynamic nature of the brain, experimental manipulations can always lead to unintended effects that could also probably contribute to the observed results; in a similar way that naturally occurring brain processes leading to a behavioral outcome involve changes in several related parameters.

Targeting GABA cells

When using Vgat-IRES-Cre mice to target GABA neurons, it should be take into account that the molecular nature of LH GABAergic cells is rather complex (see section 1.2.2), and it can be defined by the expression of different markers that do not always overlap (e.g. MCH neurons which are thought to be GABAergic but not Vgat). In addition, there is increasing recognition that Vgat might not be exclusive for loading GABA into synaptic vesicles, and other vesicular transporters such as VMAT2 could be sufficient for GABA release (Tritsch, Ding et al. 2012). Hence the use of Vgat-cre mice to target LH GABA neurons probably does not capture the function of all inhibitory cells in the area (reviewed in (Herrera, Ponomarenko et al. 2017). It is also possible that transgene penetrance in Vgat-IRES-Cre mice may be reduced compared to endogenous Vgat expression in LH, and/or that other GABAergic neurons (like MCH) express really low amounts of Vgat, which in turn could be dynamically regulated (Jennings, Ung et al. 2015).

In vivo electrophysiology

Electrophysiological recordings with movable silicon probes enabled the monitoring and acquisition of a large number of LH and RTN single and multiunits across different behaviors: 56 LH units during sleep/wake recordings, 291 LH units across free feeding paradigm, and 70 RTN units during sleep/wake recordings. One limitation of this approach is that the microdrive should be moved at least once per day (to prevent fixation of the probe to the brain and connective tissue thus it is difficult to study the activity of a given neuron along several days, which could also provide interesting information. Similarly, due to the properties of the probe-microdrive ensemble, location of the electrode might not be exactly the same over long time periods, with any minimal change resulting in the electrode contacting a different neuron. Thus, it is typically difficult to monitor the activity of a given neuron for periods longer than 1-2 hours. Therefore the present study, given the required length of many recording sessions, did not focuse in analyzing the activity of the same particular neurons across all the paradigms over days, but rather concentrated on monitoring statistically representative sets of neurons, participating in different behaviors and transitions. It would be however very interesting for future studies, with different recording lengths or employing alternative recording

methods (e.g. Ca^{2+} imaging), to follow dynamic changes in the activity of given LH neurons in a variety of behavioral paradigms, and over longer time courses.

5.2 LH_{Vgat} cells and arousal

No significant changes in firing rate or in the interspike intervals were found between NREM and wake periods in the LH_{Vgat} population as a whole, however LH_{Vgat} neurons increased transiently their firing rate upon NREM sleep to wake transitions (Figure 4.3). This increase appears to be limited to the state change, which suggests the existence of inhibitory inputs that modulate the acitivity of LH_{Vgat} neurons. One possible circuit providing negative feedback could be a subset of RTN neurons that projects directly to the LH (Barone, Cheng et al. 1994). These RTN cells are able of exerting fast (1.87 +/- 0.23 ms) inhibition on a large population of LH neurons (~ 66 %). Alternatively or simultaneously to this negative loop, when TC cells are disinhibited (see next sections) they can activate RTN neurons through their glutamatergic inputs, providing indirectly negative feedback to TC cells (Steriade 2003; Huguenard and McCormick 2007). These two proposed negative feedback loops would supress the firing of LH_{Vgat} or TC cells, respectively, and avoid uncontrolled hyperactivation of the thalamo-cortical network, which could result in pathological states (like absence epilepsy) (Huguenard and McCormick 2007; Herrera, Carus Cadavieco et al. 2016). In turn, reactivation of LH_{Vgat} neurons can occur due to the activity of local excitatory neurons in LH (e.g., Hcrt/Orx cells) as well as of fibers from the ARAS that project to the LH (Herrera, Carus Cadavieco et al. 2016) (e.g., glutamatergic cells from the parabrachial nucleus and NA neurons from the LC).

Consequently, when LH_{Vgat} cells were optogenetically stimulated during NREM sleep, a fast transition to wakefulness was observed, effect that was quantified by our collaborators Antoine Adamatidis & Carolina Gutierrez-Herrera (Herrera, Carus Cadavieco et al. 2016). This suggests that by transiently increasing their activity, LH_{Vgat} neurons can induce rapid transitions from NREM sleep to wakefulness. However, optogenetic stimulation of LH_{Vgat} cells during REM sleep did not induce any noticeable behavioral transition which indicates that the behavioral response of LH_{Vgat} neurons is selective in mediating arousal from NREM sleep state (Herrera, Carus Cadavieco et al. 2016).

Given the heterogeneity that characterizes the chemical nature of LH neurons, the degree of co-expression of LH_{Vgat} neurons that project to RTN with other markers awaits further investigation. It appears that these LH_{Vgat} population does not contain LepRb-expressing GABA cells (Herrera, Carus Cadavieco et al. 2016), since optogenetic

stimulation of the latter resulted in the opposite behavioral effect, significantly increasing the latency to wakefulness from NREM sleep (Herrera, Carus Cadavieco et al. 2016). It is also unlikely that LH_{Vgat} cells co-express MCH neuropeptide (although many MCH cells are GABAergic) or Hcrt/Orx, since recent studies have shown that these three populations don't overlap (Jennings, Ung et al. 2015), and MCH and Hcrt/Orx expressing neurons send limited projections and/ or fibers of passage to the RTN region (Bittencourt, Presse et al. 1992; Peyron, Tighe et al. 1998). Further, optogenetic stimulation of LH_{MCH} cells has been shown to increase the total duration of REM sleep (Jego, Glasgow et al. 2013; Tsunematsu, Ueno et al. 2014) and in studies, in which mainly the MCH cell cluster located in the zona incerta was optostimulated, both NREM and REM sleep were increased (Konadhode, Pelluru et al. 2013; Blanco-Centurion, Liu et al. 2016).

5.3 RTN neurons

The RTN neurons analyzed in this study displayed a narrow spike waveform (half-trough time, <0.2 ms), which is typical for inhibitory GABAergic cells (Bartho, Hirase et al. 2004), and RTN GABA neurons have been reported to display particularly sharp spikes (Gardner, Hughes et al. 2013; Halassa, Chen et al. 2014).

The majority of the recorded RTN cells (46 out of 70) displayed state-dependent changes, that is, their firing pattern changed from a more irregular firing mode (higher CV) during NREM sleep to a more regular firing mode during wakefulness (lower CV). A subset of RTN neurons (24 out of 70) did not show significant changes in their CV between NREM and wakefulness, hence their firing pattern remains similar through these behavioral changes. This is in agreement with previous studies that have described heterogeneity in the firing properties among RTN neurons, including neurons that are able of switching from bursting to regular tonic firing, and neurons which do not display bursting firing mode (Contreras, Curro Dossi et al. 1992; Lee, Govindaiah et al. 2007), and the switching between bursts and tonic firing being correlated with changes in behavioral state (Fuentealba and Steriade 2005).

Optogenetic stimulation of LH_{Vgat} projections to the RTN (Figure 4.6) decreased the activity of most of the recorded RTN neurons (77%), both of slow and fast spiking neurons, although the inhibition exerted appears to be stronger in cells that fire faster during spontaneous baseline. Interestingly, optogenetic activation of LH_{Vgat} terminals in the RTN replicated the state-dependent changes, that is, it significantly decreased the CV of RTN neurons, making their firing pattern more regular. Finally, consistently with in vivo stimulation of LH_{Vgat} somata during NREM sleep, optostimulation of their axonal projections in the RTN a fast transition from NREM sleep to wakefulness and cortical

arousal was observed, which was quantified by our collaborators Antoine Adamatidis & Carolina Gutierrez-Herrera, as measured by a prominent change in thalamocortical oscillations, with a sudden decrease of the amplitude of <4Hz oscillations (Herrera, Carus Cadavieco et al. 2016).

Taken together, these results suggest that the fast awakening from NREM sleep that occurs upon activation of the LH_{Vgat}-RTN circuit, is associated with a transient silencing of the RTN neurons (see traces in Figure 4.5). This is also indirectly confirmed by the fact that optogenetic silencing of the LH_{Vgat}-RTN circuit increased the length of NREM sleep, and enhanced the amplitude of delta oscillations, and that directly silencing RTN_{GABA} neurons with optogenetics induces arousal from NREM sleep (Herrera, Carus Cadavieco et al. 2016). During transitions from NREM sleep to wake, RTN neurons are transiently inhibited by the increased activity of LH_{Vgat} projections. This inhibition of RTN cells, in turn, results in a progressive disinhibition of TC cells, which would then switch their membrane potential from hyperpolarized to more depolarized. At more depolarized membrane potentials, TC are able to enter tonic firing mode (normally associated with cortical activation), since their low-threshold Ca^{2+} conductance becomes inactivated, resulting in the abolition of sleep-related oscillations. This depolarized state of TC neurons facilitates then the information flow through the thalamus in a way which is consistent with awaken and attentive states (McCormick and Bal 1997).

The slow depolarization of TC cells is also associated with the presence of cholinergic, serotoninergic and norepinephrinergic inputs from the ARAS, and histamine inputs from the hypothalamus, which in parallel, also exert inhibition on the RTN cells (McCormick and Bal 1997). Since the LH also receives projections from the ARAS neurons, it is possible that subcortical inputs are integrated to LH_{Vgat} cells signals in the RTN, which further controls the activity of thalamic centers (Herrera, Carus Cadavieco et al. 2016).

Consequently, the transient hyperpolarization of RTN cells, mediated by the activity of LH_{Vgat} inputs, would prevent them from participating in sleep-related oscillations. Although their low-threshold Ca^{2+} conductances allow them to fire in bursting mode at negative potentials (such as the resting membrane potential), they display a voltage-dependence which is shifted to more positive membrane values than the conductances from TC cells. Hence, a strong hyperpolarization of RTN cells would make them unable to generate the burst firing mode, which is normally associated with their participation in the slow thalamocortical oscillations during NREM sleep. Figure 5.1 displays an scheme of the described circuit.

Interestingly, optogenetic activation of the LH_{Vgat}-RTN circuit did not change the total amount of wakefulness, induced wakefulness was transient, and equal in duration to circadian-matched wake episodes in control animals (Herrera, Carus Cadavieco et al.

2016). While this circuit appears to be important for inducing fast arousal from NREM sleep, probably other arousal circuits are more specialized in consolidating wakefulness.

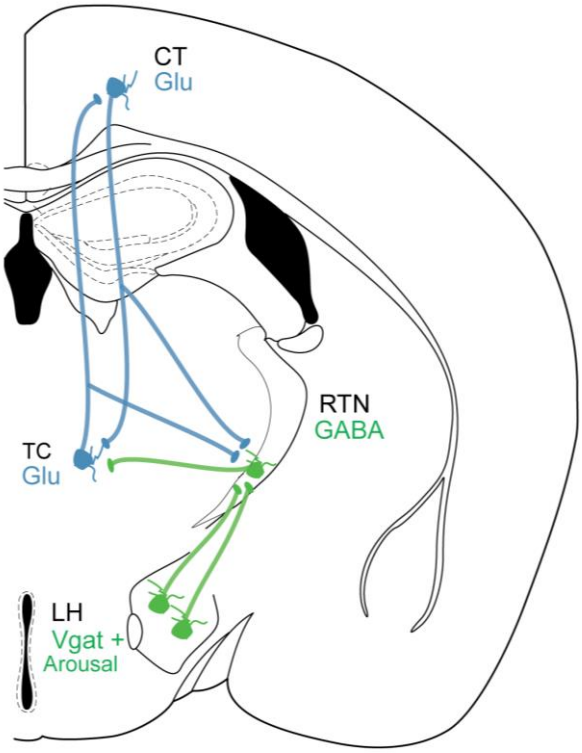

Figure 5.1 Scheme of LH_{Vgat}-RTN-thalamocortical circuit. LH_{Vgat} neurons send inhibitory projections to RTN GABA neurons, which in turn exert inhibition over glutamatergic thalamocortical cells (TC) and glutamatergic corticothalamic cells (TC). TC and CT also provide excitatory inputs to RTN neurons. Therefore, activation of LH_{Vgat} neurons indirectly disinhibits TC and CT cells. The LH_{Vgat}-RTN-thalamocortical circuit constitutes a feed-forward inhibitory circuit, capable of inducing fast arousal from NREM sleep.

It should be noted that LH_{Vgat} neurons in addition to the RTN also project to other brain regions that could be involved in the generation of arousal, as well as that they target other neuronal populations within LH. These regions include the MS, the BF, the Periventricular thalamus (PVf), the VTA, the PAG and the LC (Herrera, Carus Cadavieco et al. 2016). Optogenetic stimulation of LH_{Vgat} terminals in MS did not affect the latency to wakefulness neither from NREM nor from REM sleep. Optogenetic activation of LH_{Vgat} projections to the PVf induced arousal from NREM sleep (but not from REM sleep). However the latency to the behavioral transition was substantially longer compared with the one induced by activation of the LH_{Vgat}-RTN circuit. Optogenetic stimulation of LH_{Vgat} projections to the LC, induced a transition to wakefulness from both NREM sleep and REM sleep (Herrera, Carus Cadavieco et al. 2016). These data suggest that the LH_{Vgat}-RTN circuit is principally involved in fast arousal control, selective from NREM sleep. It

also appears that there might be some functional heterogeinity amongst the LH_{Vgat} population controlling arousal.

5.4 Regulation of food intake by LH_{Vgat} cells

Somatic optogenetic stimulation of LH_{Vgat} neurons at 20 Hz significantly increased food intake, also when mice were satiated. Consequently, optogenetic inhibition of LH_{Vgat} neural bodies decreased feeding in food-deprived mice. These results are in agreement with those published by (Jennings, Ung et al. 2015) and contrast with classical pharmacological studies, in which local injections of GABA agonist in LH mediated a decrease in feeding, while $GABA_A$ antagonists actually promoted food intake in sated rats (Kelly, Rothstein et al. 1979; Bernardis and Bellinger 1996). However in these studies the experimental manipulations affected the whole LH population, promoting a general inhibition of the LH neurons expressing GABA receptors. Hence this could affect the activity of several subgroups of LH related to feeding and metabolism, including Hcrt/Orx, MCH, and LH_{Vgat}.

Due to the wide interconnectivity of LH within the brain, LH_{Vgat} neurons are in a very good position to influence different aspects of feeding behavior. LH_{Vgat} neurons send projections to the hypothalamic paraventricular nucleus (PVN), where they exert inhibitory control, and optogenetic stimulation of this pathway increases feeding (Wu, Kim et al. 2015). Another possible circuit through which LH_{Vgat} cells mediate their effects on feeding, is through projections to the VTA, one of the brain regions that processes reward-related information (Morton, Meek et al. 2014), therefore regulating rewarding aspects of food intake. In (Jennings, Ung et al. 2015) the authors showed that besides promoting feeding, optostimulation of LH_{Vgat} neurons had reinforcement properties as well. Optogenetic activation of LH_{Vgat} neurons that project to the VTA, promotes an increase in sucrose-licking (Nieh, Matthews et al. 2015). Furthermore, optogenetic stimulation of LH_{Vgat} terminals in the VTA at different frequencies evoked differential effects, on feeding (better effects with 5-20 Hz stimulation) and reward (maximal effect with 40 Hz), which could be explained by frequency-dependent corelease of neuropeptides, as described for other neurons (Schone and Burdakov 2012).

5.5 Gamma oscillations coordinated between LS and LH

LH displays gamma oscillations during spontaneous exploration of the mice during the free-feeding paradigm. Furthermore, LH cells can be divided in two groups, according to the timing of their discharge relative to the phase of the LH gamma oscillations: the

majority (3/4) fire during the trough, while approximately ¼ fire during the rising phase and peak (Figure 4.11), and are inhibited during the trough. Thus the second group fire with a phase offset relative to the first group. By stimulating optogenetically LS terminals in LH, it was shown that LH neurons which are more responsive to LS inputs are the same ones that are more inhibited during the trough of the spontaneous gamma oscillations (both slow and fast gamma), while non-responsive cells are the ones that fire preferentially during the trough. This suggests a causal role for LS GABAergic inputs in inhibiting a subset of LH cells, enabling the phase-offset of their discharge; and it is further confirmed by the fact that optogenetic inhibition of LS projections in LH prevented the offset of LH neurons which occurred during the spontaneous gamma oscillations during the baseline, when LS GABAergic inputs were not manipulated (Carus-Cadavieco, Gorbati et al. 2017).

The subset of cells inhibited at the trough fired during the rising phase of the gamma oscillation. The reduction of inhibition is per se a robust trigger leading to spike firing (Hasenstaub, Shu et al. 2005; Fries, Nikolic et al. 2007). Simultaneously incoming excitatory inputs, e.g. from local circuits in the hypothalamus or from other brain structures coinciding with falling inhibition from the LS could be particularly effective in activating this cells.

FZ-match cells reduce prominently their firing during the trough of the spontaneous gamma oscillation and fire with higher probability during the subsequent rising phase of the gamma cycle, while FZ-mismatch cells show high excitability during the trough (Figure 4.18). The latter has been shown to be characteristic of control of discharge timing by local oscillatory inhibition in hippocampal circuits (Csicsvari, Jamieson et al. 2003), thus possibly other entrainment mechanisms (intra-LH inputs) determine activation of FZ-mismatch neurons in gamma troughs. Given that LH is most influenced by LS inhibition at the trough of the gamma oscillation, it appears that LS inputs exert inhibition over FZ-match cells, enabling a temporal separation of their firing relative to the FZ-mismatch cells. This temporal reorganization of subset of cells does not seem to be related to their neurochemical identity but rather to their function, since analysis of the phototagged LH_{Vgat} neurons revealed that their degree of inhibition during the gamma oscillation trough positively correlated with their feeding related activity.

5.5.1 LS-LH gamma oscillations specifically facilitate food seeking

Optogenetic stimulation of LS_{Sst}-LH projections at gamma frequencies induced gamma oscillations in LH and led to a significant decrease of the latency to get to the food zone, i.e. facilitated food seeking, without promoting significant changes in the amount of time spent in the FZ. Furthermore, it increases the probability of choosing to visit the FZ before

other corners of the enclosure. Notably, despite this behavioral outcome it does not affect feeding, since amount of standard or high fat food consumed was not changed. Altogether these data indicate that LS-LH gamma oscillatory input facilitates goal-directed seeking, which is specific for food, since optogenetic stimulation of this pathway at gamma frequency did not change the latency to visit the drinking zone or the time spent there. Given that food is particularly salient for mice (more than water if they are not food or water deprived), the specificity of this circuit in regulating approach to food is further verified since gamma frequency stimulation did not facilitate approach to a novel object (Carus-Cadavieco, Gorbati et al. 2017). Thus, this circuit appears to be specifically involved in food seeking, rather than novelty processing, which depends on other pathways (Takeuchi, Duszkiewicz et al. 2016)

In addition, this facilitation to food approach appears to be independent of the current nutritional state, since LS-LH gamma oscillations did not induce an increase in food intake, and led to food approach in sated mice (mice which did not consume any food during the baseline) as well as in mice who ate during the experiment, which was also in agreement with data from spontaneous recordings, where power of slow and fast gamma in the food zone was not associated with food intake (Carus-Cadavieco, Gorbati et al. 2017).

The necessity of LS-LH gamma oscillations for food-seeking behavior, is further confirmed by the fact that optogenetic inhibition of LS_{Sst}-LH projections during food approach significantly decreases the amplitude of the gamma oscillation in LH (Carus-Cadavieco, Gorbati et al. 2017) and reduces food-seeking behavior: it increases the latency to enter the FZ, and decreases the number of successful entries into the food zone upon entry in the 'approach area', where optogenetic inhibition starts, but without affecting locomotion (Carus-Cadavieco, Gorbati et al. 2017).

Moreover, optogenetic stimulation of the LS_{Sst}-LH pathway at non-gamma frequencies did not replicate any of the behavioral effects observed with 67 Hz stimulation. Neither 5 Hz stimulation nor an intensity-matched stimulation protocol at theta frequency decreased the latency to reach the food zone, or changed the preference of the FZ over food-free corners of the enclosure.

The behavioral effects of LS_{Sst}-LH gamma optostimulation are consistent with findings in electrophysiological recordings in which the mice spontaneously explored within the free-feeding paradigm, which revealed that gamma power in LH was significantly decreased when comparing food approach vs feeding (see Figure 4.12). Further, the power of the gamma oscillations in LS and in LH matched the time required to get to the FZ (i.e. the approach rate), both for slow and fast gamma. However, when moving towards the drinking zone, the power of the slow or fast gamma oscillations in LS or LH was not

related to the approach rate (Carus-Cadavieco, Gorbati et al. 2017). Consequently, the approach rate to a familiar or to a novel object did not relate to the power of the spontaneous gamma oscillations in LH. Altogether these data strengthens the notion that coordination between LS and LH at gamma frequency precisely enables food seeking (Carus-Cadavieco, Gorbati et al. 2017).

The fact that LS-LH gamma stimulation does not affect food intake, appears to contrast with a recent study (Sweeney and Yang 2016), in which chemogenetic and optogenetic activation of Vgat neurons in the septum, as well as activation of their projections to the LH resulted in a reduction of food intake. However, in this study the septal neurons targeted included GABAergic Vgat-expressing neuron in the LS, and in the MS. Both the LS and MS project to the LH, but their cellular architecture and interconnectivity with other brain regions is different (reviewed in section 1.4). Therefore, stimulation of neurons from both regions probably includes also non-Sst septal neuronal populations and recruits the activation of different circuits, with different roles than stimulation of LS_{Sst}-LH pathway (Carus-Cadavieco, Gorbati et al. 2017).

The LS and the LH displayed coordination in the gamma frequency band, both for slow gamma (30-60 Hz) and for fast gamma (60-90 Hz), and the proportion of cells that fire at the trough or at the peak of the ongoing LH gamma oscillation is similar both for slow and fast gamma. LS_{Sst}-LH stimulation during behavioral paradigms that led to food approach was applied at 67 Hz. Because it has been described that neurons can encode information differently during slow and fast gamma (Zheng, Bieri et al. 2016), it could be interesting for future studies to stimulate at slower and faster gamma frequencies, to analyze potential differences in aspects of behavior; and assess how functionally related subgroups of neurons in LH could relate to them.

Upstream circuit

As reviewed in section 1.4, the LS is one of the main outputs of the hippocampus. Furthermore, it receives also prominent excitatory projections (fibers of CaMKIIa expressing neurons) from the mPFC that terminate in the LS (Carus-Cadavieco, Gorbati et al. 2017). The LS and the hippocampus have been previously shown to be coordinated in the theta band (5-10 Hz) (Bender, Gorbati et al. 2015), however they displayed weak coherence at gamma frequencies (Carus-Cadavieco, Gorbati et al. 2017). Interestingly, mPFC and LS were coordinated in the gamma frequency band (Carus-Cadavieco, Gorbati et al. 2017). Further, optogenetic stimulation of mPFC-LS CaMKIIa ChETA-expressing axons at gamma frequency (67 Hz) led to similar behavioral effects related to food approach and food intake than those elicited by optogenetic stimulation of LS_{Sst}-LH projections. Consequently, optogenetic inhibition of mPFC-LS CaMKIIa eNPAC2.0-

expressing fibers recapitulated behavioral effects of LS_{Sst}-LH pathway inhibition (Carus-Cadavieco, Gorbati et al. 2017). In addition, mPFC-LS optogenetic stimulation at gamma frequency improved the performance of the mice in an alternating T-maze paradigm, which represents a cognitive task, by significantly increasing the number of correct trials, and very interestingly improving the temporal stability of performance (Carus-Cadavieco, Gorbati et al. 2017). Taken altogether, these data suggest that this circuit constitutes a top-down pathway, from the mPFC via the LS to the LH, which employs gamma oscillations to regulate and promote goal- directed feeding behavior (Figure 5.2) (Carus-Cadavieco, Gorbati et al. 2017; Narayanan and DiLeone 2017).

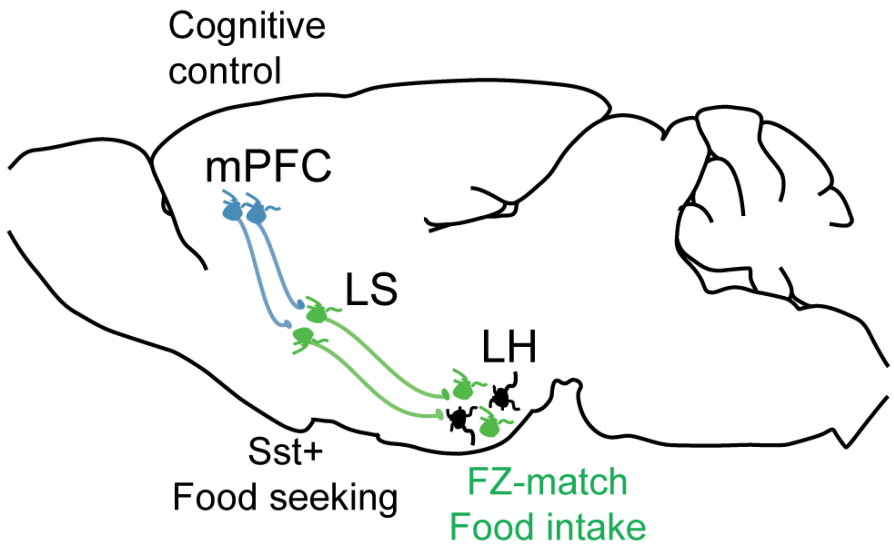

Figure 5.2 Scheme of mPFC-LS-LH top down circuit. This circuit employs gamma oscillations to regulate feeding behavior. mPFC gamma oscillations control temporal precisión of LS gamma rhythms, which in turn, enables temporal separation of signalling of LH neurons which are functionally specialized.

Successful food seeking is actually a complex cognitive task, which requires integration of multiple external and internal signals. Gamma oscillations in the mPFC have been previously associated with cognitive control and attention (Kim, Ahrlund-Richter et al. 2016; Narayanan and DiLeone 2017), therefore these data suggest that coordination of the mPFC-LS-LH circuit at gamma rhythms can underlie cognitive regulation of different aspects of feeding-related behaviors.

5.6 Function-selective coding by LH neurons

Within the free feeding paradigm, the firing of a subset of LH neurons matched the location of the food (FZ-match cells) whereas other LH cells fired preferentially at a distance from the food (FZ-mismatch cells). This suggests the presence of functional neuronal groups in LH, related to their feeding activity, since some of them are able of encoding the location of food. It has been previously shown that the activity of individual unclassified neurons in LH can be differently modulated in response to feeding related information (Ono, Nishino et al. 1981; Ono, Sasaki et al. 1986). From the optogenetically identified Vgat population, part of the LH_{Vgat} are FZ-match (13 out of 60), while part are FZ-mismatch cells (21 out of 60). This is also in agreement with recent studies in which by using Ca^{2+} imaging, subsets of LH_{Vgat} neurons were shown to display increased or reduced activity in environmental locations containing food (Jennings, Ung et al. 2015). Interestingly, despite being composed by different subgroups according to their feeding activity, the clear behavioral outcome upon optogenetic stimulation of LH_{Vgat} cells (which include both FZ-match Vgat and FZ-mismatch Vgat) is an increase in food intake (Jennings, Ung et al. 2015; Navarro, Olney et al. 2016; Carus-Cadavieco, Gorbati et al. 2017). Furthermore, this behavioral effect contrasts with the result of optogenetic stimulation of LS terminals in the same LH area where FZ-match and FZ-mismatch cells can be found, which induces goal-directed food seeking, but no changes in food intake at all. Analysis of intrahypothalamic network responses to these optogenetic manipulations revealed that stimulation of LH_{Vgat} somata (at the same frequency that leads to food intake i.e. 20 Hz) evoked an increase within seconds in the firing rate of FZ match cells, but not FZ-mismatch neurons (Carus-Cadavieco, Gorbati et al. 2017). In contrast, optogenetic stimulation of LS-LH projections at gamma frequency (at 67 Hz, the frequency that facilitates food seeking) led to a fast increase in firing of FZ-mismatch cells rather than FZ-match cells, which could explain why mice approach the food without increasing consumption (Carus-Cadavieco, Gorbati et al. 2017). As discussed in section 5.5, LS-LH gamma rhythmic inputs enables the phase-offset of FZ-match cells. Since part of the FZ-match are Vgat cells, phase-offsetting them could release FZ-mismatch cells from their inhibition, which could result in the elevated firing rates of FZ-match cells within seconds that is observed upon LS-LH stimulation (Carus-Cadavieco, Gorbati et al. 2017).

Further studies are required to determine the identity of FZ-match and FZ-mismatch cells. Besides Vgat neurons, is likely that the FZ-match subset is composed by distinct molecularly defined cells whose activity relates to feeding, e.g. Hcrt/Orx.

5.7 Consummatory and appetitive aspects of feeding

Another interesting observation from these results is that the two modes of circuit recruitment lead to different aspects of feeding behavior: appetitive (food seeking without changes in food intake) and consummatory (increase in food intake). Some Vgat cells are FZ-match while others are FZ-mismatch, which means that probably besides coding a food location subsets of Vgat cells can encode consummatory and appetitive behaviors, respectively. This is in agreement with the results from Jennings 2015, where the authors report that functionally distinct subsets of LH_{Vgat} cells can encode appetitive (cells which were responsive to not-rewarded nosepokes) and consummatory (cells responding to licking) sides of feeding, but seldomly both. It appears that different aspects of feeding behavior, can be mediated by distinct top-down pathways to hypothalamus and its diverse downstream outputs, and very likely by temporal dynamics (Carus-Cadavieco, Gorbati et al. 2017). In the context of the free feeding paradigm, our results suggest that functionally specialized firing of LH neurons appears to be LS input selective. Activation of these inputs at gamma frequencies temporally separates the activity of these specialized neurons, which leads to food approach without affecting consumption, probably due to the preferential activation of neurons mediating appetitive aspects (FZ-mismatch) (Carus-Cadavieco, Gorbati et al. 2017).

As previously described in section 1.2.1 and discussed in section 5.5.1, optogenetic manipulations of other afferents to the LH, like the BNST GABAergic inputs and LS/MS projections affected food consumption. Similarly, dopamine D1R-expressing neurons in the Nucleus accumbens shell (NAcSh, D1R-MSNs neurons), send inhibitory projections to the LH which were shown to control consumption of food by modulating LH GABA neurons activity: optogenetic inhibition of D1R-MSNs neurons extended food intake, while activation of their terminals in LH terminated ongoing ingestion, even in food deprived mice. Direct inhibition of LH GABA cells which receive projections from D1R-MSNs neurons recapitulated these effects (O'Connor, Kremer et al. 2015).

It has been reported in several studies that prolonged activation of LH_{Vgat} cells can lead to an increase in gnawing behavior, even if there is no food available (Jennings, Ung et al. 2015; Nieh, Matthews et al. 2015; Navarro, Olney et al. 2016). This is consistent with observations at early stages of this study, in which upon prolonged optogenetic stimulation of LH_{Vgat} cells at 20 Hz in the absence of food mice displayed chewing motor patterns, typical from consummatory phases of feeding behavior. Direct stimulation of LH_{Vgat} somata recruits the activation of FZ-match cells (Carus-Cadavieco, Gorbati et al. 2017), which through their activity and through their projections to other nuclei mediating consumption regulate this aspect of feeding.

Although optogenetic stimulation of LH_{Vgat} cells can be reinforcing (Jennings, Ung et al. 2015), and that electrical stimulation of LS has been described to be rewarding (Cazala, Galey et al. 1988), stimulation of the LS_{Sst}-LH pathway at gamma frequency did not appear to be rewarding (neither aversive) in a photostimulation paired chamber assay or in a self-stimulation paradigm. However it should be noted that electrical stimulation of LS, will activate all cellular types in the LS, and therefore recruit activation of different downstream nuclei. Gamma signaling within mPFC-LS-LH appears to provide cognitive regulation of food-seeking in non food-restricted mice, and precedes the processing at later stages of the feeding behavioral sequence, which includes activation of metabolic sensors, and neuronal changes related to hunger and gustation (Carus-Cadavieco, Gorbati et al. 2017). Therefore, it could be possible that rewarding properties emerge and/or increase in later stages of appetitive and consummatory phases of the feeding cycle.

Hence, an appropriate and successful feeding behavior requires precise temporal coordination between hypothalamic populations coding for appetitive and consummatory responses.

5.8 Same cell group regulates arousal, locomotion and feeding: multitasking properties of LH cells

In the same line of thought as in the previous section, a further observation from the data analyzed in this study, is that the LH cell population molecularly defined by the expression of Vgat, participates in the regulation of different innate behaviors; such as promotion of arousal from NREM sleep, locomotion, and feeding. From LH recordings across the sleep/wake cycle, 11 out 13 Vgat cells increased their firing rate upon transitions from NREM sleep to wakefulness. In the dataset that was analyzed in the context of locomotion, 11 out of 17 recorded LH units increased their activity upon the onset of locomotion; and 6 out of these were identified as GABAergic cells. In the free-feeding paradigm, from 32 LH cells that were classified as FZ-match, 13 were Vgat, and from 52 LH units that were classified as FZ-mismatch 21 were identified as Vgat. Given that the category of FZ-match and FZ-mismatch are mutually exclusive, there are at least 2 functional cell groups among the Vgat cells, according to their feeding related activity, as previously discussed in section 5.6. It would be interesting for future studies, to analyze to which extent the arousal-promoting Vgat group overlaps with the locomotion-related Vgat population and with the FZ-match or FZ-mismatch cells.

As discussed in the previous section for LH populations regulating appetitive/consummatory aspects of feeding, it is likely that selective coding properties

of LH_{Vgat} subgroups are partly dependent on their different inputs/outputs diagram, which contributes to the multitasking capacities of the whole LH_{Vgat} population (Jennings, Ung et al. 2015; Herrera, Ponomarenko et al. 2017). LS inputs to LH through gamma oscillatory activity, mediate the temporal separation of LH_{Vgat} cells firing according to their feeding related activity, contributing to the division between approach and eating (Figure 4.18, (Carus-Cadavieco, Gorbati et al. 2017). In a similar way, it could also be speculated that different LH_{Vgat} targets could mediate either arousal and/or food intake; e.g. it is unlikely that LH_{Vgat} terminals in RTN which mediate transitions to arousal, also mediate food intake (Herrera, Ponomarenko et al. 2017), but rather other LH_{Vgat} targets do that, such as the ones mentioned in section 5.4.

Two possible mechanisms are proposed in (Herrera, Ponomarenko et al. 2017) for the multitasking actions of LH_{Vgat} cells, regulating sleep and metabolism: sequential multitasking and parallel multitasking. In the sequential conception, LH_{Vgat} would first induce arousal from NREM sleep, and their prolonged activation can promote locomotion (that can lead to the food source) and mediate food intake. In the parallel scheme, the different subgroups of LH_{Vgat} cells would be simultaneously active to produce arousal and food intake during wakefulness. It should be noted that both mechanisms are not mutually exclusive and might take place simultaneously in order to enhance a given behavioral response (Herrera, Ponomarenko et al. 2017)

Thus, the temporal dynamics of specialized subgroups among LH_{Vgat} neurons could also contribute to regulating a successful coordination of innate behaviors. Results from the present study suggest that gamma oscillatory inputs from LS cause a dynamic reorganization of LH neuronal groups, which code for a similar function (Carus-Cadavieco, Gorbati et al. 2017). As reviewed in section 1.8.2, the role of gamma oscillations in coordinating and binding neuronal assemblies that process related information have been described for sensory processing in cortical areas (Singer 1993) and hippocampal circuits (Harris, Csicsvari et al. 2003). In a similar way, coordinated gamma oscillations between LS and LH can bring together on a milliseconds time scale the discharge of LH neurons that code related aspects of feeding behavior, and enabling their temporal separation from neurons that code other aspects of feeding. It could be interesting for future studies to analyse how these assemblies can be dynamically reorganized according to the current physiological need and behavioral states.

Other cell types within LH and in other hypothalamic nuclei have the ability of coordinating different innate behaviors, especially when it comes to sleep and metabolism (reviewed in section 1.2 from the introduction). In order to be successful, food seeking and feeding should occur with sufficient levels of arousal and at the same time the animal should be able to stop eating and engage in locomotion to escape if a

threat (e.g. a predator) appears in the environment (Korotkova and Ponomarenko 2017). Notably, alterations of innate behaviors are not usually isolated. Sleep restrictions lead to an increase in food intake in healthy human adults, when food is available ad libitum, and it also rises the hedonic drive for food. (Broussard and Van Cauter 2016). Eating disorders are often accompanied by changes of locomotor activity, around 80% of anorexia nervosa patients exercise excessively during the acute phase of the disorder, and in fact high-level exercise can be a strong predictor of eating disorders (Davis, Katzman et al. 1997).

5.9 Biological meaning/function of food seeking without real metabolic need

Seeking for food without having a real current nutritional need is a behavior that happens very often in nature and in modern human societies. The purpose of the consummatory side of feeding in the absence of a current necessity is perhaps more apparent. Consumption of food without a metabolic need in times of repletion can provide energy storage for times of scarcity, to cover both basic physiological functions and additional energetic-challenging demands, such as foraging for food, escape from predators and reproduction (Waterson and Horvath 2015). But beyond the consummatory aspect of feeding behavior, there are many examples in nature of appetitive feeding behavior that are not followed by food consumption, and occur long before a metabolic deficit appears. Food hoarding is an appetitive behavior, which involves foraging for food and transporting it from the source to a home or burrow where it is saved for a period of time, before its consumption (Vander Wall 1990; Schneider, Wise et al. 2013). Food-hoarders have the capacity *"to control the availability of food in space and time"*, which provides a clear adaptative advantage over non food-hoarding animals (Vander Wall 1990). A reduction of available food in the environment can be sufficient to make non-hoarders to suffer loss in body mass and/or eventually migrate. Likewise, if there is enough food but the environment becomes more hostile, due to predators or inclement weather, it becomes more difficult to forage for food without endangering the individual. Furthermore, already secured food allows animals to employ the time, that normally would be required for food seeking, to engage in different innate behaviors, that might become more relevant or important at a given moment (such as courtship or territorial defense) (Vander Wall 1990).

6 Conclusions

Based on the results obtained after subsequent analysis from experimental sessions, and on the discussion of the data, it can be concluded as follows:

- LH_{Vgat} neurons constitute a heterogeneous population in terms of functionality, being composed by different subgroups that by interactions with different target regions, and by being modulated by different inputs are able to mediate diverse innate behaviors, including arousal and food intake.

- LH_{Vgat} neurons increase their firing rate transiently upon NREM-wakefulness transitions, which causally induces fast transitions from NREM sleep to wakefulness.

- This fast promotion of arousal is mediated by the inhibitory control that LH_{Vgat} cells exert over RTN GABAergic cells.

- Optogenetic activation of LH_{Vgat} -RTN pathway results in state-dependent changes of RTN neuronal activity, which also occur during spontaneous NREM-wakefulness transitions.

- Given the connections of RTN neurons with the thalamocortical circuit, the LH_{Vgat}-RTN-thalamocortical circuit composes a feed-forward inhibitory circuit. The transient nature of LH_{Vgat} neurons increase of firing rate upon transitions to wakefulness suggest the existence of inhibitory inputs that provide feedback modulation, in order to avoid hyperactivation of the thalamocortical circuit.

- A subgroup of LH_{Vgat} neurons is preferentially active inside the food zone, being able to code its location, while another subgroup is preferentially active distantly from the food zone, allowing their classification in FZ-match cells and FZ-mismatch cells respectively.

- The firing of these two subgroups of LH_{Vgat} cells is segregated with high temporal precision during the ongoing local gamma oscillation in LH.

- Gamma oscillations in the LH are state-dependent, gamma power is increased in LH during food approach, but not during food intake.

- The LS, which sends prominent inhibitory projections to the LH, displays coordinated gamma oscillations with the LH, gamma oscillations entrain neuronal

activity in both regions. Further, LS gamma oscillatory inputs to the LH enable the temporal separation of FZ-match cells and FZ-mismatch cells.

- Optogenetic manipulation of LS GABAergic projections to LH at gamma frequency evokes gamma oscillations in LH, and drives food-seeking behavior without affecting food consumption.

- Optogenetic activation of LH_{Vgat} neuronal population mediates an increase of food intake, while its inhibition decreases food intake.

- Given that activation of projections from mPFC to LS at gamma frequency recapitulates behavioral effects of LS-LH gamma-rhythmic activation, a top-down circuit between mPFC-LS-LH utilizes gamma oscillations to mediate food-seeking.

7 Bibliography

Adamantidis, A. and L. de Lecea (2008). "Sleep and metabolism: shared circuits, new connections." Trends Endocrinol Metab **19**(10): 362-370.

Adamantidis, A. R., F. Zhang, et al. (2007). "Neural substrates of awakening probed with optogenetic control of hypocretin neurons." Nature **450**(7168): 420-424.

Agid, Y., G. Buzsaki, et al. (2007). "How can drug discovery for psychiatric disorders be improved?" Nat Rev Drug Discov **6**(3): 189-201.

Andermann, M. L. and B. B. Lowell (2017). "Toward a Wiring Diagram Understanding of Appetite Control." Neuron **95**(4): 757-778.

Aponte, Y., D. Atasoy, et al. (2011). "AGRP neurons are sufficient to orchestrate feeding behavior rapidly and without training." Nat Neurosci **14**(3): 351-355.

Atasoy, D., J. N. Betley, et al. (2012). "Deconstruction of a neural circuit for hunger." Nature **488**(7410): 172-177.

Ball, G. F. and J. Balthazart (2008). "How useful is the appetitive and consummatory distinction for our understanding of the neuroendocrine control of sexual behavior?" Horm Behav **53**(2): 307-311; author reply 315-308.

Barone, F. C., J. T. Cheng, et al. (1994). "Reticular thalamic inhibitory input to lateral hypothalamic neurons: a functional and histochemical determination." Brain Res Bull **33**(5): 575-582.

Bartho, P., H. Hirase, et al. (2004). "Characterization of neocortical principal cells and interneurons by network interactions and extracellular features." J Neurophysiol **92**(1): 600-608.

Bartho, P., A. Slezia, et al. (2014). "Ongoing network state controls the length of sleep spindles via inhibitory activity." Neuron **82**(6): 1367-1379.

Bender, F., M. Gorbati, et al. (2015). "Theta oscillations regulate the speed of locomotion via a hippocampus to lateral septum pathway." Nat Commun **6**: 8521.

Berland, C., C. Cansell, et al. (2016). "Dietary triglycerides as signaling molecules that influence reward and motivation." Curr Opin Behav Sci **9**: 126-135.

Bernardis, L. L. and L. L. Bellinger (1996). "The lateral hypothalamic area revisited: ingestive behavior." Neurosci Biobehav Rev **20**(2): 189-287.

Berridge, K. C. (2004). "Motivation concepts in behavioral neuroscience." Physiol Behav **81**(2): 179-209.

Bittencourt, J. C., F. Presse, et al. (1992). "The melanin-concentrating hormone system of the rat brain: an immuno- and hybridization histochemical characterization." J Comp Neurol **319**(2): 218-245.

Blanco-Centurion, C., M. Liu, et al. (2016). "Optogenetic activation of melanin-concentrating hormone neurons increases non-rapid eye movement and rapid eye movement sleep during the night in rats." Eur J Neurosci **44**(10): 2846-2857.

Bonnavion, P., A. C. Jackson, et al. (2015). "Antagonistic interplay between hypocretin and leptin in the lateral hypothalamus regulates stress responses." Nat Commun **6**: 6266.

Bonnavion, P., L. E. Mickelsen, et al. (2016). "Hubs and spokes of the lateral hypothalamus: cell types, circuits and behaviour." J Physiol **594**(22): 6443-6462.

Borgers, C. and N. Kopell (2003). "Synchronization in networks of excitatory and inhibitory neurons with sparse, random connectivity." Neural Comput **15**(3): 509-538.

Bremer, F. (1935). "Cerveau" isole" et physiologie du sommeil." CR Soc Biol (Paris) **118**: 1235-1241.

Brobeck, J. R., J. Tepperman, et al. (1943). "Experimental hypothalamic hyperphagia in the albino rat." The Yale journal of biology and medicine **15**(6): 831.

Broberger, C., L. De Lecea, et al. (1998). "Hypocretin/orexin- and melanin-concentrating hormone-expressing cells form distinct populations in the rodent lateral hypothalamus: relationship to the neuropeptide Y and agouti gene-related protein systems." J Comp Neurol **402**(4): 460-474.

Broussard, J. L. and E. Van Cauter (2016). "Disturbances of sleep and circadian rhythms: novel risk factors for obesity." Curr Opin Endocrinol Diabetes Obes **23**(5): 353-359.

Brown, J. A., H. L. Woodworth, et al. (2015). "To ingest or rest? Specialized roles of lateral hypothalamic area neurons in coordinating energy balance." Front Syst Neurosci **9**: 9.

Brown, R. E., R. Basheer, et al. (2012). "Control of sleep and wakefulness." Physiol Rev **92**(3): 1087-1187.

Buhl, E. H., K. Halasy, et al. (1994). "Diverse sources of hippocampal unitary inhibitory postsynaptic potentials and the number of synaptic release sites." Nature **368**(6474): 823-828.

Buzsaki, G. (2006). Rhythms of the Brain, Oxford University Press.

Buzsaki, G., C. A. Anastassiou, et al. (2012). "The origin of extracellular fields and currents--EEG, ECoG, LFP and spikes." Nat Rev Neurosci **13**(6): 407-420.

Buzsaki, G. and A. Draguhn (2004). "Neuronal oscillations in cortical networks." Science **304**(5679): 1926-1929.

Buzsaki, G. and X. J. Wang (2012). "Mechanisms of gamma oscillations." Annu Rev Neurosci **35**: 203-225.

Buzsaki, G. and B. O. Watson (2012). "Brain rhythms and neural syntax: implications for efficient coding of cognitive content and neuropsychiatric disease." Dialogues Clin Neurosci **14**(4): 345-367.

Cannon, W. B. (1932). "Homeostasis." The wisdom of the body. Norton, New York.

Canteras, N. (2012). "Hypothalamic goal-directed behavior—ingestive, reproductive and defensive." The Mouse Nervous System: 539-562.

Cardin, J. A., M. Carlen, et al. (2009). "Driving fast-spiking cells induces gamma rhythm and controls sensory responses." Nature **459**(7247): 663-667.

Cardin, J. A., M. Carlen, et al. (2010). "Targeted optogenetic stimulation and recording of neurons in vivo using cell-type-specific expression of Channelrhodopsin-2." Nat Protoc **5**(2): 247-254.

Carraway, R. and S. E. Leeman (1973). "The isolation of a new hypotensive peptide, neurotensin, from bovine hypothalami." J Biol Chem **248**(19): 6854-6861.

Carter, M. E. and L. de Lecea (2011). "Optogenetic investigation of neural circuits in vivo." Trends Mol Med **17**(4): 197-206.

Carus-Cadavieco, M., M. Gorbati, et al. (2017). "Gamma oscillations organize top-down signalling to hypothalamus and enable food seeking." Nature **542**(7640): 232-236.

Cassidy, R. M. and Q. Tong (2017). "Hunger and Satiety Gauge Reward Sensitivity." Front Endocrinol (Lausanne) **8**: 104.

Castel, M. N., J. M. Stutzmann, et al. (1989). "Effects of ICV administration of neurotensin and analogs on EEG in rats." Peptides **10**(1): 95-101.

Cazala, P., D. Galey, et al. (1988). "Electrical self-stimulation in the medial and lateral septum as compared to the lateral hypothalamus: differential intervention of reward and learning processes?" Physiol Behav **44**(1): 53-59.

Chee, M. J., E. Arrigoni, et al. (2015). "Melanin-concentrating hormone neurons release glutamate for feedforward inhibition of the lateral septum." J Neurosci **35**(8): 3644-3651.

Cho, K. K., R. Hoch, et al. (2015). "Gamma rhythms link prefrontal interneuron dysfunction with cognitive inflexibility in Dlx5/6(+/-) mice." Neuron **85**(6): 1332-1343.

Colgin, L. L., T. Denninger, et al. (2009). "Frequency of gamma oscillations routes flow of information in the hippocampus." Nature **462**(7271): 353-357.

Conductier, G., A. O. Martin, et al. (2013). "Control of ventricular ciliary beating by the melanin concentrating hormone-expressing neurons of the lateral hypothalamus: a functional imaging survey." Front Endocrinol (Lausanne) **4**: 182.

Contreras, D., R. Curro Dossi, et al. (1992). "Bursting and tonic discharges in two classes of reticular thalamic neurons." J Neurophysiol **68**(3): 973-977.

Contreras, D. and M. Steriade (1995). "Cellular basis of EEG slow rhythms: a study of dynamic corticothalamic relationships." J Neurosci **15**(1 Pt 2): 604-622.

Craig, W. (1917). "Appetites and aversions as constituents of instincts." Proceedings of the National Academy of Sciences **3**(12): 685-688.

Crosby, E. C. and R. T. Woodburne (1939). "The comparative anatomy of the preoptic area and the hypothalamus." RESEARCH PUBLICATIONS-ASSOCIATION FOR RESEARCH IN NERVOUS AND MENTAL DISEASE **20**: 52-169.

Csicsvari, J., D. A. Henze, et al. (2003). "Massively parallel recording of unit and local field potentials with silicon-based electrodes." J Neurophysiol **90**(2): 1314-1323.

Csicsvari, J., H. Hirase, et al. (1999). "Oscillatory coupling of hippocampal pyramidal cells and interneurons in the behaving Rat." J Neurosci **19**(1): 274-287.

Csicsvari, J., B. Jamieson, et al. (2003). "Mechanisms of gamma oscillations in the hippocampus of the behaving rat." Neuron **37**(2): 311-322.

Davis, C., D. K. Katzman, et al. (1997). "The prevalence of high-level exercise in the eating disorders: etiological implications." Compr Psychiatry **38**(6): 321-326.

de Andres, I., M. Garzon, et al. (2011). "Functional Anatomy of Non-REM Sleep." Front Neurol **2**: 70.

de Lecea, L., T. S. Kilduff, et al. (1998). "The hypocretins: hypothalamus-specific peptides with neuroexcitatory activity." Proc Natl Acad Sci U S A **95**(1): 322-327.

Deisseroth, K. (2015). "Optogenetics: 10 years of microbial opsins in neuroscience." Nat Neurosci **18**(9): 1213-1225.

Deisseroth, K. and P. Hegemann (2017). "The form and function of channelrhodopsin." Science **357**(6356).

Del Cid-Pellitero, E. and B. E. Jones (2012). "Immunohistochemical evidence for synaptic release of GABA from melanin-concentrating hormone containing varicosities in the locus coeruleus." Neuroscience **223**: 269-276.

Elias, C. F., C. E. Lee, et al. (2001). "Characterization of CART neurons in the rat and human hypothalamus." J Comp Neurol **432**(1): 1-19.

Engel, A. K., P. Fries, et al. (2001). "Dynamic predictions: oscillations and synchrony in top-down processing." Nat Rev Neurosci **2**(10): 704-716.

Ermentrout, G. B. and N. Kopell (1998). "Fine structure of neural spiking and synchronization in the presence of conduction delays." Proc Natl Acad Sci U S A **95**(3): 1259-1264.

Ernst, O. P., D. T. Lodowski, et al. (2014). "Microbial and animal rhodopsins: structures, functions, and molecular mechanisms." Chem Rev **114**(1): 126-163.

Felten, D. and A. Shetty (2010). "Netter's atlas of neuroscience. Saunders." Elsevier **5**: 24.

Franken, P., D. Chollet, et al. (2001). "The homeostatic regulation of sleep need is under genetic control." J Neurosci **21**(8): 2610-2621.

Fries, P., D. Nikolic, et al. (2007). "The gamma cycle." Trends Neurosci **30**(7): 309-316.

Fuentealba, P. and M. Steriade (2005). "The reticular nucleus revisited: intrinsic and network properties of a thalamic pacemaker." Prog Neurobiol **75**(2): 125-141.

Gardner, R. J., S. W. Hughes, et al. (2013). "Differential spike timing and phase dynamics of reticular thalamic and prefrontal cortical neuronal populations during sleep spindles." J Neurosci **33**(47): 18469-18480.

Gonzalez, J. A., L. T. Jensen, et al. (2016). "Inhibitory Interplay between Orexin Neurons and Eating." Curr Biol **26**(18): 2486-2491.

Goshen, I., M. Brodsky, et al. (2011). "Dynamics of retrieval strategies for remote memories." Cell **147**(3): 678-689.

Gradinaru, V., K. R. Thompson, et al. (2008). "eNpHR: a Natronomonas halorhodopsin enhanced for optogenetic applications." Brain Cell Biol **36**(1-4): 129-139.

Gradinaru, V., F. Zhang, et al. (2010). "Molecular and cellular approaches for diversifying and extending optogenetics." Cell **141**(1): 154-165.

Gray, C. M. and W. Singer (1989). "Stimulus-specific neuronal oscillations in orientation columns of cat visual cortex." Proc Natl Acad Sci U S A **86**(5): 1698-1702.

Gunaydin, L. A., O. Yizhar, et al. (2010). "Ultrafast optogenetic control." Nat Neurosci **13**(3): 387-392.

Hahn, J. D. and L. W. Swanson (2012). "Connections of the lateral hypothalamic area juxtadorsomedial region in the male rat." J Comp Neurol **520**(9): 1831-1890.

Halassa, M. M., Z. Chen, et al. (2014). "State-dependent architecture of thalamic reticular subnetworks." Cell **158**(4): 808-821.

Harris, K. D., J. Csicsvari, et al. (2003). "Organization of cell assemblies in the hippocampus." Nature **424**(6948): 552-556.

Harris, K. D., D. A. Henze, et al. (2000). "Accuracy of tetrode spike separation as determined by simultaneous intracellular and extracellular measurements." J Neurophysiol **84**(1): 401-414.

Harz, H. and P. Hegemann (1991). "Rhodopsin-regulated calcium currents in Chlamydomonas." Nature **351**(6326): 489-491.

Hasenstaub, A., Y. Shu, et al. (2005). "Inhibitory postsynaptic potentials carry synchronized frequency information in active cortical networks." Neuron **47**(3): 423-435.

Haslam, D. (2007). "Obesity: a medical history." Obes Rev **8 Suppl 1**: 31-36.

Hassani, O. K., P. Henny, et al. (2010). "GABAergic neurons intermingled with orexin and MCH neurons in the lateral hypothalamus discharge maximally during sleep." Eur J Neurosci **32**(3): 448-457.

Hassani, O. K., M. G. Lee, et al. (2009). "Melanin-concentrating hormone neurons discharge in a reciprocal manner to orexin neurons across the sleep-wake cycle." Proc Natl Acad Sci U S A **106**(7): 2418-2422.

Hazan, L., M. Zugaro, et al. (2006). "Klusters, NeuroScope, NDManager: a free software suite for neurophysiological data processing and visualization." J Neurosci Methods **155**(2): 207-216.

Hegemann, P., D. Oesterbelt, et al. (1985). "The photocycle of the chloride pump halorhodopsin. I: Azide-catalyzed deprotonation of the chromophore is a side reaction of photocycle intermediates inactivating the pump." EMBO J **4**(9): 2347-2350.

Herrera, C. G., M. Carus Cadavieco, et al. (2016). "Hypothalamic feedforward inhibition of thalamocortical network controls arousal and consciousness." Nat Neurosci **19**(2): 290-298.

Herrera, C. G., A. Ponomarenko, et al. (2017). "Sleep & metabolism: The multitasking ability of lateral hypothalamic inhibitory circuitries." Front Neuroendocrinol **44**: 27-34.

Hetherington, A. and S. Ranson (1940). "Hypothalamic lesions and adiposity in the rat." Anat Rec A Discov Mol Cell Evol Biol **78**(2): 149-172.

Hoebel, B. G. and P. Teitelbaum (1962). "Hypothalamic control of feeding and self-stimulation." Science **135**(3501): 375-377.

Huguenard, J. R. and D. A. McCormick (2007). "Thalamic synchrony and dynamic regulation of global forebrain oscillations." Trends Neurosci **30**(7): 350-356.

Huxter, J., N. Burgess, et al. (2003). "Independent rate and temporal coding in hippocampal pyramidal cells." Nature **425**(6960): 828-832.

Iaccarino, H. F., A. C. Singer, et al. (2016). "Gamma frequency entrainment attenuates amyloid load and modifies microglia." Nature **540**(7632): 230-235.

Igarashi, K. M., L. Lu, et al. (2014). "Coordination of entorhinal-hippocampal ensemble activity during associative learning." Nature **510**(7503): 143-147.

Jakab, R., C. Leranth, et al. (1995). "The rat nervous system." Academic, San Diego: 405-442.

Jego, S., S. D. Glasgow, et al. (2013). "Optogenetic identification of a rapid eye movement sleep modulatory circuit in the hypothalamus." Nat Neurosci **16**(11): 1637-1643.

Jennings, J. H., G. Rizzi, et al. (2013). "The inhibitory circuit architecture of the lateral hypothalamus orchestrates feeding." Science **341**(6153): 1517-1521.

Jennings, J. H., R. L. Ung, et al. (2015). "Visualizing hypothalamic network dynamics for appetitive and consummatory behaviors." Cell **160**(3): 516-527.

Jensen, O., J. Kaiser, et al. (2007). "Human gamma-frequency oscillations associated with attention and memory." Trends Neurosci **30**(7): 317-324.

Johnson, P. M. and P. J. Kenny (2010). "Dopamine D2 receptors in addiction-like reward dysfunction and compulsive eating in obese rats." Nat Neurosci **13**(5): 635-641.

Jones, B. E. (2005). "From waking to sleeping: neuronal and chemical substrates." Trends Pharmacol Sci **26**(11): 578-586.

Kalivas, P. W., L. Jennes, et al. (1982). "Neurotensin: topographical distribution of brain sites involved in hypothermia and antinociception." J Comp Neurol **210**(3): 225-238.

Kawauchi, H., I. Kawazoe, et al. (1983). "Characterization of melanin-concentrating hormone in chum salmon pituitaries." Nature **305**(5932): 321-323.

Kaye, W. H., J. L. Fudge, et al. (2009). "New insights into symptoms and neurocircuit function of anorexia nervosa." Nat Rev Neurosci **10**(8): 573-584.

Kelly, J., J. Rothstein, et al. (1979). "GABA and hypothalamic feeding systems. I. Topographic analysis of the effects of microinjections of muscimol." Physiol Behav **23**(6): 1123-1134.

Kempadoo, K. A., C. Tourino, et al. (2013). "Hypothalamic neurotensin projections promote reward by enhancing glutamate transmission in the VTA." J Neurosci **33**(18): 7618-7626.

Kim, H., S. Ahrlund-Richter, et al. (2016). "Prefrontal Parvalbumin Neurons in Control of Attention." Cell **164**(1-2): 208-218.

Kim, S. Y., A. Adhikari, et al. (2013). "Diverging neural pathways assemble a behavioural state from separable features in anxiety." Nature **496**(7444): 219-223.

Knoche, A., H. Yokoyama, et al. (2003). "High-frequency oscillation in the hippocampus of the behaving rat and its modulation by the histaminergic system." Hippocampus **13**(2): 273-280.

Kocsis, K., J. Kiss, et al. (2003). "Location of putative glutamatergic neurons projecting to the medial preoptic area of the rat hypothalamus." Brain Res Bull **61**(4): 459-468.

Konadhode, R. R., D. Pelluru, et al. (2013). "Optogenetic stimulation of MCH neurons increases sleep." J Neurosci **33**(25): 10257-10263.

Korotkova, T., E. C. Fuchs, et al. (2010). "NMDA receptor ablation on parvalbumin-positive interneurons impairs hippocampal synchrony, spatial representations, and working memory." Neuron **68**(3): 557-569.

Korotkova, T. and A. Ponomarenko (2017). "Optogenetic Manipulations of Neuronal Network Oscillations: Combination of Optogenetics and Electrophysiological Recordings in Behaving Mice." In Vivo Neuropharmacology and Neurophysiology: 67-88.

Korotkova, T. and A. Ponomarenko (2017). "To eat? To sleep? To run? Coordination of innate behaviors by lateral hypothalamus." e-Neuroforum **23**(2): 45-55.

Lanyi, J. K. and D. Oesterhelt (1982). "Identification of the retinal-binding protein in halorhodopsin." J Biol Chem **257**(5): 2674-2677.

Le Gros Clark, S. W. E. (1938). Morphological aspects of the hypothalamus.

Lee, M. G., O. K. Hassani, et al. (2005). "Discharge of identified orexin/hypocretin neurons across the sleep-waking cycle." J Neurosci **25**(28): 6716-6720.

Lee, S. H., G. Govindaiah, et al. (2007). "Heterogeneity of firing properties among rat thalamic reticular nucleus neurons." J Physiol **582**(Pt 1): 195-208.

Leinninger, G. M., Y. H. Jo, et al. (2009). "Leptin acts via leptin receptor-expressing lateral hypothalamic neurons to modulate the mesolimbic dopamine system and suppress feeding." Cell Metab **10**(2): 89-98.

Leinninger, G. M., D. M. Opland, et al. (2011). "Leptin action via neurotensin neurons controls orexin, the mesolimbic dopamine system and energy balance." Cell Metab **14**(3): 313-323.

Leng, G. and M. Ludwig (2008). "Neurotransmitters and peptides: whispered secrets and public announcements." J Physiol **586**(23): 5625-5632.

Li, X., D. V. Gutierrez, et al. (2005). "Fast noninvasive activation and inhibition of neural and network activity by vertebrate rhodopsin and green algae channelrhodopsin." Proc Natl Acad Sci U S A **102**(49): 17816-17821.

Lin, W., K. McKinney, et al. (2003). "Distribution of vesicular glutamate transporter-2 messenger ribonucleic Acid and protein in the septum-hypothalamus of the rat." Endocrinology **144**(2): 662-670.

Louis, G. W., G. M. Leinninger, et al. (2010). "Direct innervation and modulation of orexin neurons by lateral hypothalamic LepRb neurons." J Neurosci **30**(34): 11278-11287.

Luo, A. H., P. Tahsili-Fahadan, et al. (2011). "Linking context with reward: a functional circuit from hippocampal CA3 to ventral tegmental area." Science **333**(6040): 353-357.

Luquet, S., F. A. Perez, et al. (2005). "NPY/AgRP neurons are essential for feeding in adult mice but can be ablated in neonates." Science **310**(5748): 683-685.

Madisen, L., T. A. Zwingman, et al. (2010). "A robust and high-throughput Cre reporting and characterization system for the whole mouse brain." Nat Neurosci **13**(1): 133-140.

Maharajh, K., P. Teale, et al. (2010). "Fluctuation of gamma-band phase synchronization within the auditory cortex in schizophrenia." Clin Neurophysiol **121**(4): 542-548.

Mahler, S. V., D. E. Moorman, et al. (2014). "Motivational activation: a unifying hypothesis of orexin/hypocretin function." Nat Neurosci **17**(10): 1298-1303.

Matsuno-Yagi, A. and Y. Mukohata (1977). "Two possible roles of bacteriorhodopsin; a comparative study of strains of Halobacterium halobium differing in pigmentation." Biochem Biophys Res Commun **78**(1): 237-243.

Mattis, J., K. M. Tye, et al. (2011). "Principles for applying optogenetic tools derived from direct comparative analysis of microbial opsins." Nat Methods **9**(2): 159-172.

McCormick, D. A. and T. Bal (1997). "Sleep and arousal: thalamocortical mechanisms." Annu Rev Neurosci **20**: 185-215.

McCoy, J. G. and R. E. Strecker (2011). "The cognitive cost of sleep lost." Neurobiol Learn Mem **96**(4): 564-582.

Meszar, Z., F. Girard, et al. (2012). "The lateral hypothalamic parvalbumin-immunoreactive (PV1) nucleus in rodents." J Comp Neurol **520**(4): 798-815.

Morton, G. J., T. H. Meek, et al. (2014). "Neurobiology of food intake in health and disease." Nat Rev Neurosci **15**(6): 367-378.

Moruzzi, G. and H. W. Magoun (1949). "Brain stem reticular formation and activation of the EEG." Electroencephalogr Clin Neurophysiol **1**(4): 455-473.

Mulert, C., V. Kirsch, et al. (2012). "Hearing voices: a role of interhemispheric auditory connectivity?" World J Biol Psychiatry **13**(2): 153-158.

Muller, R. U. and J. L. Kubie (1989). "The firing of hippocampal place cells predicts the future position of freely moving rats." J Neurosci **9**(12): 4101-4110.

Nagel, G., D. Ollig, et al. (2002). "Channelrhodopsin-1: a light-gated proton channel in green algae." Science **296**(5577): 2395-2398.

Nagel, G., T. Szellas, et al. (2003). "Channelrhodopsin-2, a directly light-gated cation-selective membrane channel." Proc Natl Acad Sci U S A **100**(24): 13940-13945.

Nagy, A. (2000). "Cre recombinase: the universal reagent for genome tailoring." Genesis **26**(2): 99-109.

Narayanan, N. S. and R. J. DiLeone (2017). "Lip Sync: Gamma Rhythms Orchestrate Top-Down Control of Feeding Circuits." Cell Metab **25**(3): 497-498.

Navarro, M., J. J. Olney, et al. (2016). "Lateral Hypothalamus GABAergic Neurons Modulate Consummatory Behaviors Regardless of the Caloric Content or Biological Relevance of the Consumed Stimuli." Neuropsychopharmacology **41**(6): 1505-1512.

Nieh, E. H., G. A. Matthews, et al. (2015). "Decoding neural circuits that control compulsive sucrose seeking." Cell **160**(3): 528-541.

Nieh, E. H., C. M. Vander Weele, et al. (2016). "Inhibitory Input from the Lateral Hypothalamus to the Ventral Tegmental Area Disinhibits Dopamine Neurons and Promotes Behavioral Activation." Neuron **90**(6): 1286-1298.

Nieuwenhuys, R., L. M. Geeraedts, et al. (1982). "The medial forebrain bundle of the rat. I. General introduction." J Comp Neurol **206**(1): 49-81.

Nunez, A., R. Curro Dossi, et al. (1992). "Intracellular evidence for incompatibility between spindle and delta oscillations in thalamocortical neurons of cat." Neuroscience **48**(1): 75-85.

O'Connor, E. C., Y. Kremer, et al. (2015). "Accumbal D1R Neurons Projecting to Lateral Hypothalamus Authorize Feeding." Neuron **88**(3): 553-564.

O'Keefe, J. (1976). "Place units in the hippocampus of the freely moving rat." Exp Neurol **51**(1): 78-109.

Oesterhelt, D. and W. Stoeckenius (1971). "Rhodopsin-like protein from the purple membrane of Halobacterium halobium." Nat New Biol **233**(39): 149-152.

Oesterhelt, D. and W. Stoeckenius (1973). "Functions of a new photoreceptor membrane." Proc Natl Acad Sci U S A **70**(10): 2853-2857.

Olds, J. and P. Milner (1954). "Positive reinforcement produced by electrical stimulation of septal area and other regions of rat brain." J Comp Physiol Psychol **47**(6): 419-427.

Ono, T., H. Nishino, et al. (1981). "Long-term lateral hypothalamic single unit analysis and feeding behavior in freely moving rats." Neurosci Lett **26**(1): 79-83.

Ono, T., K. Sasaki, et al. (1986). "Feeding and diurnal related activity of lateral hypothalamic neurons in freely behaving rats." Brain Res **373**(1-2): 92-102.

Otchy, T. M., S. B. Wolff, et al. (2015). "Acute off-target effects of neural circuit manipulations." Nature **528**(7582): 358-363.

Palop, J. J., J. Chin, et al. (2007). "Aberrant excitatory neuronal activity and compensatory remodeling of inhibitory hippocampal circuits in mouse models of Alzheimer's disease." Neuron **55**(5): 697-711.

Paxinos, G. (2013). Paxinos and Franklin's the mouse brain in stereotaxic coordinates, Academic Press.

Peyron, C., D. K. Tighe, et al. (1998). "Neurons containing hypocretin (orexin) project to multiple neuronal systems." J Neurosci **18**(23): 9996-10015.

Poller, W. C., V. I. Madai, et al. (2013). "A glutamatergic projection from the lateral hypothalamus targets VTA-projecting neurons in the lateral habenula of the rat." Brain Res **1507**: 45-60.

Raimondo, J. V., L. Kay, et al. (2012). "Optogenetic silencing strategies differ in their effects on inhibitory synaptic transmission." Nat Neurosci **15**(8): 1102-1104.

Rajasethupathy, P., E. Ferenczi, et al. (2016). "Targeting Neural Circuits." Cell **165**(3): 524-534.

Ramón y Cajal, S. (1902). Estructura del septum lucidum.

Risold, P. Y. and L. W. Swanson (1996). "Structural evidence for functional domains in the rat hippocampus." Science **272**(5267): 1484-1486.

Risold, P. Y. and L. W. Swanson (1997). "Chemoarchitecture of the rat lateral septal nucleus." Brain Res Brain Res Rev **24**(2-3): 91-113.

Risold, P. Y. and L. W. Swanson (1997b). "Connections of the rat lateral septal complex." Brain Res Brain Res Rev **24**(2-3): 115-195.

Rosin, D. L., M. C. Weston, et al. (2003). "Hypothalamic orexin (hypocretin) neurons express vesicular glutamate transporters VGLUT1 or VGLUT2." J Comp Neurol **465**(4): 593-603.

Roth, T. (2007). "Insomnia: definition, prevalence, etiology, and consequences." J Clin Sleep Med **3**(5 Suppl): S7-10.

Ryan, M. D. and J. Drew (1994). "Foot-and-mouth disease virus 2A oligopeptide mediated cleavage of an artificial polyprotein." EMBO J **13**(4): 928-933.

Sachs, B. D. (2007). "A contextual definition of male sexual arousal." Hormones and Behavior **51**(5): 569-578.

Sakurai, T., A. Amemiya, et al. (1998). "Orexins and orexin receptors: a family of hypothalamic neuropeptides and G protein-coupled receptors that regulate feeding behavior." Cell **92**(4): 573-585.

Saper, C. B., P. M. Fuller, et al. (2010). "Sleep state switching." Neuron **68**(6): 1023-1042.

Sapin, E., A. Berod, et al. (2010). "A very large number of GABAergic neurons are activated in the tuberal hypothalamus during paradoxical (REM) sleep hypersomnia." PLoS One **5**(7): e11766.

Sartor, G. C. and G. S. Aston-Jones (2012). "A septal-hypothalamic pathway drives orexin neurons, which is necessary for conditioned cocaine preference." J Neurosci **32**(13): 4623-4631.

Schneider, J. E., J. D. Wise, et al. (2013). "When do we eat? Ingestive behavior, survival, and reproductive success." Horm Behav **64**(4): 702-728.

Schone, C. and D. Burdakov (2012). "Glutamate and GABA as rapid effectors of hypothalamic "peptidergic" neurons." Front Behav Neurosci **6**: 81.

Sheehan, T. P., R. A. Chambers, et al. (2004). "Regulation of affect by the lateral septum: implications for neuropsychiatry." Brain Res Brain Res Rev **46**(1): 71-117.

Shein-Idelson, M., J. M. Ondracek, et al. (2016). "Slow waves, sharp waves, ripples, and REM in sleeping dragons." Science **352**(6285): 590-595.

Sherin, J. E., P. J. Shiromani, et al. (1996). "Activation of ventrolateral preoptic neurons during sleep." Science **271**(5246): 216-219.

Sherrington, C. (1906). "Yale University Mrs. Hepsa Ely Silliman memorial lectures. The integrative action of the nervous system."

Siegel, J. M. (1999). "Narcolepsy: a key role for hypocretins (orexins)." Cell **98**(4): 409-412.

Simerly, R. (2015). "Organization of the hypothalamus." The rat nervous system. Fourth Edition. San Diego: Elsevier: 267-288.

Simerly, R. B. and L. W. Swanson (1988). "Projections of the medial preoptic nucleus: a Phaseolus vulgaris leucoagglutinin anterograde tract-tracing study in the rat." J Comp Neurol **270**(2): 209-242.

Singer, W. (1993). "Synchronization of cortical activity and its putative role in information processing and learning." Annu Rev Physiol **55**: 349-374.

Singewald, G. M., A. Rjabokon, et al. (2011). "The modulatory role of the lateral septum on neuroendocrine and behavioral stress responses." Neuropsychopharmacology **36**(4): 793-804.

Sirota, A., S. Montgomery, et al. (2008). "Entrainment of neocortical neurons and gamma oscillations by the hippocampal theta rhythm." Neuron **60**(4): 683-697.

Sohal, V. S. (2016). "How Close Are We to Understanding What (if Anything) gamma Oscillations Do in Cortical Circuits?" J Neurosci **36**(41): 10489-10495.

Sparks, P. D. and J. E. LeDoux (1995). "Septal lesions potentiate freezing behavior to contextual but not to phasic conditioned stimuli in rats." Behav Neurosci **109**(1): 184-188.

Spitzer, N. C. (2015). "Neurotransmitter Switching? No Surprise." Neuron **86**(5): 1131-1144.

Spudich, J. L., C. S. Yang, et al. (2000). "Retinylidene proteins: structures and functions from archaea to humans." Annu Rev Cell Dev Biol **16**: 365-392.

Stam, C. J., A. M. van Cappellen van Walsum, et al. (2002). "Generalized synchronization of MEG recordings in Alzheimer's Disease: evidence for involvement of the gamma band." J Clin Neurophysiol **19**(6): 562-574.

Stamatakis, A. M., M. Van Swieten, et al. (2016). "Lateral Hypothalamic Area Glutamatergic Neurons and Their Projections to the Lateral Habenula Regulate Feeding and Reward." J Neurosci **36**(2): 302-311.

Steriade, M. (2003). "The corticothalamic system in sleep." Front Biosci **8**: d878-899.

Steriade, M., D. Contreras, et al. (1993). "The slow (< 1 Hz) oscillation in reticular thalamic and thalamocortical neurons: scenario of sleep rhythm generation in interacting thalamic and neocortical networks." J Neurosci **13**(8): 3284-3299.

Sternson, S. M. (2013). "Hypothalamic survival circuits: blueprints for purposive behaviors." Neuron **77**(5): 810-824.

Swanson, L. W. (2000). "Cerebral hemisphere regulation of motivated behavior." Brain Res **886**(1-2): 113-164.

Swanson, L. W. and W. M. Cowan (1979). "The connections of the septal region in the rat." J Comp Neurol **186**(4): 621-655.

Sweeney, P. and Y. Yang (2016). "An Inhibitory Septum to Lateral Hypothalamus Circuit That Suppresses Feeding." J Neurosci **36**(44): 11185-11195.

Takeuchi, T., A. J. Duszkiewicz, et al. (2016). "Locus coeruleus and dopaminergic consolidation of everyday memory." Nature **537**(7620): 357-362.

Thompson, R. H. and L. W. Swanson (2003). "Structural characterization of a hypothalamic visceromotor pattern generator network." Brain Res Brain Res Rev **41**(2-3): 153-202.

Traub, R. D., M. A. Whittington, et al. (1996). "Analysis of gamma rhythms in the rat hippocampus in vitro and in vivo." J Physiol **493 (Pt 2)**: 471-484.

Tritsch, N. X., J. B. Ding, et al. (2012). "Dopaminergic neurons inhibit striatal output through non-canonical release of GABA." Nature **490**(7419): 262-266.

Tsunematsu, T., T. Ueno, et al. (2014). "Optogenetic manipulation of activity and temporally controlled cell-specific ablation reveal a role for MCH neurons in sleep/wake regulation." J Neurosci **34**(20): 6896-6909.

Tye, K. M. and K. Deisseroth (2012). "Optogenetic investigation of neural circuits underlying brain disease in animal models." Nat Rev Neurosci **13**(4): 251-266.

Ung, K. and B. R. Arenkiel (2012). "Fiber-optic implantation for chronic optogenetic stimulation of brain tissue." J Vis Exp(68): e50004.

van den Pol, A. N. (2012). "Neuropeptide transmission in brain circuits." Neuron **76**(1): 98-115.

van den Pol, A. N., C. Acuna-Goycolea, et al. (2004). "Physiological properties of hypothalamic MCH neurons identified with selective expression of reporter gene after recombinant virus infection." Neuron **42**(4): 635-652.

Vandecasteele, M., S. M, et al. (2012). "Large-scale recording of neurons by movable silicon probes in behaving rodents." J Vis Exp(61): e3568.

Vander Wall, S. B. (1990). Food hoarding in animals, University of Chicago Press.

Verret, L., R. Goutagny, et al. (2003). "A role of melanin-concentrating hormone producing neurons in the central regulation of paradoxical sleep." BMC Neurosci **4**: 19.

Von Economo, C. (1930). "Sleep as a problem of localization." J Nerv Ment Dis **71**(3): 249-259.

Vong, L., C. Ye, et al. (2011). "Leptin action on GABAergic neurons prevents obesity and reduces inhibitory tone to POMC neurons." Neuron **71**(1): 142-154.

Waterson, M. J. and T. L. Horvath (2015). "Neuronal Regulation of Energy Homeostasis: Beyond the Hypothalamus and Feeding." Cell Metab **22**(6): 962-970.

Weber, F. and Y. Dan (2016). "Circuit-based interrogation of sleep control." Nature **538**(7623): 51-59.

Whittington, M. A., R. D. Traub, et al. (1995). "Synchronized oscillations in interneuron networks driven by metabotropic glutamate receptor activation." Nature **373**(6515): 612-615.

Wiegert, J. S., M. Mahn, et al. (2017). "Silencing Neurons: Tools, Applications, and Experimental Constraints." Neuron **95**(3): 504-529.

Williams, E. P., M. Mesidor, et al. (2015). "Overweight and Obesity: Prevalence, Consequences, and Causes of a Growing Public Health Problem." Curr Obes Rep **4**(3): 363-370.

Wu, Z., E. R. Kim, et al. (2015). "GABAergic projections from lateral hypothalamus to paraventricular hypothalamic nucleus promote feeding." J Neurosci **35**(8): 3312-3318.

Wulff, P., A. A. Ponomarenko, et al. (2009). "Hippocampal theta rhythm and its coupling with gamma oscillations require fast inhibition onto parvalbumin-positive interneurons." Proc Natl Acad Sci U S A **106**(9): 3561-3566.

Yamamoto, J., J. Suh, et al. (2014). "Successful execution of working memory linked to synchronized high-frequency gamma oscillations." Cell **157**(4): 845-857.

Yizhar, O., L. E. Fenno, et al. (2011). "Optogenetics in neural systems." Neuron **71**(1): 9-34.

Zemelman, B. V., G. A. Lee, et al. (2002). "Selective photostimulation of genetically chARGed neurons." Neuron **33**(1): 15-22.

Zhang, F., V. Gradinaru, et al. (2010). "Optogenetic interrogation of neural circuits: technology for probing mammalian brain structures." Nat Protoc **5**(3): 439-456.

Zhang, F., J. Vierock, et al. (2011). "The microbial opsin family of optogenetic tools." Cell **147**(7): 1446-1457.

Zhang, F., L. P. Wang, et al. (2007). "Multimodal fast optical interrogation of neural circuitry." Nature **446**(7136): 633-639.

Zhao, S., C. Cunha, et al. (2008). "Improved expression of halorhodopsin for light-induced silencing of neuronal activity." Brain Cell Biol **36**(1-4): 141-154.

Zheng, C., K. W. Bieri, et al. (2016). "Spatial Sequence Coding Differs during Slow and Fast Gamma Rhythms in the Hippocampus." Neuron **89**(2): 398-408.

8 Appendix

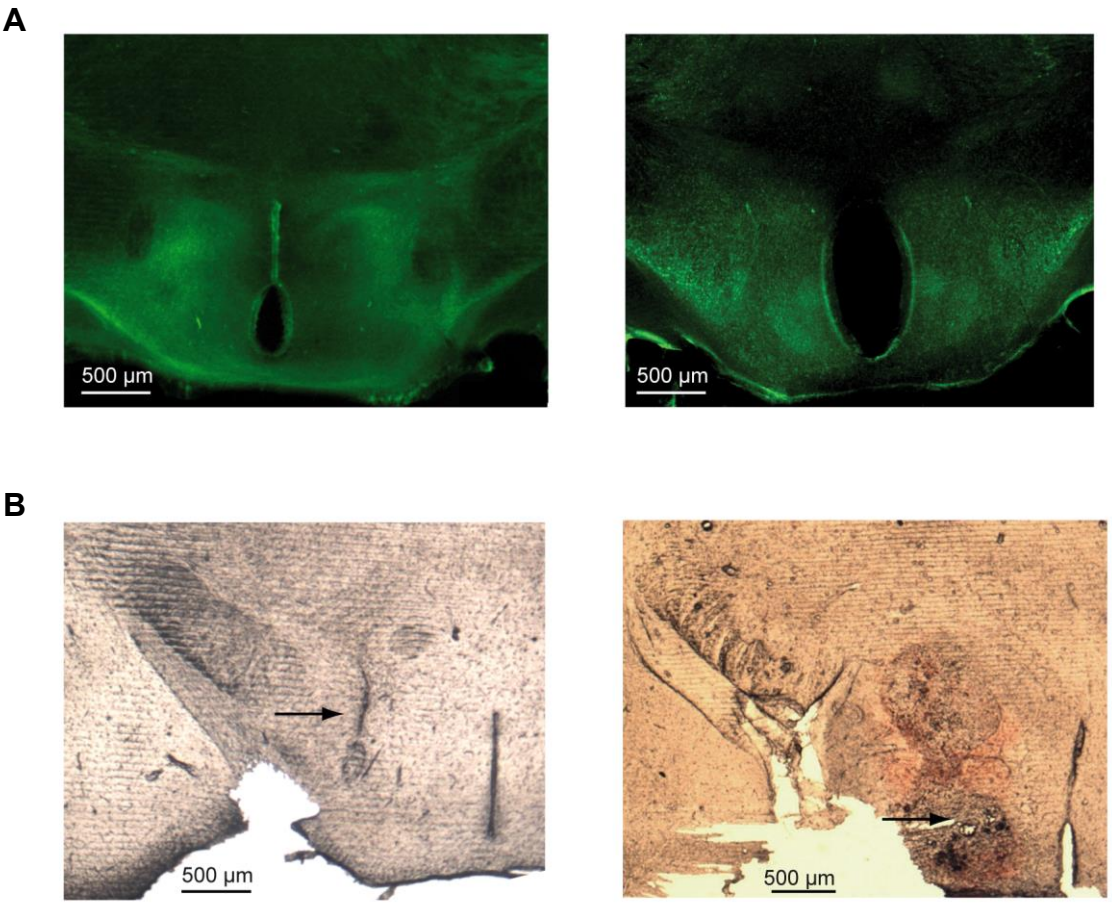

Figure 8.1 Histological verification of fluorescence expression and electrode positions in LH. **A** Representative photomicrographs of coronal brain slices from two Vgat Cre mice expressing ChETA in LH. **B** Photomicrographs of coronal brain sections from two Vgat Cre mice, showing a track left by one of the shanks of the silicon probe (left) and a lesion in the LH (right).

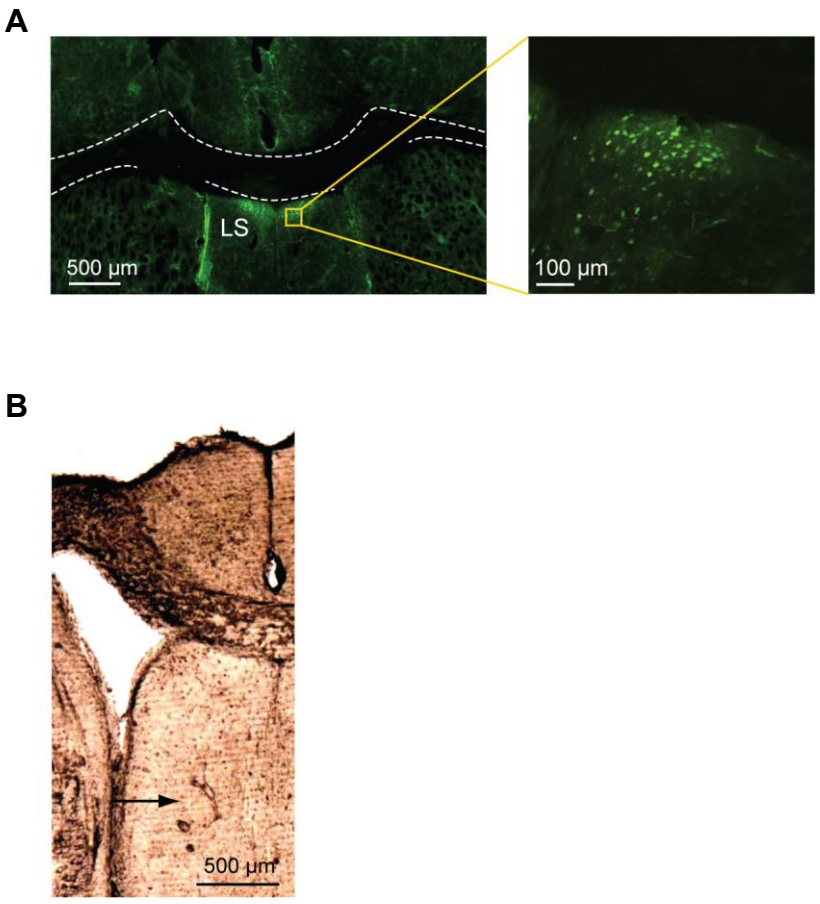

Figure 8.2 Histological verification of fluorescence expression and electrode positions in LS. **A** Photomicrograph of coronal brain slice from a Sst-Cre mouse expressing YFP in LS, right: high magnification of the same picture showing Sst-eYFP expressing neurons. **B** Photomicrograph of a coronal brain section, showing lesións from a wire array.

Acknowledgements

I would like to thank my supervisors Tatiana Korotkova and Alexey Ponomarenko who gave me the opportunity to parcipate in a very interesting and equally challenging project, for their help and their support. Moreover I would like to acknowledge our collaborators, Professor Antoine Adamantidis, Carolina Gutierrez-Herrera, Professor Karl Deisseroth and Charu Ramakrishnan. In addition I would like to especially acknowledge Suzanne van der Veldt and Natalia Denisova.

I would also like to acknowledge the reviewers of this thesis and members of the committee, for taking time to read and assess the present work.

I want to thank everyone that I have met through my time in the lab, for their motivation and enthusiam for the projects. Very special thanks go to my PhD colleagues, Franziska Bender and Maria Gorbati with whom it was a pleasure to work and share exciting scientific experiences during these years.

I am thankful also to all the colleagues I have met throughout my neuroscientific studies, especially to Ana, Elena, Mari, Sergio, for many fruitful discussions and meetings; and also Tugba, Yubin, Franziska, Camille, Kristin, Emma, Ania, Annika and Ulises.

Many thanks to Ignacio, who is gradually becoming an expert in electrophysiology and optogenetics, for his kind support during my time in Berlin.

Finally, I would like to express my gratitude to my family, for their understanding and patience; and for having supported and encouraged me throughout all the stages of my scientific studies and career.

Eigenständigkeitserklärung

Hiermit erkläre ich, die Dissertation selbstständig und nur unter Verwendung der angegebenen Hilfen und Hilfsmittel angefertigt zu haben.
Ich habe mich anderwärts nicht um einen Doktorgrad beworben und besitze keinen entsprechenden Doktorgrad. Ich erkläre, dass ich die Dissertation oder Teile davon nicht bereits bei einer anderen wissenschaftlichen Einrichtung eingereicht habe und dass sie dort weder angenommen noch abgelehnt wurde. Ich erkläre die Kenntnisnahme der dem Verfahren zugrunde liegenden Promotionsordnung der Lebenswissenschaftlichen Fakultät der Humboldt-Universität zu Berlin vom 5. März 2015.
Weiterhin erkläre ich, dass keine Zusammenarbeit mit gewerblichen Promotionsbearbeiterinnen/Promotionsberatern stattgefunden hat und dass die Grundsätze der Humboldt-Universität zu Berlin zur Sicherung guter wissenschaftlicher Praxis eingehalten wurden.

Berlin, 4.11.2017

Marta Carus-Cadavieco